Fall 2017

Saudi Aramco Journal of Technology

THE SAUDI ARAMCO JOURNAL OF TECHNOLOGY
A quarterly publication of the Saudi Arabian Oil Company

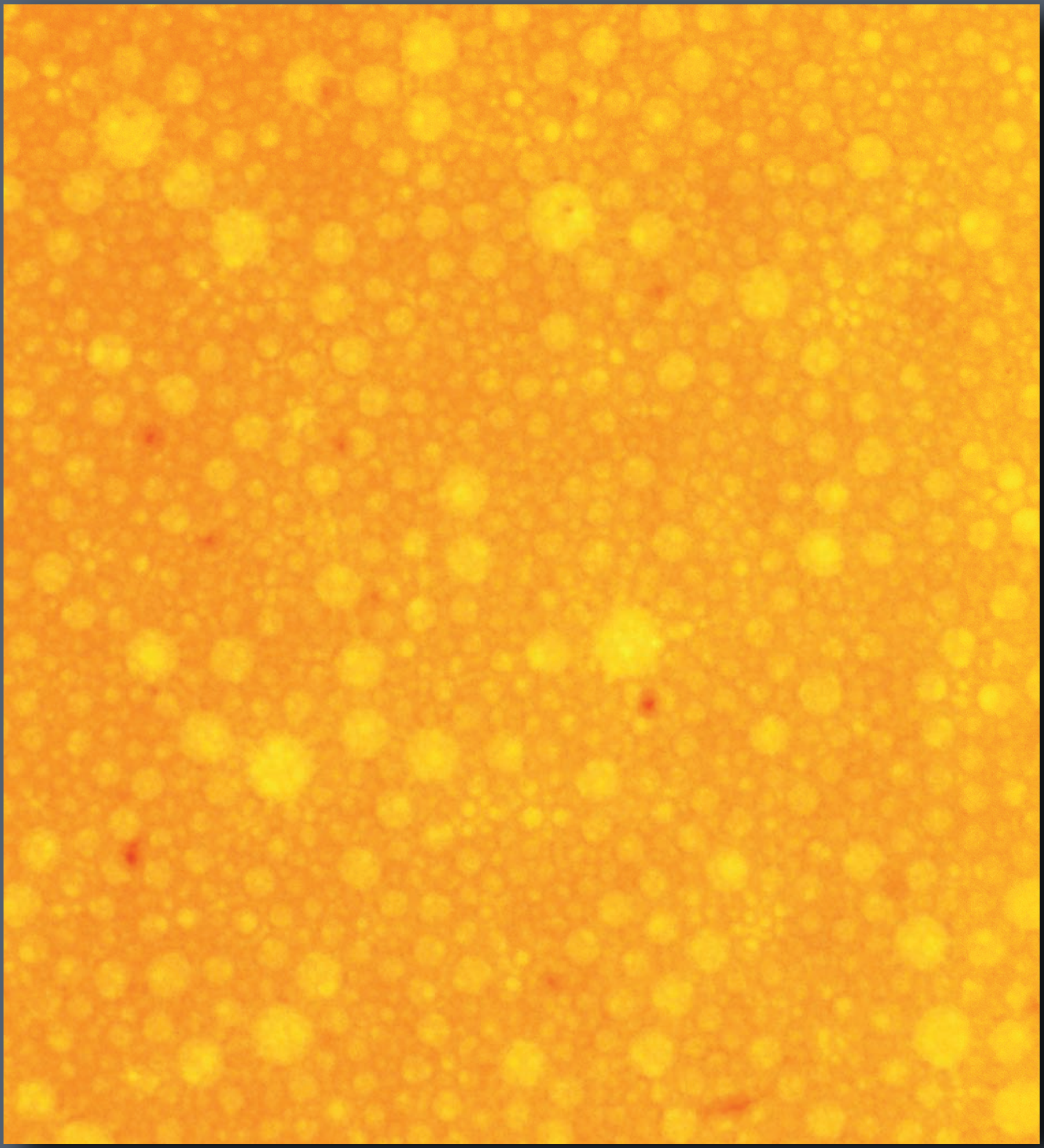

Optimizing a Stimulation Design Using Hydrajet Fracturing with Coiled Tubing in a Saudi Arabia Gas Well

see page 2

Strategies of Scale Management for Using Seawater as Fracturing Fluid

see page 17

Dr. Abdulaziz S. Al-Qasim, from Saudi Aramco's Exploration and Petroleum Engineering Center – Advanced Research Center (EXPEC ARC), evaluates the foam quality and texture during one of the foam rheology experiments.

On the Cover

Different types of surfactants were used to generate foam. Experiments were designed and conducted in a high-pressure, high temperature flow loop instrument to identify the optimum surfactant concentration and liquid/liquid ratio that can produce high quality foam and increase the supercritical carbon dioxide viscosity. During the experiment, foam characteristics were analyzed through a visual cell in terms of bubble size distribution utilizing the viewing cell.

MORE SAUDI ARAMCO JOURNAL OF TECHNOLOGY ARTICLES AVAILABLE ON THE INTERNET.

Additional articles that were submitted for publication in the *Saudi Aramco Journal of Technology* are being made available online. You can read them at this link on the Saudi Aramco Internet Website: www.saudiaramco.com/jot

The *Saudi Aramco Journal of Technology* is published quarterly by the Saudi Arabian Oil Company, Dhahran, Saudi Arabia, to provide the company's scientific and engineering communities a forum for the exchange of ideas through the presentation of technical information aimed at advancing knowledge in the hydrocarbon industry.

Complete issues of the Journal in PDF format are available on the Internet at:
http://www.saudiaramco.com
(click on "publications").

SUBSCRIPTIONS

Send individual subscription orders, address changes (see page 73) and related questions to:

Saudi Aramco Public Relations
Department
JOT Distribution
Box 5000
Dhahran 31311, Saudi Arabia
Website: www.saudiaramco.com/jot

CONTRIBUTIONS

Relevant articles are welcome. Submission guidelines are printed on the last page. Please address all manuscript and editorial correspondence to:

EDITOR

William E. Bradshaw
The *Saudi Aramco Journal of Technology*
C-11B, Room AN-1080
North Admin Building #175
Dhahran 31311, KSA
Tel: +966-013-876-0498
E-mail: william.bradshaw.1@aramco.com.sa

Unsolicited articles will be returned only when accompanied by a self-addressed envelope.

PRODUCTION COORDINATION

Richard E. Doughty

DESIGN

Graphic Engine Design Studio,
Austin, Texas, U.S.A.

ISSN 1319-2388.

The *Saudi Aramco Journal of Technology* gratefully acknowledges the assistance, contribution and cooperation of numerous operating organizations throughout the company.

أرامكو السعودية
saudi aramco

Fall 2017

THE SAUDI ARAMCO JOURNAL OF TECHNOLOGY
A quarterly publication of the Saudi Arabian Oil Company

Saudi Aramco Journal of Technology

Contents

Optimizing a Stimulation Design Using Hydrajet Fracturing with Coiled Tubing in a Saudi Arabia Gas Well

Muhammad H. Al-Buali, Ahmad N. Al-Duaij, Bruno Hardegger, Muhammad G. Bastisya and Faisal Khan

ABSTRACT

Achieving a successful evaluation and development program in a tight gas-bearing formation requires considerable analysis, not to mention optimization, to help ensure a profitable income. When problems arise and impact the performance of the well during completion, the risks associated with well intervention significantly increase. These problems sometimes prevent a hydraulic fracturing treatment from being performed. In a situation where hydraulic fracturing treatment is no longer feasible, an optimized stimulation design is needed to guarantee commercial gas production from the well while staying within current completion constraints and the allocated budget.

When this situation arose and an economical yet effective stimulation solution was needed, the hydrajet fracturing process, a stimulation technique with a proven success rate in onshore applications, was implemented. To increase the treatment efficiency, a novel acid-soluble abrasive material was used to create the perforations that connect the reservoir to the wellbore, which helped avoid the need for sand clean out time and for the use of additional chemicals. The hydrajet fracturing was followed by a pinpoint acid stimulation to unlock the hydrocarbons in a low-pressure area of the reservoir.

The post-treatment results were very promising: The gas rate achieved was approximately double the rate expected by using a conventional bullhead acid fracturing treatment. This has demonstrated the value of hydrajet fracturing to the industry.

This article not only discusses the results achieved using the hydrajet fracturing technique, compared to wells completed and evaluated with different completion schemes, but also presents a best practice for using the method to stimulate a well. The success of this operation resulted in the introduction of an alternative approach to completing a well where hydraulic fracturing is not possible, and achieving success relatively faster and more cost effectively.

INTRODUCTION

The Ghawar oil and gas field is by far the largest conventional oil and gas field in the world. It began production in 1951, and the reservoir comprises sandstones and carbonate formations ranging from the highly permeable formation “Y” to tight spots in formation “Z.” Thousands of vertical and horizontal wells have been drilled in both the carbonate and sandstone formations. Several carbonate gas wells have a low permeability profile, and some are characterized by low reservoir pressure.

To maximize gas production from these formations and to reduce the skin factor near the wellbore, it is essential to develop deep penetrating stimulation treatments to provide the longest, cleanest and most permeable channel possible for the gas and condensate to flow into the wellbore. To enable these stimulation treatments, most wells are completed either with ball-drop multistage fracturing completions or as cased hole with cemented liners followed by plug and perf acid fracturing treatments.

This particular well was designed to be completed with a plug and perf acid fracturing operation, so a 4½”, 13.5 lb/ft liner was set and cemented in place, Fig. 1. Subsequent drilling in the horizontal build section resulted in 52.99° of dogleg severity in the 4½” section, thereby making it impossible to carry out the plug and perf operation with wireline — the maximum length of a bottom-hole assembly (BHA) that can pass through this dogleg does not allow for the use of conventional guns.

Under these conditions, rather than sidetracking the well, efforts were made to identify a solution that would be both feasible and economically viable. A state-of-the-art perforating and stimulating technique was engineered. As several sets of perforations were essential to cover most of the good quality pay zone, conservative abrasive perforating was not considered a workable solution because of the time it would take, the solids utilized and the large fluid volumes required to clean all of the sand from the wellbore after the operation. Yet, abrasive perforations generate the best connectivity from the wellbore to the formation. Therefore, an innovative solution was developed to provide the best option for achieving deep acid penetration, while taking into account the low pressures in the wellbore, and to increase gas productivity without placing the wellbore completion at risk.

This article explains the design principle of the intervention, the tests performed before the operation and a brief review of the results of the operation.

WELL CHALLENGE AND PRELIMINARY DESIGN

To determine the best possible way to design the perforation and stimulation treatment within the constraints posed by the wellbore described above, a comprehensive analysis of reservoir and well data was performed. The porosity, permeability and stresses along the pay zone were reviewed through an evaluation of the open hole logs to generate a simulation model for use in deciding how the treatment was to be placed and designed.

From all this data, it was concluded that a total of four clusters were needed with five perforating stages/stops per cluster. It was also necessary to optimize the amount of the chemicals and time that the operation would require to avoid exceeding the budgeted cost while preserving maximum efficiency and treatment results. It was decided to use coiled tubing (CT) after every abrasive jetting stage in each cluster to force a hydrajet-assisted acid fracture. Each abrasive jetting perforation stage would be followed by pumping 2,100 gallons of high concentration acid — 20%, which would be followed by a relative permeability modifier-based diverting agent. This relative permeability modifier-based diverting agent was used to complement the influence of the dynamic diversion and help ensure the placement of treatment only in the stage being hydrajetted with abrasive material and not the previous ones.

PERFORATING TECHNIQUE BACKGROUND

Abrasive perforating techniques have roots going as far back as the 1950s. At that time, the objective of the abrasive perforating was to provide an alternative to conventional perforating, one that would create channels to connect the formation to the wellbore without causing any perforation-induced skin in the perforation tunnel itself, while also meeting the constraints imposed by the wellbore geometry. The conventional perforating method was associated with the creation of a crushed section around the perforated channel, thereby resulting in a damaged zone filled with debris[1]. Also, wellbore constraints often meant many runs were needed to perforate the single stage with conventional guns.

In earlier times, the abrasive perforating technique required a relatively long operational time to complete the treatment, which made it impractical for common usage. Given these limitations, further research was abandoned, and the technique was left unattended until several decades later. In the last decade, with additional research and more advanced tools, abrasive jetting has been identified as having several advantages, predominantly when it comes to very tight formations. This advanced technique significantly decreases the breakdown pressures and allows fracture treatments to be performed using less horsepower. Because of these advantages, abrasive jetting today significantly supersedes, in most of the cases, the performance exhibited by conventional perforating guns. These advantages also include cost savings and the elimination of logistical challenges related to the transportation of explosives[2-4].

Abrasive jetting creates a larger diameter hole as compared to conventional perforating guns, and the ability to reduce the near wellbore damage by reducing the tortuosity that results from the smaller diameter holes created by

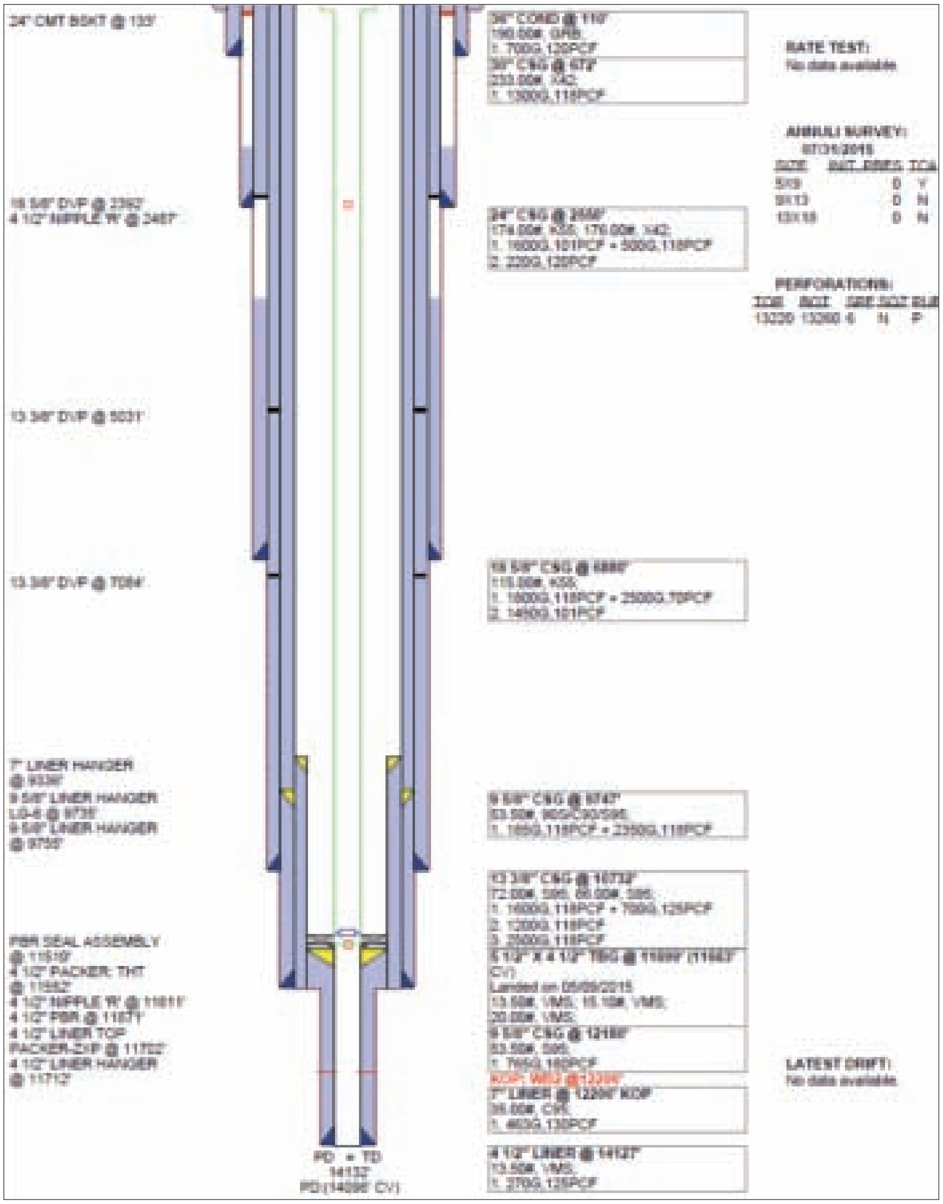

Fig. 1. Well schematic.

conventional perforating techniques is one of the most crucial advantages offered by the abrasive jetting technique in hydraulic fracturing and acid stimulation operations. Near wellbore tortuosity is an important rock characteristic, and its presence often restricts both hydrocarbon flow from the formation to the wellbore and fluid injection into the formation during hydraulic fracturing and acid stimulation treatments. Abrasive hydrajetting has another significant advantage over perforating guns in that it eliminates the formation damage caused by the shaped charges when they pierce the liner and the formation, which creates an area of crushed debris that in many instances plugs some or most of the perforated tunnels. The channels/slots created during the hydrajetting perforations are not plugged because any debris generated during the hydrajetting operation is removed with the abrasive slurry used to break the formation[5].

PERFORATING TECHNIQUE DESIGN AND YARD TESTING

As mentioned earlier, significant time is required to perform conventional abrasive perforations, particularly because the technique involves at least one additional CT run for sand clean out. So a different approach was devised to minimize the operational time needed to perform the abrasive perforations and to be as efficient as possible with the fluids that would be pumped, all without compromising the end results. The team sourced out a newly developed acid-soluble abrasive material, which created the same quality of perforations as did the conventional sand but did not require a clean out run since the acid from the stimulation would dissolve the abrasive material. This saved an additional CT run, ~350 barrels (bbl) of water and 100 bbl of linear gel, in addition to eliminating two CT operational days.

To test the hardness of the acid-soluble abrasive material, several yard tests were conducted to determine if the material had the same abrasive characteristics as common 20/40-mesh or 100-mesh sand. The time it required to penetrate the cement and steel was recorded and compared with the time when using common sand. It was necessary to establish a benchmark with this abrasive material to determine if additional penetration time and more fluid resources were required to obtain the same penetration as that achieved by the common sand. This was particularly essential since conventional silica sand has a Mohs hardness of approximately 6.7, while the acid-soluble abrasive material has a Mohs value ranging from 4.5 to 4.7, which meant it was approximately 33% less abrasive.

Several tests were performed. A control test with 20/40-mesh sand was run first, and then the same test setup was prepared to pump the acid-soluble abrasive material using the same configuration of the jetting tool and the same pumping rates. Conventional sand cut the pipe and penetrated the cement completely in 3.3 minutes of pumping time with the abrasive slurry, while the acid-soluble material achieved the same results in 4.8 minutes. It also eventually cracked the cement annulus, Fig. 2. These tests provided a better understanding of the additional pumping time, and therefore, the different amount of fluids required to create a channel of a specific length with the new acid-soluble product compared to the conventional sand.

Once the tests were completed, the design of the operation began. An optimized design was required so the volumes of fluids and abrasive materials could be controlled and costs

Fig. 2. Cracked cement annulus after acid-soluble test (left), and perforation hole diameter on the 6.625" casing (right).

Perforating Recommendation		Nozzle/Jet Calculations	
OD of Hydrajet Tool	3.06"	Nozzle Size	3/16
Casing Size	4.5"	Number of Nozzles	4
Grade	N-80	Cv	0.8
Wt	13.5	Flow Rate Total	210 gpm
ID of Casing	3.920"	Flow Rate Total	5.0 bpm
Drift Diameter	3.795"	Base Fluid Density	8.34 ppg
Pipe Wall	0.290	Sand lb per gal of Base Fluid	1 ppg
*Desired Penetration Depth into Formation	4.7"	Specific Volume of Sand	0.0456 gal/lb
Standoff Assume Centralized	0.430"	Flow Rate each Nozzle	52.5 gpm
Sand Pump Time to Penetrate Steel	0.37 min	Pressure Drop each Nozzle	4,190 psi
*Recommended Pump Time of the 1 ppg Stage to Cut Single Perforations (Berea Sand)	9.0 min	Nozzle Exit Velocity	608 ft/sec
		Perf Diameter from Jetted Hole	0.69"

Fig. 3. Hydrajetting calculations for conventional 20/40-mesh sand.

could be maintained at a reasonable level. Several perforations were needed if the best portion of the pay zone were to be stimulated. After it was determined from the logs which spots offered the best porosity and permeability characteristics, it was decided to complete a total of four perforation clusters with five stages per each cluster and four holes in each stage, equaling a total of 80 perforations. During the test, it was determined that the pumping time to achieve a similar effect would be 45% longer while using the acid-soluble material as compared to using conventional sand. After using the spreadsheet to calculate the time necessary to penetrate 4.7" into the formation with conventional 20/40-mesh sand, Table 1, it was decided to increase the expected time to 13 minutes for the acid-soluble material — approximately 45% additional time — for operational ease.

STIMULATION OPERATION DESIGN

The two main criteria of this stimulation technique were that it had to be deployed with the maximum wellhead pressure (WHP) limited to 6,000 psi and it had to provide deep acid penetration. The reason for seeking a deep penetrating treatment was to achieve the primary goal: The creation of a combination, or at least a network, of multiple fractures and/or extensive wormholes[6]. The hydrajet-assisted acid fracturing approach met both criteria, leveraging the Bernoulli principle to achieve dynamic diversion and deep penetration by means of CT. The hydrajet-assisted acid injection takes advantage of the dynamics of fluid moving at a very high velocity to direct flow to a specific entry point in front of the nozzle[1, 7].

The dynamic diversion is achieved by generating a low-pressure zone in the CT wellbore annulus immediately in front of the jetting tool, which draws fluid from the annulus into the jetted cavity. Upon entering the cavity, the commingled fluids hit the wall of the cavity, where they transform their high kinetic energy into potential energy since the pressure at the wall of the cavity is much higher than at the entrance. This pressure at a foremost boundary of the cavity — stagnation pressure — can exceed the annulus pressure by more than 3,000 psi, Fig. 3, thereby exceeding the fracture initiation pressure at this point. Because of this, a fracture will be initiated at the point where the nozzle is stationed.

The hydrajetting and stimulation stage design was developed, and a pumping schedule was optimized to attain the highest efficiency possible within practical feasible pumping rates. To determine whether the acid-soluble abrasive material could connect the formation to the wellbore as anticipated, the first two stages were planned as a diagnostic action. If the first stage had not been successful in connecting the reservoir to the wellbore, the CT would have been moved to the next stage. If, after hydrajetting, the second stage did not connect the reservoir to the wellbore, then hydrajetting alone would be performed for the rest of the stages and the acid stimulation would be done through bullheading. If successful injectivity was observed, then the rest of the stages would be completed as designed, with the stimulation performed immediately after each hydrajet stage. The reason for hydrajetting and performing the stimulation in sequence is that it is necessary to locate the nozzle at the same point where the perforation is created to achieve full dynamic divergence and for the hydrajet acid fracturing effect to occur. A spacer pill of linear gel was pumped to increase the pH of the environment in the pipe to prevent premature dissolution of the abrasive material while traversing the treating iron and CT.

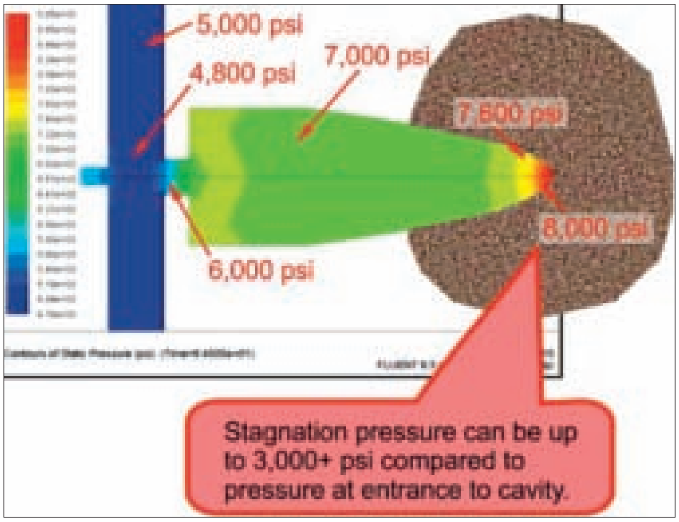

Fig. 3. Stagnation pressure exceeding the fracture initiation pressure.

Table 2 shows the pumping schedule for the abrasive perforating operation. The spacer was to be followed by 50 bbl of 20% hydrochloric (HCl) acid with a gelling agent for deeper penetration and friction reduction. These steps would be repeated until the entire four clusters of the operation were completed.

OPERATIONAL REPORT

The equipment, chemicals and personnel were mobilized to the location, and the equipment was rigged up per Saudi Aramco's requirements. The first run was a drifting and casing collar locater (CCL) run performed with a memory gauge to achieve precise depth correlation for the perforating and stimulating stages. The CCL run was completed successfully, and the depth offset was corrected with the flags made on the pipe. Another CT run was made with the perforating/jetting tool to perform the hydrajetting and stimulation as per the design. The CT depth was corrected and the CT was stationed at the first stage's corrected depth — again as per the design.

As noted above, the plan was to perform the first stage and then do an injectivity test to verify the effectiveness of the abrasive material. Due to the initial pump pressure settings, the first stage could not be executed in the first attempt as designed, and the injectivity test showed that the reservoir was not connected to the wellbore. The pump settings were changed, and the first stage was repeated successfully with a

				CT Pumping Status					
								Status of CT-Tbf Annulus	
Fracture Port No./Perf. Depth (ft)	Stage Description	Fluid Type	Volume (gal)	Volume (bbl)	Avg. CT Rate (bbl/min)	Necessary CT Pressure (psi)	Time (min)	Choke Status	Expected WHP (psi)
	Preflush	30-lbm liner gel	3,360	80	5	6,300	16	Open	500 to 800
Perf. No. 1 CT depth 13,260	Hydrajetting	Acid-soluble abrasive Slurry	2,520	60	5	6,500	12	Open	500 to 800
	Spacer	30-lbm liner gel	840	20	5	6,300	4	Open	500 to 800
	Acid Squeeze	20% HCl acid	2,100	50	5	6,300	10	Close	500 to 800
	Diversion	Diversion gel	504	12	4	6,300	3	Close	500 to 800

Table 2. Hydrajetting and stimulation pumping schedule per stage

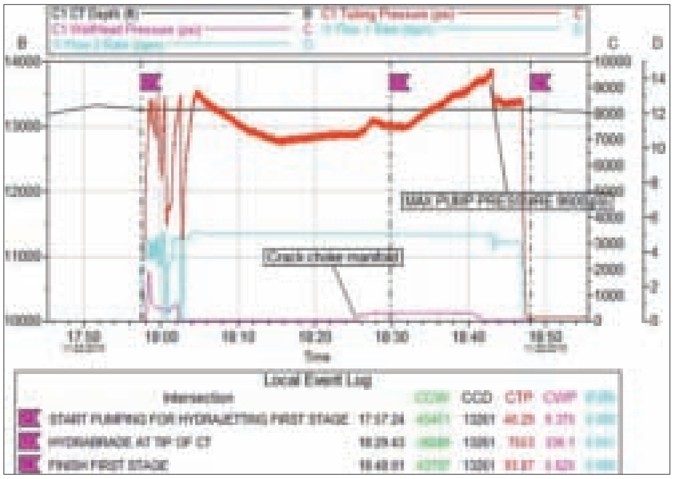

Fig. 4. First stage of hydrajetting.

maximum pumping rate of 5 barrels per minute (bpm) and at a maximum pumping pressure of 9,600 psi, Fig. 5. The BHA used during the operation is shown in Table 3.

The injectivity test after the second attempt at the first hydrajetting stage showed a steady pressure drop, indicating that the reservoir had been successfully connected with the wellbore. Based on the injectivity test results, 50 bbl of 20% HCl acid was squeezed into the formation with CT at the same depth so as to increase injectivity in case the face of the formation had been plugged. The injectivity test following the acid squeeze showed good results, Fig. 5. Based on the injectivity test results, it was decided to perform the rest of the stages as planned.

Proceeding as per the initial design, the CT was pulled out to the second stage's depth and 65 bbl of abrasive slurry was pumped, followed by 20 bbl of spacer, then 50 bbl of 20% HCl acid, then 12 bbl of gel as a diversion; this comprised the main treatment to perforate the casing. Maximum CT pressure during hydrajetting of the second stage was 9,500 psi at 4.9 bpm. When the acid was at the tip of the CT, the choke manifold was closed to squeeze the acid into the formation while pumping it at a rate of 4.8 bpm; maximum WHP reached to 3,500 psi during the acid squeeze.

After the second stage, the pump rate was dropped to 2 bpm to move the CT to the third stage at 13,240 ft. All three stages for the first cluster were pumped as designed, and after each hydrajetting stage, 50 bbl of 20% HCl acid was pumped to squeeze the acid into the formation, Figs. 6 and 7. An increase in the pumping pressure was observed while performing the hydrajetting operation with the acid-soluble abrasive slurry. This corresponded to the additional frictional pressure in the reel when it was being loaded with the higher density abrasive material-laden fluid. The pressure then dropped as the slurry entered into the section of CT in the well. The pumping pressure increased again when the acid entered the reel and ultimately hit the formation. It then dropped once the acid dissolved the near wellbore damage in the face of the perforation and reduced the skin.

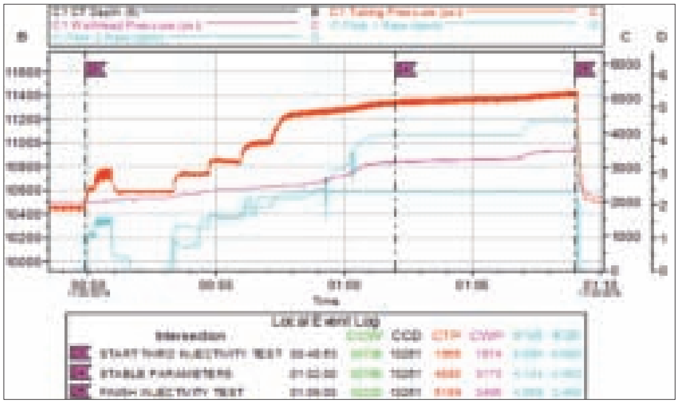

Fig. 5. Injectivity test after the first stage of hydrajetting and acid squeeze.

Item	Tool Description	Tool Connections	Tool O/D (in.)	Tool I/D (in.)	T-Length (in.)	Drop Ball
1	CT Connector for 2⅜" CT	2.388" PAC Pin			5	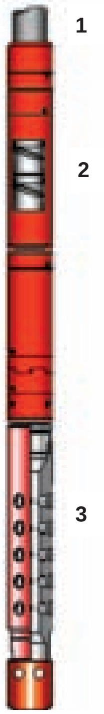
2	MHA	2.388" PAC Pin 2.388" PAC Box			33	
3	Hydrajet Tool String Tool	2.388" PAC Box			40	
	Maximum Tool String OD:		0			
	Minimum Tool String ID:			0		
	Total Length of BHA in Feet:				6.50	

Table 3. Hydrajetting BHA.

Once all the stages for the first cluster were done, the CT was run in hole to total depth and performed one bottoms up run to clean any undissolved abrasive material. While the CT performed the bottoms up run, the WHP increased to 5,000 psi and high hydrogen sulfide was detected at the surface. Once the bottoms up run was completed, the decision was made to pull out the CT to monitor the WHP and flow back the well. Later, after the flow back test results came in, it was decided to conclude the operation without perforating the rest of three clusters because the well was flowing at more than twice the flow rate expected from the original plug and perf operation design and also at substantially higher WHP. So, the job objective was achieved from only one set of the perforations.

CONCLUSIONS

The well was originally planned for a plug and perf job, but due to high dogleg severity, it was decided to complete the well with abrasive hydrajetting and hydrajet-assisted acid stimulation. Four clusters consisting of five stages were planned to be completed with abrasive hydrajetting. When twice the desired

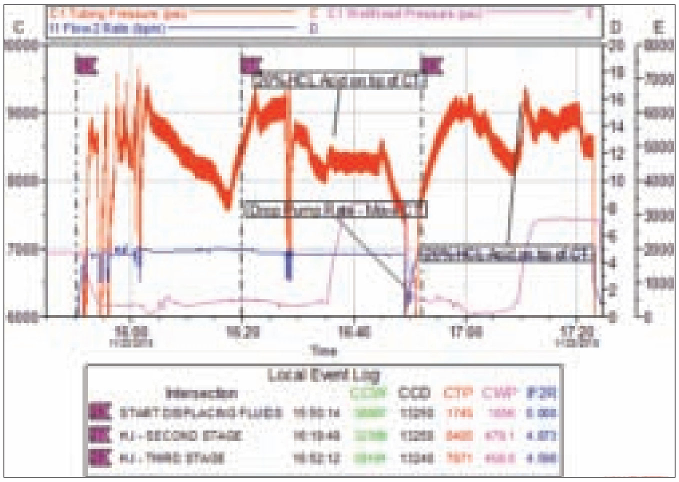

Fig. 6. Abrasive jetting and hydrajetting-assisted acid stimulation for the second and third stage (one of four clusters).

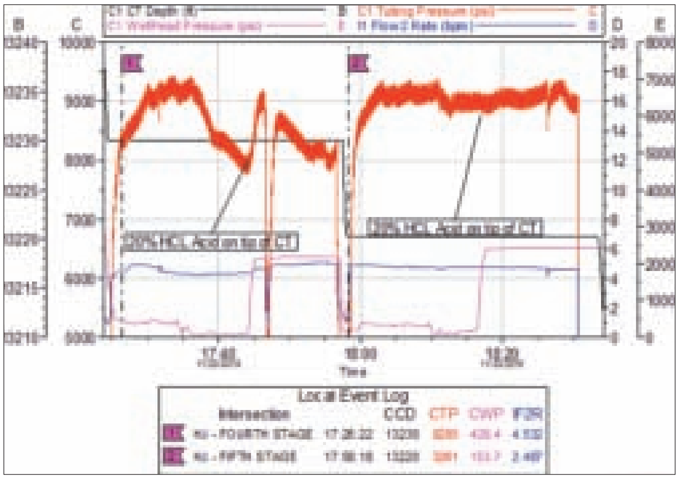

Fig. 7. Abrasive jetting and hydrajetting-assisted acid stimulation for the fourth and fifth stage (one of four clusters).

gas rates were achieved after completing only one cluster, the well was flowed back for constant gas rate measurement.

After a constant gas rate was obtained, the CT was demobilized from the location, and the flow back continued to clean up the treatment. Eventually, the well stabilized at ~20 million standard cubic ft per day (MMscfd) from a single cluster, which is an outstanding figure; the expected flow rate had been about 10 MMscfd from four clusters. Currently, the treatment technique is being evaluated for possible implementation on additional candidates, particularly those with low reservoir pressure, to perform similar stimulation treatments to help enhance productivity.

The operation was performed successfully, and the entire treatment was conducted as planned. The acid-soluble abrasive material was deemed a total success, given that the perforations were completed as planned and allowed for the full acid treatment to be pumped. The placement of the perforations with respect to the target pay zone and the subsequent acid treatment paid great dividends. Again, the final flow back results came in at least twice as much as expected by the Reservoir Engineering Department and from a single set of perforation clusters.

ACKNOWLEDGMENTS

The authors would like to thank the management of Saudi Aramco and Halliburton for their support and permission to publish this article.

This article was presented at the Middle East Oil and Gas Show and Conference, Manama, Kingdom of Bahrain, March 6-9, 2017.

REFERENCES

1. Rees, M.J., Khallad, A., Cheng, A., Rispler, K.A., et al.: "Successful Hydrajet Acid Squeeze and Multifracture Acid Treatments in Horizontal Open Holes Using Dynamic Diversion Process and Downhole Mixing," SPE paper 71692, presented at the SPE Annual Technology Conference and Exhibition, New Orleans, Louisiana, September 30-October 3, 2001.
2. Solares, J.R., Amorocho, R., Bartko, K.M., Leising, L., et al.: "Successful Field Trial of a Novel Abrasive Jetting Tool Designed to Create Large Diameter Long Cavities in the Formation to Enhance Stimulation Treatments," SPE paper 121794, presented at the SPE/ICoTA Coiled Tubing and Well Intervention Conference and Exhibition, The Woodlands, Texas, March 31-April 1, 2009.
3. Nunez Garcia, W., Solares, R., Leal Jauregui, J.A., Duarte, J.E., et al.: "First Successful Low Cost Abrasive Perforation with Wireless Assisted Coiled Tubing in Deviated High-Pressure, High Temperature Gas Well," SPE paper 136906, presented at the Abu Dhabi International Petroleum Exhibition and Conference, Abu Dhabi, UAE, November 1-4, 2010.
4. McDaniel, B.W., East, L.E. and Surjaatmadja, J.B.: "Use of Hydrajet Perforating to Improve Fracturing Success Sees Global Expansion," SPE paper 114695, presented at the CIPC/SPE Gas Technology Symposium Joint Conference, Calgary, Alberta, Canada, June 16-19, 2008.
5. Smith, C.G., Khiat, S. and Al-Badraoui, D.: "An Effective Technique to Reduce Bottom-hole Friction Pressure during Hydraulic Fracturing Treatments," SPE paper 112422, presented at the SPE International Symposium and Exhibition on Formation Damage Control, Lafayette, Louisiana, February 13-15, 2008.
6. Alzaid, M.R., Al-Ghazal, M.A., Al-Driweesh, S., Al-Ghurairi, F., et al.: "Dual Lateral Open Hole Coiled Tubing Acid Stimulation in Deep HPHT Sour Gas Producer Wells — Field Experience and Lessons Learned from the Ghawar Field," SPE paper 164326, presented at the SPE Middle East Oil and Gas Show and Conference, Manama, Bahrain, March 10-13, 2013.
7. Eberhard, M.J., Surjaatmadja, J.B., Peterson, E.M., Lockman, R.R., et al.: "Precise Fracture Initiation Using Dynamic Fluid Movement Allows Effective Fracture Development in Deviated Wellbores," SPE paper 62889, presented at the SPE Annual Technical Conference and Exhibition, Dallas, Texas, October 1-4, 2000.

BIOGRAPHIES

Muhammad H. Al-Buali is now a Chemical Engineer after starting his career working as a Production Engineer for oil, water and gas wells. Since 2010, he has worked in the Gas Well Completion Operation Department, executing and supervising all rigless activities related to fracturing and stimulation, well intervention and well testing on Saudi Aramco's onshore gas wells. Muhammad is currently a Division Head in the Southern Area Gas Well Completion Operations Department.

He is a member of the Society of Petroleum Engineers (SPE) and has participated in many SPE events as an author, presenter and delegate.

In 2002, Muhammad received his B.S. degree in Applied Chemical Engineering from King Fahd University of Petroleum and Minerals (KFUPM), Dhahran, Saudi Arabia.

Ahmad N. Al-Duaij joined Saudi Aramco in 2011 as a Technical Support Engineer, working in the Well Completion Engineering Support Unit of the Southern Area Well Completion Operations Department supporting gas well completion operations. He completed a one-year assignment working as a Production Engineer with the Ghawar Gas Production Engineering team handling the Ghawar gas wells, developing completion programs that include, but are not limited to, perforation programs, proppant fracturing and acid fracturing programs, among others.

Following this assignment, Ahmad was sent to Houston to work with Halliburton in their Unconventional Gas Resources Program for one year. After successfully completing this assignment, he returned to Saudi Arabia to work as an Operations Foreman executing critical rigless operations, starting from the perforation stage and progressing to the fracturing stage, utilizing state-of-the-art technologies.

Currently, Ahmad is working as an Operations Foreman for the Ghawar Gas Well Completion Engineering Support Unit.

He received his B.S. degree in Petroleum Engineering from King Fahd University of Petroleum and Minerals (KFUPM), Dhahran, Saudi Arabia.

Bruno Hardegger leads the Production Solutions Operations as Country Manager in Saudi Arabia for Halliburton, responsible for designing jobs utilizing state-of-the-art technologies, superlative safety and flawless execution that maximizes the customer asset's value through the most economic, efficient and time effective solutions. He has 27 years of diversified experience in oil field operations and management.

Bruno develops and maintains customer relations for the purpose of assessing local needs, service quality, monitors upcoming challenges and implementation of new technologies to meet the ever increasing demands and challenges encountered during the life of the well.

He started his career with Conoco in 1990 in Europe, working in different field positions, making his way up to Lead Supervisor before he joined Halliburton in 2004 in Canada. Bruno worked in various positions in Canada and at other international assignments before going to work for Halliburton Saudi in 2009.

In 1981, he received a Diploma in Oil Heating Systems from BZ Rorschach, Rorschach, Switzerland.

Muhammad G. Bastisya started his career with Halliburton in 2009 in Indonesia, supporting multiple national/multinational oil companies in coiled tubing (CT) job design and operations. His experience includes knowledge in fishing and milling operations, stimulation and hydrajetting operations, descaling, water shut off and other CT operations.

Muhammad joined Halliburton Saudi Arabia in 2013 as a Senior Engineer supporting critical operations related to CT and stimulation. He has been involved in designing multiple CT stimulation projects in the Southern Area Well Completions Operations Department.

In 2009, Muhammad received his B.S. degree in Petroleum Engineering from the Institut Teknologi Bandung, Bandung, Indonesia. Currently, he is completing his M.S. degree program at the Delft University of Technology, Delft, Netherlands.

Faisal Khan is now a Principal Account Representative with Halliburton Production Solutions where he supports Saudi Aramco in designing coiled tubing (CT) and stimulation operations in the Ghawar Gas Production Engineering Department. Faisal joined Halliburton in 2013 as a Senior Technical Engineer, executing critical well operations, including but not limited to hydrajetting, surgi-squeeze, multilateral stimulations, water shut off, descaling, milling, perforating, and real time distributed temperature surveys, and other CT operations.

He started his career with ENI Pakistan as a Completions and Stimulations Engineer in 2009. Faisal was involved in the designing of stimulation operations and completion designs in the high-pressure, high temperature wells.

He received his B.S. degree in Petroleum Engineering from the University of Engineering and Technology, Lahore, Pakistan.

A Laboratory Study of In-depth Gel Treatment to Improve Oil Recovery

Dr. Jinxun Wang, Dr. Ammar J. Alshehri, Dr. Abdulkareem M. AlSofi and Abdullah M. Al-Boqmi

ABSTRACT

The extreme heterogeneity of carbonate reservoirs, in the form of fracture corridors and super-permeability thief zones, challenges the efficient sweep of oil in both secondary and tertiary recovery operations. In such reservoirs, conformance control is crucial to ensure injected water and any enhanced oil recovery (EOR) chemicals optimally contact the remaining oil with minimal throughput. Gel-based conformance control has been successfully applied in both sandstone and carbonate reservoirs. In-depth conformance control in high temperature reservoirs is still a challenge, though, due to severe gel syneresis and the associated significant reduction in gelation time.

In this work, a laboratory study was conducted on a polymer/chromium gel system for a high temperature carbonate reservoir to evaluate the gelant formulation's potential for diversion and recovery improvement. We performed four oil displacement experiments on carbonate core samples to demonstrate oil recovery improvement by the gel treatment. In these tests, the gel solution was injected into specially prepared heterogeneous carbonate composite core samples in which different configurations of high permeability channels had been created.

Gel treatment was conducted after waterflooding and was followed by chase waterflooding while monitoring the oil production during both floods. Oil recovery improvement using gel treatment varied by the type of channel in the sample: 18% of original oil in core (OOIC) was recovered in the composite core with high permeability channels extending midway through the composite, while 38% of OOIC was recovered in the composite core with channels extending all the way through the composite. This indicates that the high permeability channels were effectively blocked and the bypassed oil was successfully mobilized after gel treatment.

This laboratory study provides more insight into the mechanisms of oil recovery improvement using gel treatment. Moreover, it clearly demonstrates the potential of in-depth gel systems for improving oil recovery in heterogeneous reservoir applications at high temperature.

INTRODUCTION

Fractures or high permeability zones are often observed in carbonate reservoirs. During waterflooding and enhanced oil recovery (EOR), this causes channeling of injected fluids toward producers and consequently poor sweep of the oil residing in the matrix. Conformance control is therefore crucial in such heterogeneous reservoirs during these processes, and the poor performance of many earlier EOR projects was attributed to conformance problems[1]. Conformance control ensures EOR chemicals efficiently contact the remaining oil with minimal throughput. Different types of conformance control methods are reviewed by Sydansk and Romero-Zerón (2011)[2]. Among chemical conformance methods, polymer gels are widely used due to their relatively low cost and ease of application at well sites. When a gelant solution consisting of a water-soluble polymer and crosslinker(s) is injected, an elastic, solid-like gel system is formed after a certain time in response to the elevated reservoir temperature. This blocks the fractures or high permeability zones, so any subsequent injection water will be diverted to the unswept or less completely swept regions, leading to an improvement in sweep efficiency.

Many gel systems have been suggested[3-9] for use. Han et al. (2014)[10] reviews numerous in-depth, gel-based fluid diversion technologies, including weak gels, sequential injection for generating in situ gels, colloidal dispersion gels, microgels and preformed particle gels. The most commonly used polymers to form gels are polyacrylamides that can have various degrees of hydrolysis and various molecular weights. Polyacrylamides can be cross-linked by either metallic crosslinkers or organic crosslinkers. In the first case, gels can be formed through chemical bonding between the negatively charged carboxylate groups of the polymer and the multivalent cations of a metallic crosslinker such as trivalent chromium (Cr(III)). Sydansk and Southwell (1998)[1] review more than 12 years of experience in developing and applying the widely applied Cr(III) carboxylate/acrylamide polymer gel technology. In the second case, gels can be generated through covalent bonding between organic crosslinkers and the functional groups of the polymer[11-14].

The selection of a given gel formulation mainly depends on the specific conformance problem and reservoir conditions. For a successful field application, adequate gelation time is required to maintain the gelant in a solution state while it is pumped to the target treatment region. The polymer and crosslinker types and their concentrations, as well as the reservoir temperature, salinity and pH, all have influences on gelation time. Temperature has a significant impact: higher temperatures result in shorter gelation time. Although polymer gel technology has been widely used in both injectors and producers, most of the applications have been in moderate temperature reservoirs. Applying such technology in high temperature reservoirs remains a challenge.

In this work, a laboratory study was conducted on a polymer/chromium gel system for a high temperature carbonate reservoir based on our previous studies on this gel[15]. Oil displacement experiments were performed on carbonate core samples to demonstrate the potential of oil recovery improvement using this gel treatment. For these experiments, the gel solution was injected into specially prepared heterogeneous carbonate composite core samples in which different configurations of high permeability channels had been created.

EXPERIMENTS

Materials

Carbonate core samples were used in this study. A total of five 1½” diameter core plugs were prepared for the tests. Their ambient porosity and air permeability ranged from 18.7% to 28.2% and 706 millidarcies (md) to 957 md, respectively. Plug properties are listed in Table 1. Four sets of dual plug composite core samples were assembled for the coreflooding tests. Varied levels of heterogeneity were tested; the one homogeneous composite had no artificial heterogeneity, while the three remaining composites had different configurations of high permeability channels, including channels halfway through and all the way through.

Dead crude oil collected from a Middle Eastern carbonate reservoir was used to prepare the core samples for the coreflooding tests. The oil was filtrated through a 5 µm filter for test use. At room temperature, the density and viscosity were 0.8663 g/cm^3 and 12 centipoise (cP), respectively. At 95 °C, the density and viscosity were 0.8159 g/cm^3 and 2.78 cP, respectively. The brine used in this study was heavy water (D_2O) with 6,000 mg/L sodium chloride. D_2O was used in place of water to eliminate the protons of the aqueous phase and to focus further nuclear magnetic resonance studies[16] on oil displacement inside the cores.

A sulfonated polyacrylamide was used as the polymer in the gel system. It is a copolymer of acrylamide and acrylamide tert-butyl sulfonate with a sulfonation degree of about 25%. The molecular weight of the polymer was 12 million Daltons. The crosslinker used in this study was Cr(III), and its stock solution was prepared using Cr(III) acetate.

Gelation Time

The time when the gelant solution starts to form a gel is important for field applications. Adequate gelation time is required to place the gelant solution into the target treatment region. This is crucial for in-depth conformance, since the gelation time must be long enough to achieve deep placement. This is especially challenging for high temperature reservoirs. Bottle tests are often used to observe and rapidly assess the gelation time, but the observation criteria can be different for different researchers. Sydansk (1990)[17] first determines the gelation rate and gel strength by bottle tests, then proposes a code system from “A” to “J” to describe 10 different levels of gel strength based on visual observation. This present experiment followed the method described by Lockhart and Albonico (1994)[18] to estimate the gelation time. According to them, at the gelation point, the gelant will flow to the cap when the sample bottle is capped and inverted, but when it is uncapped and inverted, an elastic, tongue-shaped gelant will partially flow out, with the “tongue” several centimeters long. This roughly corresponds to the gel strength code of “D”[17] in the 1990 study, which is a moderately flowing gel. The solution can flow at this point, but its flowability is limited.

Bottle tests were conducted on different gelant solutions. The polymer and crosslinker stock solutions were prepared first. Then, gelant solutions with different concentrations of the polymer and crosslinker were prepared, and 10 ml of each solution was placed into a 20 ml glass bottle and sealed with a plastic cap. Each sample was put into an oven at 95 °C and then periodically removed to observe the gelant flowability by slightly tilting and inverting the bottle until a gelation time was determined.

Plug Sample	Length (cm)	Diameter (cm)	Ambient Porosity (%)	Ambient Air Permeability (md)	Grain Density (g/cm^3)
1	4.607	3.771	28.2	934	2.71
2	4.274	3.781	26.1	957	2.70
3	4.404	3.788	19.3	819	2.72
4	4.306	3.789	18.7	743	2.71
5	4.342	3.772	23.7	706	2.69

Table 1. Basic properties of the core plug samples

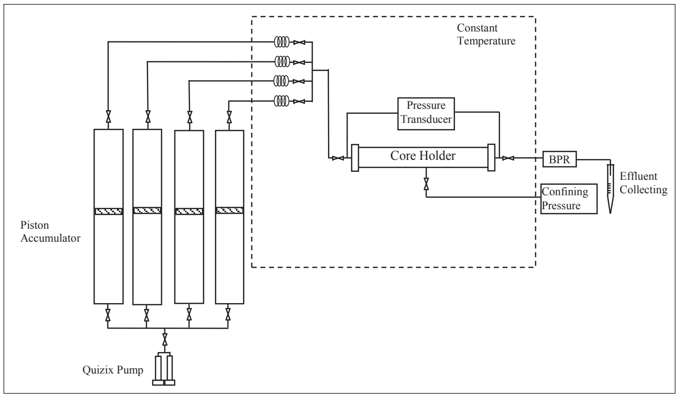

Fig. 1. Schematic diagram of the equipment used for the coreflooding test.

Coreflooding Study

Oil displacement tests were conducted using a coreflooding system; Fig. 1 shows the system schematic. The main components of the apparatus are a core holder, confining pressure system, back pressure regulator, instruments for pressure drop measurement and temperature control, and fluid injection and effluent collection systems. A hydrostatic core holder was horizontally mounted in the oven. Test fluids, including oil, injection water and gelant solution, were loaded into individual piston accumulators and were injected into the core plugs using a computer controlled Quizix pump. The pressure drop across the core sample was measured by digital differential pressure transducers and recorded through the computer data acquisition system. The back pressure was applied and controlled by the computer control systems.

Before coreflooding tests, the clean and dried plug samples were vacuum saturated with brine, and then initial water saturation was established by using a centrifuge method. The plug samples were then submerged in dead crude oil and aged for four weeks. For the test, each two-plug composite core sample was loaded into a core holder, and a confining pressure of 1,400 psi and back pressure of 200 psi were applied. The system was heated to 95 °C overnight to allow it to reach thermal equilibrium. The core sample was flushed with dead crude oil until the pressure drop stabilized before waterflooding, which was conducted by injecting brine at a constant flow rate of 0.5 ml/min until oil production was negligible. Gel treatment was then performed by injecting around 0.5 pore volumes (PVs) of gelant solution, composed of 4,000 mg/L of polymer, 100 mg/L of Cr(III) and 6,000 mg/L of sodium chloride (NaCl) in D_2O. With the gel slug in core, the sample was aged at reservoir conditions overnight. Waterflooding by brine was then resumed until oil production was negligible.

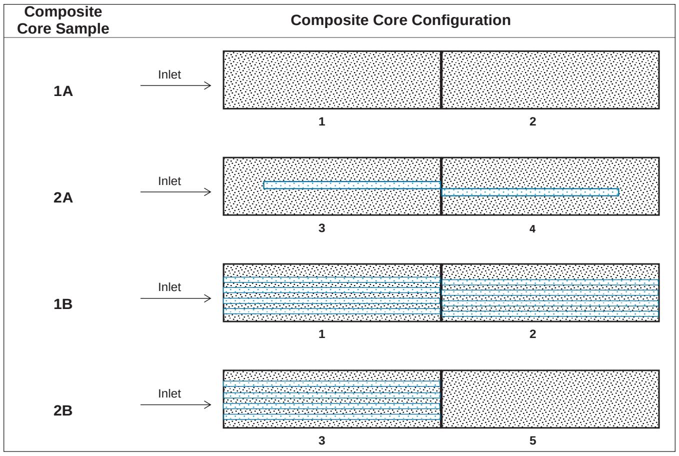

Fig. 2. Configurations of the composite core samples for coreflooding tests.

The gel treatment's potential for improving oil recovery was evaluated by conducting four coreflooding tests, just described, on core samples with varied heterogeneities. Dual plug composite core samples were used in two rounds of coreflooding tests, with two sets of samples in each round. Figure 2 presents the four dual plug composite core configurations used for the four coreflooding tests. Samples 1A and 2A were flooded in the first round, while Samples 1B and 2B were flooded in the second round. One homogeneous composite core sample (1A) and one heterogeneous composite core sample (2A) were used in the first round of tests. For the heterogeneous sample, small holes were drilled halfway through both plugs of the composite core to create a high permeability flow channel. The diameters of the small holes were 3.5 mm to 4 mm, around one-tenth of the core plug diameter, 3.81 cm. This heterogeneity was created after the oil permeability measurement. The composite core sample was then reloaded into the core holder and oil was flushed until pressure was stabilized.

Three of the four plugs in the first round of tests, Plugs 1, 2 and 3, Fig. 2, were reused to form the composite core samples for the second round of tests. The oil and salts in the plugs were fully cleaned away after the first round of coreflooding. Additional smaller holes, with a diameter of approximately 1 mm to 2 mm, were then drilled all the way through the three reused core plugs. As presented in Fig. 2, Sample 1B had channels all the way through both plugs. Sample 2B, which used one new undrilled plug, had channels all the way through the inlet plug only.

RESULTS AND DISCUSSIONS

Gelation Time

The gelant solution selected for the coreflooding studies was composed of 4,000 mg/L of polymer, 100 mg/L of Cr(III) and 6,000 mg/L of NaCl in D_2O. Based on bottle tests, the gelation time of the studied gelant solution at 95 °C is around 2 hours. It should be noted that the gel system used in this study was merely selected to have an appropriate gelation time for the coreflooding tests. For in-depth treatment of high temperature reservoirs, a much longer gelation time is required and a different gel system will be needed. Using a retardant agent to elongate the gelation time is one of the possible options to achieve a long enough gelation time for deep injection of the gel system.

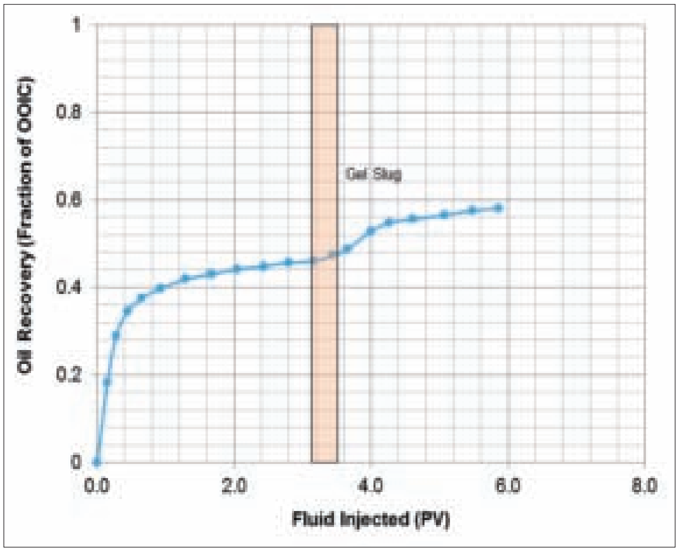

Fig. 3. Oil recovery curve of waterflooding and gel treatment on Sample 1A.

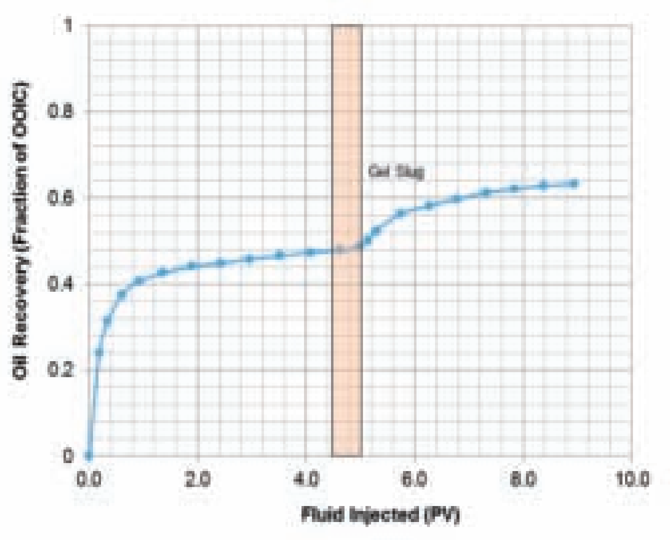

Fig. 4. Oil recovery curve of waterflooding and gel treatment on Sample 2A.

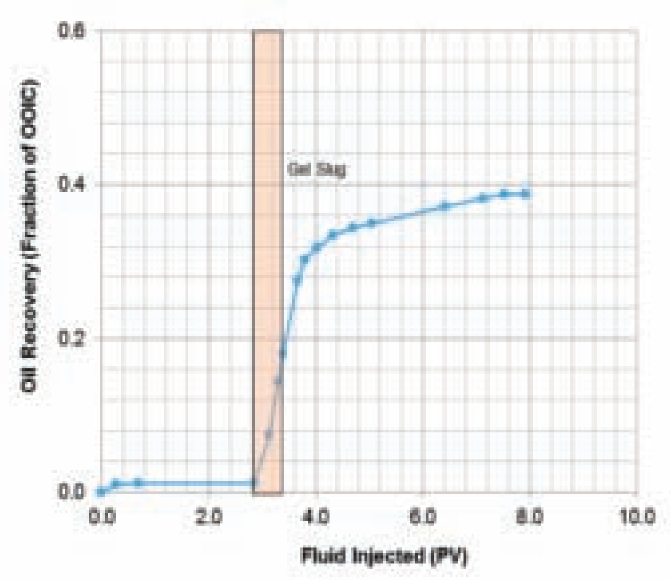

Fig. 5. Oil recovery curve of waterflooding and gel treatment on Sample 1B.

Oil Recovery Improvement by Gel Treatment

Figures 3 to 6 plot the oil recovery curves of the four coreflooding tests. Results show that initial waterflooding oil recovery ranged from 41.5% to 47.8% of original oil in core (OOIC) in all composites except for Sample 1B, with channels all the way through the composite core. The waterflooding oil recovery of Sample 1B was only 1.1% OOIC because the high permeability channels extended straight through the composite core.

The oil recovery improvement by gel treatment ranged from 12% to 37.6% OOIC. The highest incremental oil recovery of 37.6% OOIC was achieved in Sample 1B, where the initial waterflooding recovery had been extremely low as most of the oil was bypassed due to the extreme heterogeneity of this composite core with channels all the way through. Significant improvements, with oil recovery of 15.4% and 18.4% OOIC, were also obtained, respectively, in Sample 2A, with a channel halfway through both plugs, and Sample 2B, with channels all the way through the inlet plug only. Among the four tests, the lowest incremental oil recovery of 12% OOIC was obtained in the composite core without any artificial heterogeneity — Sample 1A.

These results indicate that gel treatment effectively blocked the high permeability channels in the heterogeneous core samples, leading to significant improvement in sweep efficiency. The incremental oil recovery following gel treatment also tended to be larger for the core sample with more severe heterogeneity.

The oil recovery data are summarized in Table 2. The incremental oil recovery is expressed in terms of OOIC, in terms of remaining oil in core (ROIC) and as a ratio to the waterflooding oil recovery. All of the incremental recovery data show the same trend. The largest incremental oil recovery was obtained from the most heterogeneous core sample, and the lowest incremental recovery was from the core without any artificial

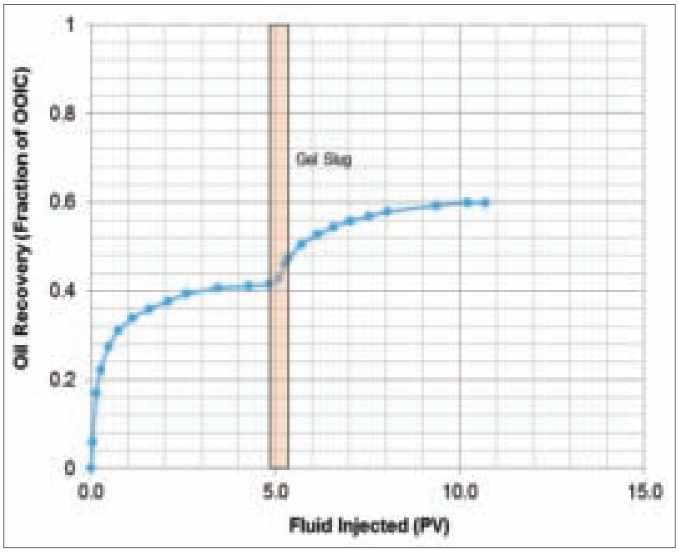

Fig. 6. Oil recovery curve of waterflooding and gel treatment on Sample 2B.

Composite Core Sample	Swi (%)	Recovery Process	Cumulative Oil Recovery (OOIC)	Incremental Oil Recovery			Remaining Oil Saturation
				(OOIC)	(ROIC)	(ORWF)*	
1A	18	Waterflooding	46%	—	—	—	44.2%
		Gel Treatment	58%	12%	22.2%	26%	34.3%
2A	22.9	Waterflooding	47.8%	—	—	—	40.3%
		Gel Treatment	63.2%	15.4%	29.5%	32%	28.4%
1B	20.3	Waterflooding	1.1%	—	—	—	78.8%
		Gel Treatment	38.7%	37.6%	38%	3.418%	48.9%
2B	22.7	Waterflooding	41.5%	—	—	—	45.2%
		Gel Treatment	59.9%	18.4%	31.5%	44%	31%
* ORWF: oil recovered normalized by waterflooding recovery.							

Table 2. Summary of oil recovery results by waterflooding and gel treatment

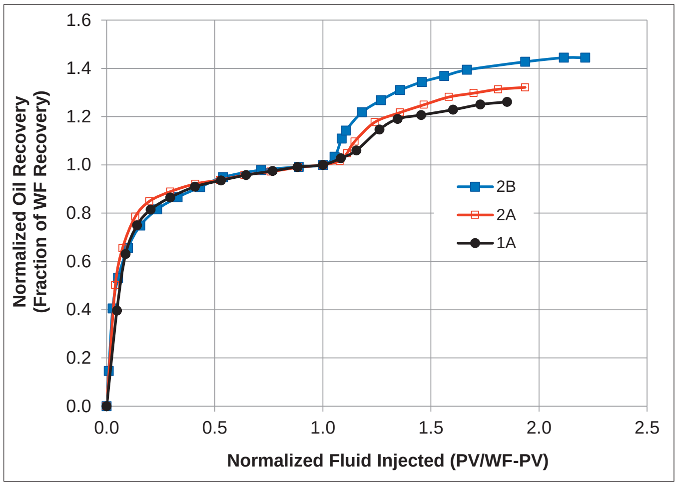

Fig. 7. Normalized oil recovery curves of waterflooding and gel treatment.

heterogeneity.

For further illustration, normalized oil recovery curves for three of the samples are plotted in Fig. 7. In this figure, the oil recovery was normalized based on waterflooding oil recovery, and the fluid injection (PV) was normalized based on the waterflooding injection period. Sample 1B, with extreme heterogeneity, was excluded because initial waterflooding oil recovery was so low. Figure 7 also clearly demonstrates that the realized improvement in recovery is directly correlated to the severity of heterogeneity. Moreover, the huge improvement observed in Sample 2B — with channels throughout — highlights the potential value of in-depth gel treatment in reservoirs with super-permeability thief zones. Subsequently, the effective placement of gel across such thief zones must be assured to achieve substantial oil recovery improvement.

CONCLUSIONS

A polymer gel consisting of polyacrylamide and Cr(III) was studied for application in projects to improve oil recovery in heterogeneous carbonate reservoirs at high temperature. Gelation time guided the selection of the gelant formulation for the coreflooding tests. A gelant solution composed of 4,000 mg/L of polymer, 100 mg/L of Cr(III) and 6,000 mg/L of NaCl in D_2O was selected. The gelant exhibited a gelation time of around 2 hours at 95 °C. This gelation time is appropriate for the coreflooding tests. For in-depth treatment in the field, a much longer gelation time is required. Four oil displacement tests were performed on specially prepared heterogeneous carbonate composite core samples in which different configurations of high permeability channels had been created. The following conclusions were drawn from these test results:

1. Waterflooding oil recovery averaged around 45% of the OOIC. The exception was the sample with channels all the way through the composite plugs. The waterflooding oil recovery of this extremely heterogeneous case was only 1.1% OOIC because the water easily broke through the high permeability channels.
2. Incremental oil recovery following gel treatment ranged from 12% to 37.6% OOIC.
3. The realized improvement in oil recovery is directly correlated to the severity of heterogeneity. The lower incremental oil recovery, 12% OOIC, was obtained from the composite core without any artificial heterogeneity. The largest incremental oil recovery, 37.6% OOIC, was achieved from the sample with channels all the way through the composite plugs. For intermediate heterogeneities, i.e., channel(s) not all the way through, significant oil recovery improvement was also observed — 15.4% to 18.4% OOIC — but the difference compared to the homogeneous case was much smaller.

In general, results of this study demonstrate the potential of the studied polymer gel system for increasing oil recovery in carbonate reservoirs at high temperature. The results also indicate that gel treatment is very effective in improving oil recovery for reservoirs with severe heterogeneity if the gel can be effectively placed deep into the high permeability channels.

ACKNOWLEDGMENTS

The authors would like to thank the management of Saudi Aramco and the EXPEC Advanced Research Center for their support and permission to publish this article.

This article was presented at the SPE Kingdom of Saudi Arabia Annual Technical Symposium and Exhibition, Dammam, Saudi Arabia, April 24-27, 2017.

REFERENCES

1. Sydansk, R.D. and Southwell, G.P.: "More Than 12 Years of Experience with a Successful Conformance Control Polymer Gel Technology," SPE paper 49315, presented at the SPE Annual Technical Conference and Exhibition, New Orleans, Louisiana, September 27-30, 1998.
2. Sydansk, R.D. and Romero-Zerón, L.: *Reservoir Conformance Improvement*, Vol. 8, Society of Petroleum Engineers, Richardson, Texas, 2011, 138 p.
3. Moradi-Araghi, A.: "A Review of Thermally Stable Gels for Fluid Diversion in Petroleum Production," *Journal of Petroleum Science and Engineering*, Vol. 26, Issues 1-4, May 2000, pp. 1-10.
4. Vossoughi, S.: "Profile Modification Using In Situ Gelation Technology — A Review," *Journal of Petroleum Science and Engineering*, Vol. 26, Issues 1-4, May 2000, pp. 199-209.
5. Zaitoun, A., Tabary, R., Rousseau, D., Pichery, T.R., et al.: "Using Microgels to Shut Off Water in a Gas Storage Well," SPE paper 106042, presented at the International Symposium on Oil Field Chemistry, Houston, Texas, February 28-March 2, 2007.
6. El-Karsani, K.S.M., Al-Muntasheri, G.A. and Hussein, I.A.: "Polymer Systems for Water Shutoff and Profile Modification: A Review Over the Last Decade," *SPE Journal*, Vol. 19, Issue 1, February 2014, pp. 135-149.
7. Al-Maamari, R.S., Al-Hashmi, A.R., Al-Sharji, H.H., Dupuis, G., et al.: "Development of Thermo-Gels for In-depth Conformance Control," SPE paper 174640, presented at the SPE Asia Pacific Enhanced Oil Recovery Conference, Kuala Lumpur, Malaysia, August 11-13, 2015.
8. Dupuis, G., Lesuffleur, T., Desbois, M., Bouillot, J., et al.: "Water Conformance Treatment Using SMG Microgels: A Successful Field Case," SPE paper 179765, presented at the SPE EOR Conference at Oil and Gas West Asia, Muscat, Oman, March 21-23, 2016.
9. Johnson, L.M., Norton, C.A., Huffman, N.D., Mecham, J.B., et al.: "Nanocapsules for Controlled Release of Waterflood Agents for Improved Conformance," SPE paper 181547, presented at the SPE Annual Technical Conference and Exhibition, Dubai, UAE, September 26-28, 2016.
10. Han, M., Alshehri, A.J., Krinis, D. and Lyngra, S.: "State-of-the-Art of In-depth Fluid Diversion Technology: Enhancing Reservoir Oil Recovery by Gel Treatments," SPE paper 172186, presented at the SPE Saudi Arabia Section Technical Symposium and Exhibition, al-Khobar, Saudi Arabia, April 21-24, 2014.
11. Clampitt, R.L., Al-Rikabi, H.M. and Dabbous, M.K.: "A Hostile Environment Gelled Polymer System for Well Treatment and Profile Control," SPE paper 25629, presented at the Middle East Oil Show, Manama, Bahrain, April 3-6, 1993.
12. Dovan, H.T., Hutchins, R.D. and Sandiford, B.B.: "Delaying Gelation of Aqueous Polymers at Elevated Temperatures Using Novel Organic Crosslinkers," SPE paper 37246, presented at the International Symposium on Oil Field Chemistry, Houston, Texas, February 18-21, 1997.
13. Hardy, M., Botermans, W., Hamouda, A., Valdal, J., et al.: "The First Carbonate Field Application of a New Organically Crosslinked Water Shutoff Polymer System," SPE paper 50738, presented at the SPE International Symposium on Oil Field Chemistry, Houston, Texas, February 16-19, 1999.
14. Al-Muntasheri, G.A., Nasr-El-Din, H.A. and Zitha, P.L.J.: "Gelation Kinetics of an Organically Cross-linked Gel at High Temperature and Pressure," SPE paper 104071, presented at the First International Oil Conference and Exhibition in Mexico, Cancun, Mexico, August 31-September 2, 2006.
15. Wang, J., Al-Sofi, A.M. and Al-Boqmi, A.M.: "Development and Evaluation of Gel-based Conformance Control for a High Salinity and High Temperature Carbonate," SPE paper 179796, presented at the SPE EOR Conference at Oil and Gas West Asia, Muscat, Oman, March 21-23, 2016.
16. Kwak, H.T., Wang, J. and Al-Sofi, A.M.: "Close Monitoring of Gel-based Conformance Control by NMR Techniques," SPE paper 183719, presented at the SPE Middle East Oil and Gas Show and Conference, Manama, Bahrain, March 6-9, 2017.
17. Sydansk, R.D.: "A Newly Developed Chromium (III) Gel Technology," *SPE Reservoir Engineering*, Vol. 5, Issue 3, August 1990, pp. 346-352.
18. Lockhart, T.P. and Albonico, P.: "New Chemistry for the Placement of Chromium (III)/Polymer Gels in High Temperature Reservoirs," *SPE Production & Facilities*, Vol. 9, Issue 4, November 1994, pp. 273-279.

BIOGRAPHIES

Dr. Jinxun Wang works at Saudi Aramco's Exploration and Petroleum Engineering Center – Advanced Research Center (EXPEC ARC) as a Petroleum Engineer in the chemical enhanced oil recovery focus area of the Reservoir Engineering Technology Division. Before joining Saudi Aramco, he worked with Core Laboratories Canada Ltd. as a Project Engineer in their Advanced Rock Properties group. Jinxun's experience also includes 10 years of research and teaching reservoir engineering at petroleum universities in China.

Jinxun received his B.S. degree from the China University of Petroleum, his M.S. degree from the Southwest Petroleum Institute, China, and his Ph.D. degree from the Research Institute of Petroleum Exploration and Development, Beijing, China, all in Petroleum Engineering. He received a second Ph.D. degree in Chemical Engineering from the University of Calgary, Calgary, Alberta, Canada.

Jinxun is a member of the Society of Petroleum Engineers (SPE) and the Society of Core Analysts (SCA).

Dr. Ammar J. Alshehri is a Reservoir Engineer working with the chemical enhanced oil recovery focus area of the Reservoir Engineering Technology Division of Saudi Aramco's Exploration and Petroleum Engineering Center – Advanced Research Center (EXPEC ARC). He has several years of experience in areas related to enhanced oil recovery, petrophysics, production engineering, reservoir management and numerical reservoir simulation. Ammar is currently a member of the chemical enhanced oil recovery team and a member of Upstream's Carbon Management team.

He has several technical papers and articles published in several venues. Ammar is an active member of the Society of Petroleum Engineers (SPE) and has had several leading roles in SPE-KSA section. He is also a technical reviewer for the *SPE Journal* and the *Journal of Petroleum Science and Engineering*.

In 2005, Ammar received his B.S. degree in Petroleum Engineering from the Colorado School of Mines, Golden, CO; in 2009, an M.S. degree and in 2013, his Ph.D. degree, both in Petroleum Engineering from Stanford University, Stanford, CA.

Dr. Abdulkarim M. Al-Sofi is a Reservoir Engineer with the Reservoir Engineering Technology Division of Saudi Aramco's Exploration and Petroleum Engineering Center – Advanced Research Center (EXPEC ARC). He is currently the Champion of the chemical enhanced oil recovery focus area and is leading a new research initiative on heavy oil mobilization and recovery. Abdulkarim has also worked with the Reservoir Management, Reservoir Description and Simulation, and Reserves Assessment Departments.

He is the recipient of the 2009 Society of Petroleum Engineers (SPE) Annual Technical Conference and Exhibition Young Professional Best Paper Award in reservoir engineering, the recipient of the 2011 EXPEC ARC Best Presentation Award and the recipient of the 2013 Middle East Young Engineer of the Year Award.

Abdulkarim has authored 15 conference papers and seven peer-reviewed journal papers.

In 2006, he received his B.S. degree from the University of Texas at Austin, Austin, TX, and in 2010, Abdulkarim received his Ph.D. degree from Imperial College London, London, U.K., both degrees in Petroleum Engineering.

Abdullah M. Al-Boqmi is a Lab Technician with the chemical enhanced oil recovery focus area of the Reservoir Engineering Technology Division of Saudi Aramco's Exploration and Petroleum Engineering Center – Advanced Research Center (EXPEC ARC). He received his training from Saudi Aramco's Industrial Training Center (ITC) and Jubail Industrial College, Jubail, Saudi Arabia.

Abdullah is a co-inventor in two granted U.S. patents. He is an active member of the Society of Petroleum Engineers (SPE) and the coauthor of two SPE papers in the area of surfactant/polymer screening and conformance control efforts.

Strategies of Scale Management for Using Seawater as Fracturing Fluid

Dr. Tao Chen, Ahmed BinGhanim, Dr. Mohammed A. Bataweel and Dr. Raed Rahal

ABSTRACT

Continuous efforts are made to save freshwater resources in the Middle East, and using seawater-based fluid for fracturing has a high potential to save millions of gallons of freshwater in hydraulic fracturing applications.

Scale deposition is one of the major technical challenges for using seawater as fracturing fluid. To understand scale deposition and the means for its mitigation when fracturing using a seawater-based fluid, a series of dynamic and static performance tests, compatibility tests and thermal stability tests were conducted.

Results show that harsh scale forms when raw seawater is mixed with formation water having high total dissolved solids (TDS) at high temperature under both dynamic and static conditions. Scale inhibitors cannot effectively inhibit this scale deposition due to issues of brine compatibility and the performance at static conditions.

Tests were then run using nano-filtered seawater. The filtration removes most of the sulfate ions in seawater and significantly reduces the scaling tendency when mixing the filtered seawater with high TDS formation water during fracturing. By combining a nano-filtration technique with scale inhibitor application, the scale issue during fracturing using the filtered seawater-based fluid can be effectively mitigated and the fluid made suitable for field application. The scale inhibitor showed good compatibility with nano-filtered seawater. The dynamic tests were passed when the proper scale inhibitor at an optimum concentration was used, while the static tests did not form any precipitation. Thermal aging resulted in a color change for all tests, as was expected, and the performance of the thermal aged scale inhibitor was also evaluated.

This article provides insight into scale deposition and its inhibition when using seawater-based fluid for fracturing at high temperatures up to 300 °F, and it furthers the effective strategies to address the scale issue raised by using a seawater-based fluid.

INTRODUCTION

Effective stimulation of oil and gas wells requires the use of efficient fracturing fluids that can perform under a variety of conditions. Hydraulic fracturing primarily uses water-based fluids to initiate and extend an open crack in the formation where gas or oil is located. Proppants are then used to keep the fracture, and therefore the conductive pathway, open once the treatment fluid is removed[1]. In a typical hydraulic fracturing operation, from 1 to 4 million gallons of freshwater is consumed[2]. The availability of freshwater for use as a fracturing fluid is one of the major challenges facing the oil and gas industry, especially in the Arabian Penisula and similar arid regions. In addition, a considerable amount of time is required to transport freshwater to locations in offshore operations, which adds to the inconvenience and impracticality of storing large quantities of freshwater offshore[3]. The lack of available freshwater resources and the high cost involved in its transport and servicing are major disadvantages.

Using seawater to make fracturing fluid can help conserve freshwater and reduce costs for hydraulic fracturing applications. In addition, formation damage due to the swelling of clay that occurs when using freshwater for fracturing can be prevented because the high salt concentration of seawater precludes such swelling.

Using seawater to make fracturing fluids, however, also poses several new challenges. One of the major challenges is the viscosity buildup that occurs when the guar gum polymer used in the hydration step prior to developing the complete fracturing fluid is altered by the high salt content in seawater. The resulting high ionic strength can negatively affect the reservoir and the rheology of the fluid, causing formation damage[4]. Another major challenge is that the high salinity of seawater leads to a propensity for scaling. The reason for this has to do with the different factors and chemical properties that influence the process of developing fracturing fluids. Compared to freshwater used for fracturing fluid development, which does not pose scaling problems as much, seawater causes sulfate scales to form, primarily due to the mixing of two incompatible waters: seawater, which contains a high concentration of sulfate ion, and formation water, which contains a high concentration of barium, calcium and strontium ions. Table 1 shows the water chemistry of typical freshwater and seawater.

The formation of mineral scale is a persistent and expensive problem in oil and gas production. It may create technical problems, including pipe or valve blockage, and cause

	Freshwater (mg/l)	Arabian Gulf Seawater (mg/l)
Na^+	27	16,180
Ca^{2+}	144	650
Mg^{2+}	55	173
K^+	2	700
Sr^{2+}	0	< 1
Ba^{2+}	0	0
Cl^-	53	31,000
SO_4^{2-}	60	4,020

Table 1. Water chemistry of typical freshwater and seawater

underdeposit corrosion, formation damage, and even more importantly, unscheduled equipment shutdown[5-7]. The effects of scale in an oil field can be dramatic, and mitigation costs can be enormous. Scaling is a significant issue that should be considered when fracturing using a seawater-based fluid, which can potentially cause well blockage, reduce the efficiency of fracturing, etc.

In most cases, scale prevention through chemical inhibition is the preferred method of maintaining well productivity. To prevent scale from forming in the system, a chemical inhibitor must be injected continuously and/or by periodic squeeze treatments[8, 9].

To understand scale deposition and its mitigation using a scale inhibitor during fracturing operations with a seawater-based fluid, dynamic and static performance tests, compatibility tests and thermal stability tests of a selected scale inhibitor were conducted. Dynamic scale loop tests were conducted at temperatures up to 300 °F and pressures up to 3,000 psi. Static performance tests were conducted at 300 °F for 2 and 24 hours. For the thermal stability test, the scale inhibitor was thermally aged to test its molecular stability and inhibition performance after a period of time at high temperature. Results show that harsh scale forms when raw seawater is mixed with formation water having high total dissolved solids (TDS) at high temperatures under dynamic and static conditions. Scale inhibitors cannot effectively inhibit scale deposition due to issues of brine compatibility and the performance at static conditions.

To solve the scale issues posed by fracturing using a seawater-based fluid, a nano-filtration unit was introduced to remove most of the sulfate ions and the concentrations of other salts in the seawater[10]. This significantly reduces the scaling tendency when the seawater-based fluid is mixed with high TDS formation water.

By combining a nano-filtration technique with a scale inhibitor application, the scale issue during fracturing using a seawater-based fluid can be effectively mitigated and the fluid made suitable for field application. The scale inhibitor showed good compatibility with the nano-filtered seawater. The dynamic tests were passed when the proper scale inhibitor at an optimum concentration was used, and the static tests did not form any precipitation. Thermal aging resulted in a color change for all tests, as was expected, and the performance of the thermal aged scale inhibitor was also evaluated.

MATERIALS AND METHODS

Brines

All brines tested were prepared to synthetically represent the specific formation water, seawater and nano-filtered seawater found in the Middle East region. Table 2 shows the water chemistry of the seawater, filtered seawater and high salinity formation water.

Scale Inhibitor

The scale inhibitor used for all tests met the passing criteria by satisfying different requirements, such as calcium compatibility, seawater and formation water compatibility, thermal aging, high inhibition performance, etc. The polymer-based scale inhibitor that was selected was pushed to the limits to perform effectively at temperatures up to 300 °F.

TEST PROCEDURES

Brine Compatibility Test

The goal of the compatibility test was to verify the compatibility of scale inhibitors with seawater and formation water at test conditions. The scale inhibitor must be compatible with the formation water at the appropriate application concentration under field temperatures.

Synthetic seawater and high salinity formation water without bicarbonate/sulfate were prepared to match the water chemistry provided in Table 2. The freshwater was made by dissolving all the salts in de-ionized water before filtering and

Ion	Tested Formation Water (ppm)	Arabian Gulf Seawater (ppm)	Nano-filtered Seawater (ppm)
Na^+	7,000	16,180	16,280
Ca^{2+}	25,000	650	213
Mg^{2+}	2,000	1,730	256
K^+	4,000	700	519
Sr^{2+}	2,000	1	< 1
Ba^{2+}	4,000	< 1	0
Cl^-	160,000	31,000	26,401
SO_4^{2-}	200	4,020	297
HCO_3^-	0	126	103

Table 2. Water chemistry of formation water, Saudi Arabia seawater and nano-filtered seawater

degassing the brine under vacuum. High temperature glass tubes were filled with the appropriate mixtures of scale inhibitor and seawater or scale inhibitor and high salinity formation water. Scale inhibitor concentrations were 250 ppm, 500 ppm, 5,000 ppm, 1% (vol) and 5% (vol) in the synthetic seawater (or nano-filtered seawater) and high salinity formation water. The appearance of the tubes at room temperature was noted. The tubes were then placed in a preheated oven at 300 °F for 24 hours. Appearances were noted twice: after 2 hours and and the end of the 24 hours.

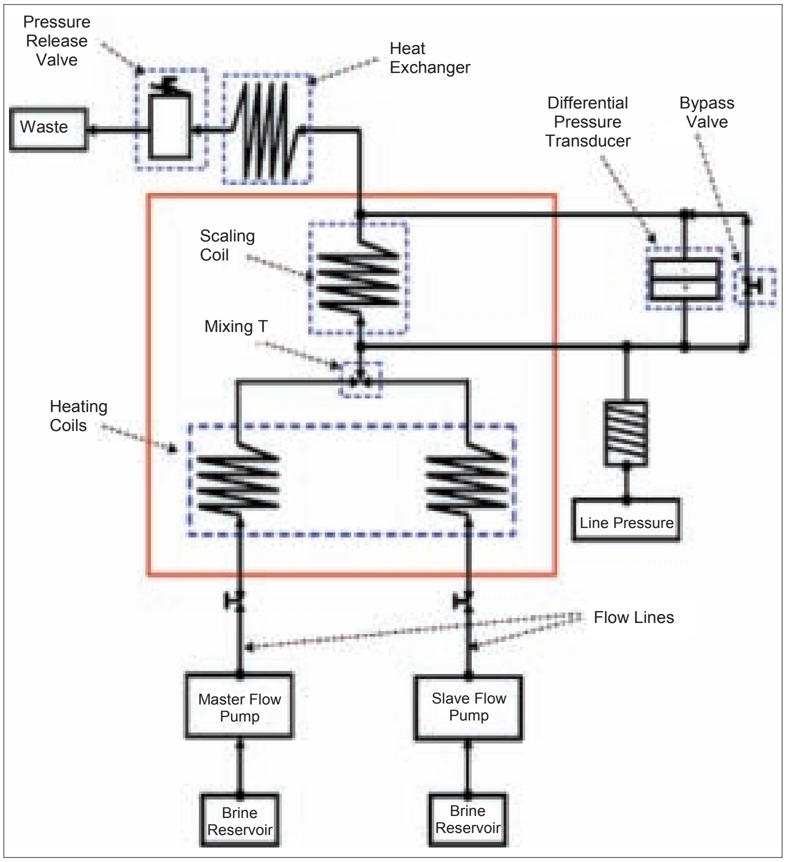

Fig. 1. Flow diagram of the dynamic loop system.

Static Scale Inhibition Efficiency Tests

Static scale inhibitor efficiency tests for calcium sulfate ($CaSO_4$) and barium sulfate ($BaSO_4$) were performed with the selected scale inhibitor. Tests were conducted with a mixture of 20% high salinity formation water and 80% seawater or nano-filtered seawater, which is the worse case scenario for sulfate scaling at a reservoir temperature of 300 °F, to evaluate the performance of the selected scale inhibitor. The water was filtered through a 0.45 µm membrane prior to use.

After dosing a set of 120 ml high temperature and high- pressure glass jars with 50 mL of anion brine, a certain concentration of the scale inhibitor was added to each jar. A blank was prepared with 50 mL of anion brine and no scale inhibitor, and a control was prepared with 50 mL of deionized water. All jars were prepared in duplicate. Similarly, after dosing another set of jars with 50 ml of cation brine, a certain concentration of the scale inhibitor was added to each jar. All the jars were sealed and placed into the oven at 195 °F. After 1 hour, the anion jars were mixed with the cation jars, and placed in another oven at 300 °F. Visual appearance was noted at the initial mixing, at 2 hours and at 24 hours.

Dynamic Loop Tests

Dynamic scale loop tests were performed to detect the worse case scenarios for scaling as a result of mixing seawater and formation water and to evaluate the performance of scale inhibitors under dynamic conditions. The water chemistries of the high salinity formation water, seawater and filtered seawater used in these tests were previously summarized in Table 2. Tests were carried out using different ratios of formation water and seawater. The dynamic scale inhibition test was conducted using a DSR 6000 machine.

The dynamic flow apparatus used was a high-pressure, high temperature (HPHT) test system. Figure 1 is a flow diagram of the apparatus used. The test consisted of the individual injection of two scaling test brines, anion and cation, at equal rates into the apparatus. Both brines passed into heating coils within the oven set at the test temperature. At a T-junction, the brines mixed together and passed into the scaling coil. The differential pressure (DP) is measured across this scaling coil and rises once scale formation and adhesion to the coil walls causes a blockage. When that happened, the DP was recorded as a function of time[6].

Table 3 lists all tests that were performed, using the standard text conditions.

Each test began with a blank run with no scale inhibitor present. For the following tests, including scale inhibitors, it is an industry standard to triple the time of the blank test time. This was done for each different temperature or brine composition.

Standard Test Conditions	
Scaling coil length	1 m
Scaling coil internal diameter	~1 mm
Coil	Alloy 600 coils
Total brine flow rate	6 ml/min
Back pressure	3,000 psi
pH	Ambient 6.5 ± 0.3
Pass criteria	< 3 psi rise in DP over set time
Temperature	300 °F
Brine	Different ratios of formation water and seawater

Table 3. Standard test conditions utilized for all tests

Thermal Stability Test

For an inhibitor to be safely deployed in HPHT wells, it must be thermally stable at field temperatures. The thermal stability test conditions are summarized as:

- Concentration: Neat scale inhibitor
- Test temperature: 300 °F
- Test duration: 3 days

The tested scale inhibitor was aged at 300 °F for 3 days. The samples were sparged with nitrogen prior to thermal aging. Each sample was assessed visually.

The thermal aged samples were later used for the dynamic loop testing to check if heating the chemicals had any effect on their performance.

RESULTS

Sulfate Scale Prediction

As part of a scale risk review, scale prediction is undertaken to both review scaling tendency and predict oversaturation. The scale prediction here was performed using one of the recognized industry standards — the ScaleSoftPitzer program, Version 2010.

The scale prediction calculations provide values for the supersaturation ratio — a parameter indicating the thermodynamic driving force for the formation of each scale type and also the possible mass of scale precipitate. ScaleSoftPitzer (and other similar scale prediction codes) calculate the supersaturation ratio using either the ion pairing or the Pitzer equation. It should be recognized that scale predictions are used only to provide a guide to the likely nature and extent of the scaling challenge and to investigate the impact of a process change on the likely severity of scaling. It is also the case that different programs may interpret the level of risks slightly differently.

The formula for the supersaturation ratio is given in Eqn. 1:

$$S_\alpha = (\alpha_1 \times \alpha_2)/K_{(P.T)} \qquad (1)$$

where $a = \gamma \times C$.

S_a is the supersaturation ratio and a is the activity of the separate species. α_1 and α_2 are the activity of scaling cation and scaling anion in the solution, respectively. K is normally called the solubility product, which depends on the pressure, P, and the temperature, T. C is the concentration of the ions in the solution, and γ is the ionic activity coefficient.

Scale can occur at any point in the oil and gas production system where supersaturation is generated. A supersaturated solution is the primary cause of scale formation. It occurs when the concentration of ions is above their equilibrium concentration. The degree of supersaturation, or the scaling, S_a, is the driving force for the precipitation reaction and suggests the likelihood for scale precipitation. Guideline values for the interpretation of the S_a values are provided in Table 4.

Supersaturation Ratio Values	Interpretation
< 1	Undersaturated for this scale type, so non-scaling.
1 – 3	Slightly supersaturated, so likelihood of scale formation is marginal.
3 – 10	Scale likely, but should not be severe.
10 – 100	Scale almost certain to occur and is expected to be strongly scaling.
> 100	Severe scaling likely.

Table 4. Interpretation of supersaturation ratio values

Sulfate Scale Prediction of Mixing Seawater and High Salinity Formation Water

$BaSO_4$, $CaSO_4$ and strontium sulfate ($SrSO_4$) scales were predicted to form when high salinity formation water and seawater were mixed at 300 °F, Fig. 2.

The worse case condition for $BaSO_4$ precipitation of scale at predicted points is the mixing of 60% to 80% seawater and 20% to 40% formation water, with a S_a of 2,100 to 2,232. An extremely harsh $BaSO_4$ S_a was predicted with the mixing of seawater and formation water at 300 °F. This was coupled to a huge mass precipitation, between 1,450 mg/L and 2,859 mg/L. Harsh $BaSO_4$ scale deposition is certain to occur with mixed formation and seawater at these ratios.

For $CaSO_4$, the saturation ratio is between 0 and 27. The worse case condition for $CaSO_4$ precipitation of scale at predicted points is the mixing of 70% to 90% seawater and 10% to 30% formation water, with a high mass precipitation of 3,836 mg/L to 4,679 mg/L. $CaSO_4$ scale deposition is certain to occur and will be severe due to the high mass precipitation.

For $SrSO_4$, the saturation ratio is between 0 and 19. The worse case condition for $SrSO_4$ precipitation of scale at predicted points is the mixing of 20% to 60% seawater and 40%

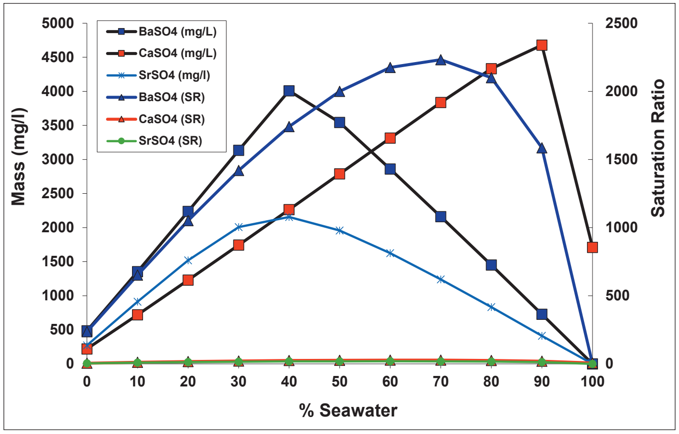

Fig. 2. Sulfate scale prediction — mixing formation water and seawater at 300 °F.

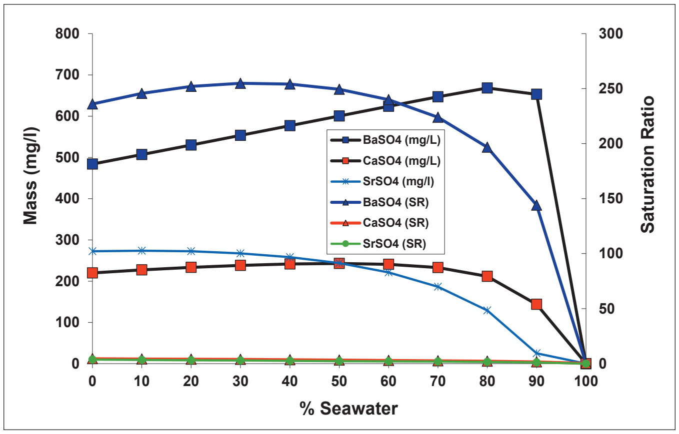

Fig. 3. Sulfate scale prediction — mixing formation water and nano-filtered seawater at 300 °F.

to 80% formation water, with a mass precipitation of 1,520 mg/L to 2,156 mg/L. $SrSO_4$ scale deposition is certain to occur and will be severe due to the high mass precipitation.

In comparison to the $BaSO_4$ scale predictions, the likelihood of $CaSO_4$ and $SrSO_4$ scale precipitation is lower due to a lower S_a. Yet the mass deposition of $CaSO_4$ and $SrSO_4$ is high, which predicts that a large mass deposit will form if $CaSO_4$ and $SrSO_4$ precipitates scale.

By balancing the saturation ratio and the mass precipitation of sulfate scales, the mixing ratio of 80% seawater and 20% formation water was selected for further performance tests in the absence and in the presence of scale inhibitors.

Sulfate Scale Prediction of Mixing Nano-Filtered Seawater and High Salinity Formation Water

$BaSO_4$, $CaSO_4$ and $SrSO_4$ scales were predicted to form when high salinity formation water and nano-filtered seawater were mixed at 300 °F, Fig. 3.

$BaSO_4$ scale was predicted at a mixing ratio of 0% to 90% seawater and 10% to 100% formation water, with a S_a of 144 to 254. A harsh $BaSO_4$ S_a was predicted at 300 °F, coupled to a medium mass precipitation, between 484 mg/L and 668 mg/L. $BaSO_4$ scale deposition is certain to occur with mixed formation and seawater at these ratios.

For $CaSO_4$, the saturation ratio is between 2 and 4 when the mixing ratio is 0% to 90% seawater and 10% to 100% formation water, along with 144 mg/L to 243 mg/L $CaSO_4$ deposition.

The predicted saturation ratio of $SrSO_4$ is 1 to 4 at the mixing ratio of 0% to 90% seawater and 10% to 100% formation water, along with 25 mg/L to 274 mg/l deposition. $CaSO_4$ and $SrSO_4$ scale deposition is likely to occur, but the scaling will not be harsh.

In a comparison of scale tendency between using seawater and using nano-filtered seawater, the scaling tendency is substantially reduced with the application of a nano-filtration treatment.

Formation Water Compatibility

The incompatibility between scale inhibitors and the seawater, nano-filtered seawater and high salinity formation water the inhibitors would encounter under field temperatures can potentially cause formation damage in the reservoir. For an inhibitor to be safely deployed in a reservoir, it should be compatible with the deployed seawater or nano-filtered seawater at the application dose rate. In addition, it should be compatible with the high salinity formation water at field conditions and at the

	Concentration	Initial	2 Hours	24 Hours
	Blank (0 ppm)	Clear	Clear	Clear
Scale Inhibitor in Seawater	250 ppm	Clear	Clear	Clear
	500 ppm	Clear	Clear	Clear
	5,000 ppm	Clear	Clear	Clear
	1%	Clear	Clear	Clear
	5%	Clear	Clear	Clear
Scale Inhibitor in Nano-filtered Seawater	250 ppm	Clear	Clear	Clear
	500 ppm	Clear	Clear	Clear
	5,000 ppm	Clear	Clear	Clear
	1%	Clear	Clear	Clear
	5%	Clear	Clear	Clear
Scale Inhibitor in High Salinity Formation Water	250 ppm	Clear	Clear	Clear
	500 ppm	Precipitate	Precipitate	Precipitate
	5,000 ppm	Precipitate	Precipitate	Precipitate
	1%	Precipitate	Precipitate	Precipitate
	5%	Precipitate	Precipitate	Precipitate

Table 5. Compatibility of selected scale inhibitor in seawater, nano-filtered seawater and formation water at 300 °F

field application dose rate. The synthesized seawater, nano-filtered seawater and high salinity formation water, previously listed in Table 2, were used to evaluate the compatibility of the selected scale inhibitor at 300 °F. The results are summarized in Table 5.

The selected scale inhibitor was fully compatible at all concentrations tested in the seawater and nano-filtered seawater on initial mixing at room temperature and after 24 hours at 300 °F. No precipitation or gel was observed in any of the concentrations tested after 24 hours.

Compatibility tests of the selected scale inhibitor with the high salinity formation water showed all tested concentrations were precipitated at the initial room temperature and after 24 hours at 300 °F.

Because there is no incompatibility between the inhibitor and seawater or the inhibitor and nano-filtered seawater, no compatibility issue should arise when the scale inhibitor deploys in seawater or nano-filtered seawater. Consequently, the incompatibility of the scale inhibitor with the high salinity formation water could be a cause for concern when the scale inhibitor, deployed in seawater or nano-filtered seawater, mixes with the high salinity formation water in the formation, especially for scale inhibitor dose rates above 500 ppm.

Dynamic Loop Tests Using Seawater

The dynamic efficiency loop testing was carried out to determine the minimum inhibitor concentration (MIC) of the selected inhibitor under dynamic conditions. The mixing ratio of 80% seawater and 20% formation water was selected for the dynamic loop test, the worse case scenario determined by scale prediction.

The results of the dynamic loop performance tests with seawater (80%) and formation water (20%) at 300 °F were previously shown in Fig. 3. The blank loop test in the absence of the scale inhibitor was carried out to determine the length of time required for testing the scale inhibitor at different concentrations against the pass criteria. The blank run scaled at about 12 minutes after the anion and cation brine mixed, so the hold time for each dose was 21 minutes (three times the blank time), Fig. 4.

The scale inhibitor was tested at concentrations of 1,000 ppm, 1,500 ppm, 2,000 ppm, 2,500 ppm and 3,000 ppm. The DP increased up to 1 psi at 8.5 minutes, 13 minutes, 17 minutes, 21 minutes and 23 minutes in the presence of 000 ppm, 1,500 ppm, 2,000 ppm, 2,500 ppm and 3,000 ppm, respectively. Results indicate that the MIC of the tested scale inhibitor under this test condition is 2,500 ppm.

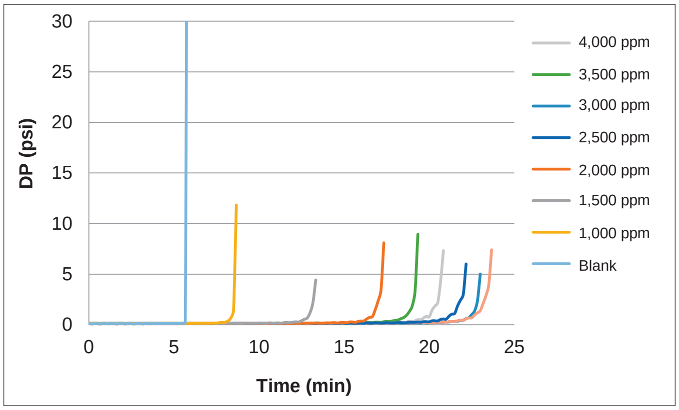

Fig. 4. Dynamic loop tests with seawater (80%) and formation water (20%) at 300 °F.

Static Efficiency Testing Using Seawater as Fracture Fluid

Static scale inhibitor efficiency tests were carried out in 20% formation water and 80% seawater to evaluate the performance of the selected scale inhibitor on sulfate scale under static conditions. The detected MIC of the candidate scale inhibitor by dynamic loop test is 2,500 ppm. The dose rates for the static test were 2,500 ppm, 5,000 ppm, 7,500 ppm and 10,000 ppm. A summary of the visual appearance of the samples following the static efficiency test for sulfate scale is noted in Table 6. A scale deposit was noticeable immediately after mixing the cations and anions, after 2 hours and after 24 hours in all tested concentrations. These results indicate that the scaling is too harsh to be effectively inhibited under static conditions, even with high concentrations of scale inhibitor.

Dynamic Loop Tests Using Nano-Filtered Seawater

As previously noted, because it is difficult to effectively inhibit scale deposition using seawater as a fracturing fluid, a

Chemical	Dose (ppm)	Appearance		
		At Mix	2 Hours	24 Hours
Blank	N/A	Precipitate	Precipitate	Precipitate
Control	N/A	Clear	Clear	Clear
Test Scale Inhibitor	2,500	Precipitate	Precipitate	Precipitate
	5,000	Precipitate	Precipitate	Precipitate
	7,500	Precipitate	Precipitate	Precipitate
	10,000	Precipitate	Precipitate	Precipitate

Table 6. Visual appearance of samples after static efficiency tests for sulfate scale at 300 °F in seawater (80%) and formation water (20%)

nano-filtration technique to remove most of the sulfate ions and concentrations of other salts in seawater, which significantly reduces the scaling tendency when mixed with high TDS formation water, is advisable. The improvement was previously shown in Fig. 2 and Fig. 3.

The dynamic efficiency loop testing was carried out to determine the MIC of the selected inhibitor under dynamic conditions using nano-filtered seawater as a fracturing fluid. The mixing ratio of 80% seawater and 20% formation water was again selected for the dynamic loop test, the worse case scenario determined by scale prediction.

Figure 5 shows the results of the dynamic loop performance tests with nano-filtered seawater (80%) and formation water (20%) at 300 °F. When the blank loop test in the absence of scale inhibitor was carried out and scaled at about 22 minutes after the anion and cation brine mixed, the hold time for each dose was set at 66 minutes (three times the blank time).

The scale inhibitor was tested at concentrations of 250 ppm and 500 ppm. The DP did not increase up to 1 psi after 66 minutes in the presence of 250 ppm and 500 ppm concentrations of scale inhibitor. These results indicate that the MIC of the scale inhibitor under this test condition is less than 250 ppm.

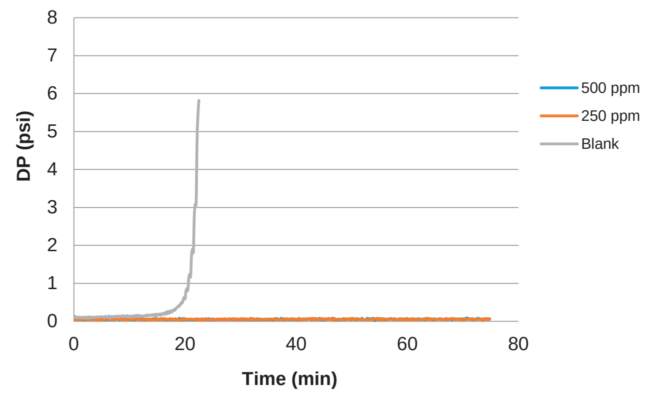

Fig. 5. Dynamic loop tests with nano-filtered seawater (80%) and formation water (20%) at 300 °F.

Static Efficiency Testing Using Nano-Filtered Seawater as Fracture Fluid

Static scale inhibitor efficiency tests were carried out in 20% formation water and 80% nano-filtered seawater to evaluate the performance of the selected scale inhibitor on sulfate scale under static conditions. The detected MIC of the candidate scale inhibitor by dynamic loop test is less than 250 ppm. The dose rates for the static test were 250 ppm, 500 ppm, 750 ppm and 1,000 ppm. Table 7 is a summary of the visual appearance of the samples following the static efficiency tests for sulfate scale. Slight haziness and precipitation were observed after 2 hours and after 24 hours, respectively, in the blank test. There was no noticeable scale formation in the dosed scale inhibitor jars with concentrations of 250 ppm to 1,000 ppm scale inhibitor. The MIC of SI-A and SI-B is less than 250 ppm on sulfate scale under this test condition based on the static jar test. This indicates that the sulfate scaling under this test condition can be effectively inhibited with a 250 ppm concentration of scale inhibitor.

Thermal Stability Test

To evaluate the thermal stability of the scale inhibitor under conditions of field application, the scale inhibitor was thermally aged at 300 °F for 3 days, then a dynamic loop performance test at 300 °F was conducted on the thermal aged samples.

The color of the scale inhibitor changed to a darker color, but no precipitate occurred over the 3 days of the thermal stability test, Fig. 6.

Figure 7 shows the results of the dynamic loop test, which was carried out to evaluate if heating the chemicals had any effect on its performance. The DP built up after about 13 minutes in the presence of a 1,500 ppm scale inhibitor and after 20 minutes in the presence of a 1,500 ppm thermal aged scale inhibitor. These results show that thermal age had no negative effect on the performance of the scale inhibitor. Instead, an improved scale inhibition performance was observed after the thermal age treatment.

Chemical	**Dose (ppm)**	**Appearance**		
		At Mix	**2 Hours**	**24 Hours**
Blank	N/A	Clear	Slightly Hazy	Slightly Precipitate
Control	N/A	Clear	Clear	Clear
Test scale Inhibitor	250	Clear	Clear	Clear
	500	Clear	Clear	Clear
	750	Clear	Clear	Clear
	1,000	Clear	Clear	Clear

Table 7. Visual appearance of samples following static efficiency tests for sulfate scale at 300 °F in nano-filtered seawater (80%) and formation water (20%)

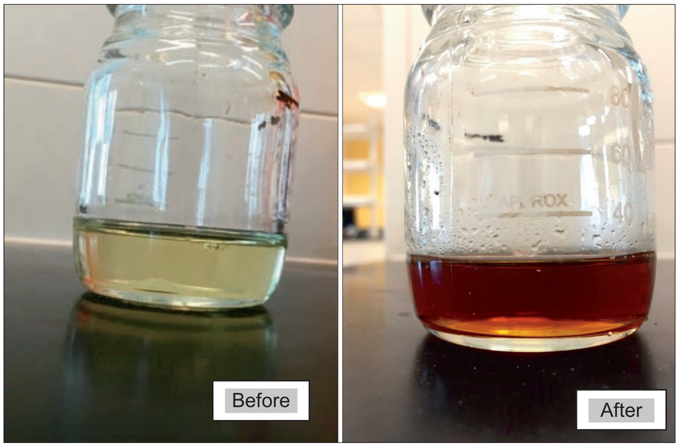

Fig. 6. Observation of non-aged and aged scale inhibitor at 300 °F after 3 days.

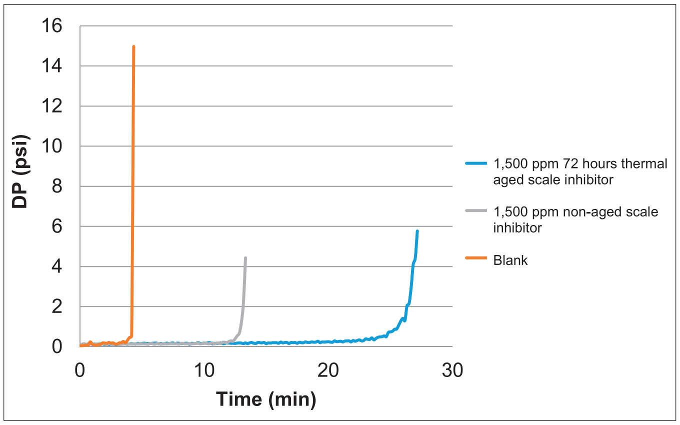

Fig. 7. Dynamic loop tests of thermal aged scale inhibitor with seawater (80%) and formation water (20%) at 300 °F.

Other Tests to Qualify the Chemical Package for Fracturing Use

Scale inhibitor qualification is essential for developing fracturing fluid using seawater. To qualify the final chemical package for fracturing using seawater, more tests should be carried out, including a linear gel hydration test to understand the hydration behavior of the guar gum when it is used in nano-filtered seawater for the targeted hydraulic fracturing conditions. Also needed are a rheology test to determine the proppant carrying capacity of the cross-linked fracturing fluid; constant shear rate and shear sweep tests to assess the fracturing fluid sensitivity to shear degradation by simulating the shear history during the fracturing operation; and a coreflood test and proppant pack damage test to evaluate the potential formation damage and the conductivity. Detailed qualification procedures and results are reported in BinGhanim et al. (2017)[11].

CONCLUSIONS

1. Using seawater to make fracturing fluid can help conserve freshwater and reduce the costs for hydraulic fracturing applications.
2. Sulfate scale deposition is one of the major challenges when using seawater as a fracturing fluid. Sulfate scales that form are primarily due to mixing two incompatible waters: seawater that contains a high concentration of sulfate ions and high salinity formation waters that contain high concentrations of barium, calcium and strontium ions. Scaling is a significant issue that should be considered when conducting fracturing operations using seawater as a fracturing fluid.
3. A nano-filtration unit can effectively remove sulfate and significantly reduce the scaling tendency of seawater when it is mixed with high TDS formation water during fracturing. By combining a nano-filtration technique with scale inhibitor application, the scale issue during fracturing using a seawater-based fluid can be effectively mitigated and the fluid made suitable for field application.

ACKNOWLEDGMENTS

The authors would like to thank the management of Saudi Aramco and Halliburton for their support and permission to publish this article.

This article was presented at the SPE Kingdom of Saudi Arabia Annual Technical Symposium and Exhibition, Dammam, Saudi Arabia, April 24-27, 2017.

REFERENCES

1. Alohaly, M., BinGhanim, A., Rahal, R. and Rahim, S.: "Seawater Fracturing Fluid Development Challenges: A Comparison between Seawater-based and Freshwater-based Fracturing Fluids Using Two Types of Guar Gum Polymers," SPE paper 182799, presented at the SPE Kingdom of Saudi Arabia Annual Technical Symposium and Exhibition, Dammam, Saudi Arabia, April 25-28, 2016.
2. van Domelen, M. and Haggstrom, J.: "Methods for Minimizing Freshwater Requirements in Unconventional Reservoir Fracturing Operations," WPC paper 20-0422, presented at the 20th World Petroleum Congress, Doha, Qatar, December 4-8, 2011.
3. Gao, Y., Shi, Y., Zhou, F., Xu, M., et al.: "Development and Application of Continuously Mixing Seawater-based Fracturing Fluid System," SPE paper 176494, presented at the SPE/IATMI Asia Pacific Oil and Gas Conference and Exhibition, Nusa Dua, Bali, Indonesia, October 20-22, 2015.
4. Karadkar, P., Al Dahlan, M., Sahman, F., Marshad, K., et al.: "Elimination of Scaling Potential of Seawater in Downhole Environment through the Innovative Use of Nanofiltration and Scale Inhibitor," SPE paper 182759, presented at the SPE Kingdom of Saudi Arabia Annual Technical Symposium and Exhibition, Dammam, Saudi Arabia, April 25-28, 2016.

5. Yang, Q., Liu, Y., Gu, A., Ding, J., et al.: "Investigation of Calcium Carbonate Scaling Inhibition and Scale Morphology by AFM," *Journal of Colloid Interface Science*, Vol. 240, Issue 2, August 2001, pp. 608-621.
6. Liu, X., Chen, T., Chen, P., Montgomerie, H., et al.: "Understanding the Co-deposition of Calcium Sulfate and Barium Sulfate and Developing Environmental Acceptable Scale Inhibitors Applied in HTHP Wells," SPE paper 156013, presented at the SPE International Conference on Oil Field Scale, Aberdeen, U.K., May 30-31, 2012.
7. Nasr-El-Din, H.A.: "New Mechanisms of Formation Damage: Lab Studies and Case Histories," SPE paper 82253, presented at the SPE European Formation Damage Conference, The Hague, the Netherlands, May 13-14, 2003.
8. Cowan, J.C. and Weintritt, D.J.: *Water-Formed Scale Deposits*, Gulf Publishing Company, Texas, December 1976, 606 p.
9. Montgomerie, H., Chen, P., Hagen, T.H., Vikane, O., et al.: "Development of a New Polymer Inhibitor Chemistry for Downhole Squeeze Applications," *SPE Production & Operations*, Vol. 24, Issue 3, August 2009, pp. 459-564.
10. Heatherly, M.W., Howell, M.E. and McElhiney, J.E.: "Sulfate Removal Technology for Seawater Waterflood Injection," OTC paper 7593, presented at the Offshore Technology Conference, Houston, Texas, May 2-5, 1994.
11. BinGhanim, A., Al-Hussain, A.M., Karadkar, P., Al-Ohaly, M., et al.: "High Temperature Fracturing Fluid Based on Nanofiltered Seawater," SPE paper 189048, presented at the SPE Kingdom of Saudi Arabia Annual Technical Symposium and Exhibition, Dammam, Saudi Arabia, April 24-27, 2017.

BIOGRAPHIES

Dr. Tao Chen is a Petroleum Engineering Specialist working with the Production Technology Team of Saudi Aramco's Exploration and Petroleum Engineering Center – Advanced Research Center (EXPEC ARC). His interests are production chemistry and flow assurance in the oil and gas industry, specializing in oil field scale management.

Prior to joining Saudi Aramco in 2014, Tao spent more than 15 years on oil field scale management in the Eastern Hemisphere and worked at Clariant, Champion Technologies, Nalco Champion and LR Senergy in Aberdeen, U.K.

He has published mor than 60 technical publications about scale management in oil fields.

Tao received both his B.S. and M.S. degrees in Chemical Engineering from Dalian University of Technology, China, and his Ph.D. degree in Chemical Engineering from Heriot-Watt University, Edinburgh, U.K. Tao also received an MBA from Warwick University, Coventry, U.K.

Ahmed BinGhanim joined Halliburton in 2015 as a scientist working on the Production Enhancement Team. His interests in the oil and gas industry are in the areas of designing fracturing fluids, scale management and proppant pack conductivity.

Ahmed has four published articles related to scale, water-based fracturing fluids and permeability.

He received his B.S. degree in Chemical and Biological Engineering with a minor in Biomedical Engineering from Colorado State University, Fort Collins, CO.

Dr. Mohammed A. Bataweel is a Research Engineer with the Production Technology Division of Saudi Aramco's Exploration and Petroleum Engineering Center – Advanced Research Center (EXPEC ARC). He has represented his department on several field development, asset and multidisciplinary teams. Mohammed's research interests include formation damage due to drilling and completion fluids, investigation and mitigation of injectivity decline, conformance control, sand production prediction, special core analysis, chemical enhanced oil recovery, productivity enhancement technologies, visualization of fluid flow in porous media and oil field chemicals. Currently, he is a focus area champion for the Smart Fluid Group of the Production Technology Team.

Mohammed is an active member of the Society of Petroleum Engineers (SPE) where he has served on several conference boards. He initiated and co-chaired several SPE advanced technical workshop series in the region. Mohammed has published more than 20 SPE papers in local/international conferences and refereed journals.

He received his B.S. degree in Mechanical Engineering from King Fahd University of Petroleum and Minerals (KFUPM), Dhahran, Saudi Arabia. Mohammed also received his M.S. degree in Petroleum Engineering from Heriot-Watt University, Edinburgh, U.K. He received his Ph.D. degree in Petroleum Engineering from Texas A&M University, College Station, TX.

Dr. Raed Rahal is a Principal Scientist for Production Enhancement at the Halliburton Dhahran Technology Center, Saudi Arabia. He is currently managing a production enhancement technology portfolio of fluids and additives for oil field applications in Saudi Arabia. Raed is an upstream oil and gas professional with a diversified technical background in well stimulation techniques and chemicals, including hydraulic fracturing, acidizing, and sand and water control chemicals. Prior to joining Halliburton in 2013, he had over 10 years of commendable experience in the area of nanotechnology, sol gel chemistry, photocalysis, nanoparticles design and surface functionalization.

Raed received both his M.S. and Ph.D. degrees in Material Science from Claude Bernard University, Lyon, France.

During his career, Raed has published more than 25 papers and has been awarded four patents.

Date Seed-Based Particulate LCM "ARC Plug" — Its Development, Laboratory Testing and Trial Test Results

Dr. Md. Amanullah, Mohammed K. Al-Arfaj, Ahmed E. Gadalla, Rami F. Saleh, Ihab M. El-Habrouk, Bader N. Al-Dhafeeri and Abdullah M. Khayat

ABSTRACT

Saudi Aramco has developed a novel sized particulate lost circulation material (LCM) using eco-friendly natural date seeds as the raw material. The Kingdom of Saudi Arabia generates more than 150,000 tons of date seeds each year as a waste byproduct. Currently, there is no industrial use for the vast amount of date seeds available in the Kingdom. Because there is a sustainable source of date seeds in the Kingdom, they are a potential raw material for local product development, which is needed to reduce import costs and fulfill the goals of Vision 2030 of Saudi Arabia. Their use here will boost the growth of local industries and enterprises, create new job opportunities for the local communities and uplift the social and economic condition of the date farming communities.

Experimental evaluation of the mechanical characteristics of the various date seeds available in the Kingdom indicated their suitability for developing sized particulate LCMs since most of them have similar physical and mechanical characteristics. While some seeds showed relatively inferior mechanical behavior compared to others, they can still be used in combination with other date seeds for preparing sized particulate LCMs without any major impact on the behavior of the admixture. Therefore, a single type of date seed or a blend of all the date seeds can be used as the raw material. Based on this assumption, a novel sized particulate LCM, named "ARC plug," has been developed using a blend of various date seeds as the raw material.

The performance of the newly developed, date seed-based sized particulate LCM, or ARC plug, was evaluated using a permeability plugging test (PPT) apparatus with a 2 mm slotted disc at 250 °F and 1,500 psi pressure. A commercially equivalent product derived from walnut shells was also evaluated for comparison with the performance of the date seed-based ARC plug. The results demonstrated the good sealing and plugging efficiency of the ARC plug with virtually no loss of whole mud.

To find out if the ARC plug performance in the lab changed under field conditions, two trial tests were conducted in two different hole sections of offset wells that showed partial losses. The trial tests showed effective control of partial losses in these hole sections, which confirmed the same sealing and plugging behavior observed in the laboratory. The ARC plug also fulfilled all the key performance indicators in the comprehensive evaluation. Based on the laboratory and field trial test results, it can be concluded that the locally developed, date seed-based sized particulate ARC plug is a viable alternative to imported sized particulate LCM products supplied by various vendors and service companies.

INTRODUCTION

Historical analyses surveying challenges encountered while drilling indicate that loss of circulation is one of the major challenges while drilling in Saudi Aramco fields. It increases the total drilling cost significantly due to the exponential increase in nonproductive time (NPT) that it causes, especially in extreme drilling environments. It is a particular drilling challenge in the Middle East due to the unique characteristics of the subsurface geology of this region. In addition to creating problems by itself, loss of circulation can also trigger other drilling problems, such as borehole instability, kick and blowout, pipe sticking, etc., which can increase the NPT dramatically as well[1]. As a result, it can be a very costly drilling problem if not controlled immediately after its occurrence.

Even a single loss of circulation event, once problems start to cascade, can lead to huge monetary losses up to a million dollars or more[2]. Therefore, preventing loss of circulation is a much better strategy than trying to cure it once it happens. The huge number of uncertainties and unknown factors associated with subsurface formations and loss zone characteristics, however, make it difficult to prevent loss of circulation in many cases. As a result, a drilling strategy should include all corrective/curative measures and arrangements to eliminate or minimize any scope of losses while drilling or cementing a wellbore.

To prevent loss of circulation early on, appropriate loss circulation materials (LCMs) or a suitable LCM blend is usually incorporated into an active mud system to take action immediately once the well starts to take losses. The main objective of this type of preventive strategy is to strengthen the near wellbore formation and increase the fracture gradient of the formation, which will widen the mud weight window and reduce the scope of the induced loss of circulation[3]. Experts have developed several models to predict the strengthening effect on the near wellbore formation of this preventive method using LCMs. One of the models that predicts the near wellbore strengthening effect is the stress cage model described by Alberty and McLean (2004)[4].

This prediction model is based on the linear elastic fracture mechanic theory. According to this theory, an increase in the near wellbore hoop stress due to the bridging or wedging effect of LCMs will improve the fracture gradient of the formation and so forestall the induced loss of circulation. Other models include the fracture closure model described by Dupriest (2005)[5] and the elastic-plastic fracture model described by Aadnoy and Belayneh (2004)[6]. These models also highlight the effect of LCMs on curing the losses as soon as they occur by increasing the fracture gradient of the near wellbore formation.

The corrective or curative strategy involves taking certain action to address the loss after a loss of circulation event has occurred. In this approach, LCMs are added continuously to an active mud system to control the loss to an acceptable level or cure it totally, if possible. Alternatively, LCMs designed in pill form are spotted at the loss zone to control or prevent the mud losses. This type of corrective approach requires a special design strategy that specifies the mixing procedure and placement techniques for successful completion of the LCM treatment. Sometimes, a rapidly dehydrating slurry designed to combat loss of circulation is used in depleted, poorly consolidated, highly permeable, super-K, fractured and vugular formations. According to Wang et al. (2005)[7], LCMs that are capable of creating deformable, viscous and cohesive plugs are likely to be more effective in the corrective approach to loss of circulation due to their favorable physical properties, such as cohesiveness, ductility, flexibility, etc.

Given the variation in the intensity of mud losses and in the nature of the formations causing such losses, different types of LCMs, such as fibrous, flaky or granular LCMs, engineered blends, gel-forming materials, etc., have been developed to control loss of circulation.

Drilling reports use two major criteria to classify loss of circulation. Depending on the hourly loss of drilling mud, it is classified as seepage, moderate or severe; and depending on the amount of mud returning from the wellbore to the surface, it is classified as partial or complete. In cases of complete loss of circulation, there is no return of flow, while for partial loss of circulation, there is some return of the drilling mud to the surface. Various types of conventional LCMs composed of fibrous, flaky and sized particulates are commonly used to control partial loss of circulation[8, 9]. Currently, Saudi Aramco imports all of these conventional LCM products because the Kingdom lacks local alternatives to them. It costs a huge amount of foreign currency each year to import these LCMs. Therefore, the establishment of conventional LCM production using locally available raw materials would cost much less while providing a sustainable source of affordable LCM products for controlling partial loss of circulation.

A granular LCM is frequently used in controlling natural and induced loss of circulation. It is also used in strengthening the near wellbore formation to widen the mud weight window. According to Nayberg (1987)[10] and Howard and Scott (1951)[11], sized particulate LCMs, i.e., granular LCMs, are capable of forming a seal or bridge at the formation face or within the fracture to prevent the loss of whole mud into thief zones. Examples of the materials composing the granular LCMs used by the oil and gas industry are ground or sized limestone, marbles, wood granules, nut shells, formica particles, etc. These LCMs are used either alone in strengthening the near wellbore formation or in combination with other loss control additives to prevent moderate to severe loss of circulation. They can easily be produced locally in Saudi Arabia by using the waste seeds of the date farming industry.

The date farming industry in both the Kingdom and the whole Middle East produces various waste byproducts, such as date seeds, dead palm trees, yearly pruning wastes, fruit-bearing panicles and caps, etc., in huge quantities each year. The date seeds could be a source of sustainable raw materials for manufacturing various mud additives locally[1]. Due to the organic nature of the raw materials, mud additives derived from them would be eco-friendly, nontoxic and biodegradable. As a result, these plant-based green products would play an important role in protecting the Kingdom's environment. They are also in line with the industry's constant shift toward green products/additives for oil and gas field applications in response to the enactment of increasingly strict environmental laws and regulations by regional and global environmental protection agencies. This shfit is reflected in the increasing number of research activities directed toward finding or developing virtually nontoxic, readily biodegradable and environmentally benign green chemicals and polymers for designing high performance drilling and completion fluids[12-14].

Date seeds are one of the major green waste products produced by the date palm industry. They are a prominent candidate for use in green products and mud additives developed locally for oil and gas field applications. Due to the good mechanical properties of date seeds, they could be used to make good quality sized particulate LCMs to replace the equivalent commercial products now imported by Saudi Aramco.

This article describes the laboratory and field tests that evaluated the performance of the locally developed, date seed-based sized particulate LCM named "ARC plug" to demonstrate its suitability as an alternative to commercial products.

TYPES OF DATE SEEDS

Various types of date fruits are produced in the Kingdom, leaving behind a wide variety of date seeds as waste byproducts. The various types of date seeds available in the Kingdom may have noticeable variations in chemical composition, physical characteristics, mechanical properties, etc. Compositional analyses using appropriate techniques and technologies can provide the chemical composition of date seeds, along with the types and amount of minerals and bioactive compounds, such as fibers and polyphenols, present in them. Physical analyses can provide information about the size, shape, ovality, density, moisture content, water absorption capacity, etc., of each of the various types of date seeds available. Mechanical characterization can provide information on the strength, stiffness, hardness, toughness, ductility, impact resistance, etc., of the various available date seeds. Any of these parameters can be used to assess the date seeds' similarities or dissimilarities from a mechanical point of view.

These mechanical characteristics of the various date seeds are important if they are to be used as a raw material for sized particulate LCMs in oil and gas field applications. For comparison, the toughness of commercial sized particulate LCMs was first evaluated using a patented method. A detailed description of the method can be found in Amanullah et al. (2011)[12]. The goal of the following evaluation of date seed toughness, i.e., enough resistance to hydrodynamic and mechanical impact force to prevent disintegration and size reduction, was to identify the types of date seeds with the best resistance. Material toughness is measured by the percentage of loss after two hours of rolling in a test cell that simulates an aggressive hydrodynamic environment and a scaled down version of the impact force condition of a borehole environment. Date seed-based LCMs need to show similar or equivalent performance to that of currently used granular LCMs.

The types of seeds and their stability index determined from that evaluation are shown in Table 1, summarized in a loss-on-grinding index (LOGI) value. The experimental data clearly indicate that the sized particulate LCMs developed using various date seeds have very similar material toughness, with the exception of LCMs made of Shahal, Khalas and Hatemy date seeds. The difference is not significant, however; compare the LOGI values for those seeds to the values of conventional equivalent sized particulate LCM materials ("Nut Plug"). In general, all of the date seeds showed acceptable mechanical properties and demonstrated their enormous potential as locally available raw materials for local production of sized particulate LCMs to be used as an alternative to imported sized particulate LCM products. Therefore, all these seeds as a whole can be used in manufacturing the sized particulate LCMs irrespective of the type and source of the seeds.

DATE SEEDS AVAILABLE PER YEAR

Date farming is one of the major agricultural sectors in the arid and semi-arid regions of the world, especially in the dry Middle East and North Africa regions. Statistical information indicates that there are more than 120 million date trees worldwide, which produce huge quantities of date fruits as well as waste date seeds per year. According to the statistical data of the Food and Agricultural Organization of the United Nations[15], more than 7 million tons of date fruits were produced worldwide in 2010. The top 10 countries producing date fruits are Egypt, Iran, Saudi Arabia, United Arab Emirates (UAE), Pakistan, Algeria, Sudan, Iraq, Oman and Libya. They provide more than 90% of the world's total date production. According to the *Al-Watan* newspaper (September 25, 2003), the number of registered palm trees in Saudi Arabia stands at 20 million. This is in addition to the 3.7 million unregistered palm trees in the Kingdom. Based on the historical exponential growth of the date farming industry, the current number of date trees in the Kingdom is likely much higher than the

English Name	Size (Microns+)	Initial Mass (g)	Initial Dry Mass after Washing (g)	Final Dry Mass after Grinding Test (g)	Lost Mass due to Grinding (g)	LOGI
Ruzeiz	600	20	13.95	13.31	0.64	4.59
Shaishee	600	20.24	15.86	15.68	0.18	1.13
Shahal	600	20.2	15.15	13.06	2.09	13.80
Sagae	600	20.04	13.81	13.53	0.28	2.03
Wossely	600	20.13	13	12.7	0.3	2.31
Khalas	600	20.31	18.3	16.79	1.51	8.25
Khalas	600	20.24	18.2	16.29	1.94	10.66
Sefri	600	20.36	14.95	14.68	0.27	1.81
Safawi	600	20.03	13.94	13.78	0.16	1.15
Hatemy	600	20.21	15.1	12.85	2.25	14.90
Hatemy	600	20.2	16.1	14.45	1.65	10.25
Nut Plugs	600	20.33	19.91	18.19	1.72	8.64
Nut Plugs	600	20.57	20.24	18.08	2.16	10.67
$CaCO_3$	600	20.78	20.1	19	1.1	5.47
$CaCO_3$	600	20.37	20.14	19.15	0.99	4.92

Table 1. The LOGI values for various date seed-based sized particulate LCMs, nut plug LCMs and $CaCO_3$ LCMs

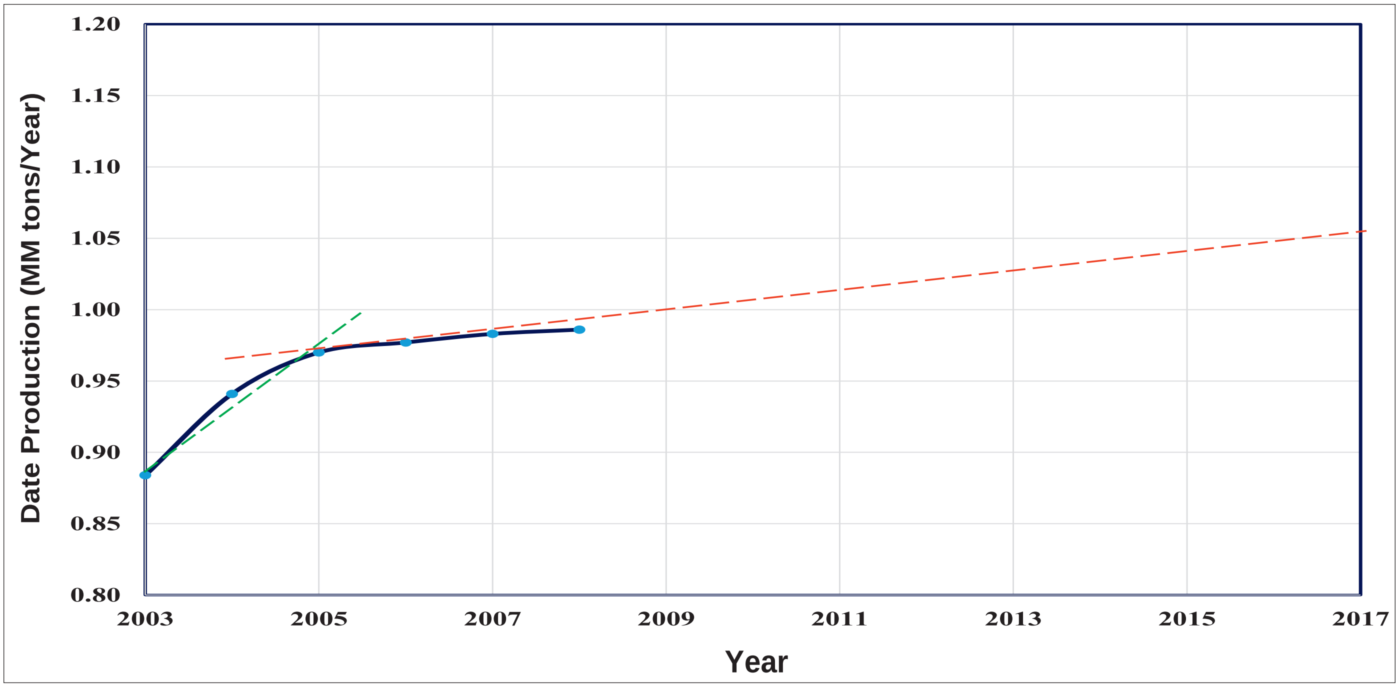

Fig. 1. Year vs. date fruit production history of Saudi Arabia from 2003-2008[16, 17].

registered plus unregistered numbers. According to the *Al-Hayat* newspaper (January 24, 2002), estimated date production in Saudi Arabia is about 800,000 tons per annum, and it is expected to grow to 2 million tons per annum within three to five years. This statistical information highlights the availability of a sustainable source of date tree waste in the Kingdom for use in local development of some mud additives.

An extrapolation of the historical production data of the Kingdom of Saudi Arabia published in MOA (2008)[16] and MOA (2009)[17] is shown graphically in Fig. 1.

The data clearly indicates a bilinear trend line, i.e., rapid growth in the early stage starting from 2003 to 2005 and then progressive growth in the later stage starting after 2005. Extrapolation of the progressive production data trend line indicates about 1.05 million tons of date production in 2017. Assuming the present date production in the Kingdom is about 1.05 million tons per year, we can estimate the amount of waste date seeds available per year as a raw material for manufacturing sized particulate LCMs and other mud additives.

Published information indicates about 11% to 18% of the date fruit weight comes from the date seed[18, 19]. Estimating the average percentage weight of date seeds at about 14.5%, the calculated amount of date seeds available as a waste byproduct in the Kingdom is more than 150,000 tons per year. Verbal communication from the Al-Hasa Date Research Center also indicated the availability of more than 150,000 tons of date seeds per year as waste byproducts generated from various date processing plants, such as factories producing pitted dates, date powders, date syrup, date juice, chocolate-coated dates, date confectionery, etc. Currently, most of the date seeds are discarded as there is no major industrial use for them in the Kingdom or in the Middle Eastern region. Only a minor quantity is used as animal feed or solid fuel; some date seeds are roasted and ground into smaller sizes to use as a caffeine-free coffee substitute or to mix with normal coffee[20]. Therefore, a huge amount of waste date seeds is available as a raw material for various products and additives used in different industrial applications.

Given the long-lasting and sustainable source of date seeds in the Kingdom alone, it is a highly viable raw material for local development of products for oil and gas field applications. If we consider the whole Middle Eastern region, the amount of date seeds available to use as a raw material to produce additives for oil and gas field applications is more than enough not only for local consumption but also for the global consumption.

ARC PLUG MANUFACTURING PROCESS

Figure 2 is a flow diagram of the preparation process for making the date seed-based sized particulate LCM or ARC plug. Initially, waste date seeds are collected from various date processing plants. The leftover skin of the date flesh is removed by washing the date using the hydrodynamic forces of a water jet and the mechanical agitation forces of vanes fitted in a closed loop circulation system. The date seeds are collected in a large bag placed at the outlet of the close loop washing system. The

Fig. 2. Flow diagram for manufacturing the ARC plug, a date seed-based sized particulate LCM.

seeds are next routed through a rotating heating drum to dry before crushing and grinding. The thermal treatment of the seeds improves the ability to grind the date seeds into various size ranges.

For bulk production of date seed-based sized particulate LCMs, an industrial grade washing system, dryer, crusher, grinder and sieves of various sizes would be required to produce large quantities of the material within a short processing time. Particle size distribution is varied to meet the operational requirements of a particular field.

PHYSIO-MECHANICAL CHARACTERISTICS

Various physical tests, such as tests measuring moisture content, specific gravity, bulk density and volumetric swelling, along with chemical and mechanical tests, such as an acid solubility test and a loss-on-grinding test, were conducted to characterize the date seed-based sized particulate LCM product for comparison with a widely used sized particulate LCM product available in the market. Table 2 shows the characteristic parameters of the date seed-based ARC plug along with the characteristic parameters of the walnut shell-based commercial sized particulate LCM. The results demonstrate the suitability of the newly developed date seed-based ARC plug as an alternative to and/or substitute for commercial sized particulate LCMs derived from walnut shells.

MUD SYSTEMS USED FOR ARC PLUG PERFORMANCE EVALUATION

Four different water-based muds commonly used in drilling operations were selected to evaluate the performance of the ARC plug using a standard permeability plugging test (PPT) apparatus. Table 3 shows the mud systems along with the concentrations of the ARC plug and the equivalent commercial walnut shell-based particulate LCM product used in the evaluation.

LABORATORY TESTING AND EVALUATION OF ARC PLUG PERFORMANCE

Figure 3 shows the PPT apparatus used to evaluate the performance of the newly developed, date seed-based sized particulate LCM ARC plug. It consists of a 500 ml cell that has a movable piston at the bottom to pressurize the LCM containing mud system. The tests were conducted by incorporating 10 ppb and 30 ppb date seed-based sized particulate LCMs into a 65 pcf bentonite mud, 80 pcf NaCl polymer mud, 73 pcf KCl polymer mud and 90 pcf $CaCl_2$ polymer mud.

The ARC plug LCM was mixed properly into the mud system for a homogeneous distribution of the sized particles into

Fig. 3. PPT apparatus and the 2 mm slotted disc used for testing the ARC plug.

Specifications	Date Seed-based Particulate LCM (ARC Plug)	Walnut Shell-based Particulate LCM
Physical Appearance	Light Brown	Tan to Brown
Specific Gravity	1.3 to 1.4	1.2 to 1.4
Water Solubility	Insoluble	Insoluble
Acid Solubility	Insoluble	Insoluble
Bulk Density	0.60 to 0.75 gm/cc	0.58 to 0.64 gm/cc
LOGI	< 8%	< 8%
Volumetric Swelling	0.38 cc/gm	0.27 cc/gm
Moisture Content	< 5%	< 5%

Table 2. Comparison of date seed-based and walnut shell-based sized particulate LCMs

Mud Systems	Date Seed-based Particulate LCM — ARC Plug (ppb)		Walnut Shell-based Particulate LCM (ppb)	
65 pcf Bentonite Mud	10	30	10	30
73 pcf KCl Polymer Mud	10	30	10	30
80 pcf NaCl Polymer Mud	10	30	10	30
90 pcf $CaCl_2$ Polymer Mud	10	30	10	30

Table 3. Mud systems and sized particulate LCM concentrations used in tests

the mud system, and then a sample of the mud was placed into the test cell. Next, a 2 mm slotted disc was fixed at the appropriate position on the test cell. Then a top cap with a slightly greater slot aperture (> 2 mm) was fixed above the slotted disc for collecting any drilling fluid lost during the test interval. During the test, the cell was heated to a temperature of 250 °F, and a pressure of 1,500 psi was applied at the bottom of the test cell using a hand pump. A built-in heating jacket surrounding the test cell allowed the heating of the LCM containing drilling mud to simulate its exposure to a comparable bottom-hole temperature.

Two different concentrations of the sized particulate ARC plug were tested and evaluated. A commercial sized particulate LCM, manufactured using walnut shells as the raw materials, was also tested using the same mud systems, a similar concentration and identical test conditions for comparative evaluation of the performance of the newly developed, date seed-based sized particulate LCM.

DISCUSSION

Table 4 shows the conventional walnut shell-based (nut plug) and the newly developed, date seed-based (ARC plug) sized particulate LCM performances at 10 ppb and 30 ppb concentrations in the presence of a 65 pcf unweighted bentonite mud. The tests assess the bridging and plugging efficiency of each sized particulate LCM by whether it forms an impermeable barrier or plug in the constant area's natural fracture simulating slots of the slotted disc. Compared to the commercial walnut shell-based sized particulate LCM, a very similar performance in sealing and blocking is seen for the date seed-based sized particulate ARC plug at 10 ppb concentration and a similar sealing and plugging performance is seen at 30 ppb concentration.

In spite of the high differential pressure — 1,500 psi — the newly developed, date seed-based sized particulate LCM showed complete sealing and blocking within a very short time, just like the conventional walnut shell-based sized particulate LCM. This is reflected by the fact that both the commercial and the newly developed sized particulate LCM products saw virtually no loss of mud spurt, mud filtrate or whole mud during the PPTs. The similar performance of the newly developed, date seed-based sized particulate ARC plug compared to the commercial walnut shell-based sized particulate nut plug demonstrates the ARC plug's suitability as a viable alternative to the imported product. The date seed-based sized particulate LCMs are therefore a reliable, locally made substitute for the commercial sized particulate LCMs for use in preventing and correcting loss of circulation, and also in formation strengthening while drilling.

Table 5 shows the plugging efficiency test results conducted by incorporating 10 ppb and 30 ppb date seed-based and walnut shell-based sized particulate LCMs into a 73 pcf KCl polymer mud. The results again show the effective sealing and blocking efficiency of the date seed-based sized particulate LCM, both at 10 ppb and at 30 ppb concentrations, like the commercially available and widely used walnut shell-based sized particulate LCMs.

The results further indicate that the date seed-based sized particulate LCMs can be incorporated in saltwater-based mud to combat loss of circulation while drilling without compromising the performance of the LCMs. That it has a sealing and plugging performance similar to that of the commercial walnut shell-based sized particulate LCMs undoubtedly proves its ability to replace the commercially available imported products.

Table 6 shows the plugging efficiency test conducted by incorporating 10 ppb and 30 ppb date seed-based and walnut shell-based sized particulate LCMs into an 80 pcf NaCl polymer mud. The results clearly indicate the effective sealing and blocking capacity of both the date seed-based and walnut shell-based sized particulate LCMs. This again proves the suitability of the date seed-based sized particulate LCMs in replacing the

Mud System	LCM	Concentration	Spurt Loss	Fluid Loss	Total Leakoff	Cake Thickness	PPT Value
65 pcf Bentonite Mud	ARC Plug	10 ppb	0	0.2	0.2	N/A	0.4
65 pcf Bentonite Mud T2	Nut Plug	10 ppb	0	0	0	N/A	0
65 pcf Bentonite Mud	ARC Plug	30 ppb	0	0	0	N/A	0
65 pcf Bentonite Mud	Nut Plug	30 ppb	0	0	0	N/A	0

Table 4. Comparison of the sealing and blocking efficiency of date seed-based and walnut shell-based LCMs in unweighted bentonite mud

Mud System	LCM	Concentration	Spurt Loss	Fluid Loss	Total Leakoff	Cake Thickness	PPT Value
73 pcf KCl Polymer Mud	ARC Plug	10 ppb	0	0	0	N/A	0
73 pcf KCl Polymer Mud T3	Nut Plug	10 ppb	0	0	0	N/A	0
73 pcf KCl Polymer Mud	ARC Plug	30 ppb	0	0	0	N/A	0
73 pcf KCl Polymer Mud	Nut Plug	30 ppb	0	0	0	N/A	0

Table 5. Comparison of the sealing and blocking efficiency of date seed-based and walnut shell-based LCMs in KCl polymer mud

Mud System	LCM	Concentration	Spurt Loss	Fluid Loss	Total Leakoff	Cake Thickness	PPT Value
80 pcf NaCl Polymer Mud	ARC Plug	10 ppb	0	0	0	N/A	0
80 pcf NaCl Polymer Mud T2	Nut Plug	10 ppb	0	0	0	N/A	0
80 pcf NaCl Polymer Mud	ARC Plug	30 ppb	0	0	0	N/A	0
80 pcf NaCl Polymer Mud	Nut Plug	30 ppb	0	0	0	N/A	0

Table 6. Comparison of the sealing and blocking efficiency of date seed-based and walnut shell-based LCMs in NaCl polymer mud

Mud System	LCM	Concentration	Spurt Loss	Fluid Loss	Total Leakoff	Cake Thickness	PPT Value
90 pcf $CaCl_2$ Polymer Mud	ARC Plug	10 ppb	0	0	0	N/A	0
90 pcf $CaCl_2$ Polymer Mud	Nut Plug	10 ppb	0.1	2.8	2.9	N/A	5.8
90 pcf $CaCl_2$ Polymer Mud	ARC Plug	30 ppb	0	0	0	N/A	0
90 pcf $CaCl_2$ Polymer Mud	Nut Plug	30 ppb	0	0	0	N/A	0

Table 7. Comparison of the sealing and blocking efficiency of date seed-based and walnut shell-based LCMs in $CaCl_2$ polymer mud

commercially available imports.

The results also further demonstrate that the compositional variation of the water-based muds used in this study had no effect on the date seed-based sized particulate LCM's technical performance in creating flow barriers or an impermeable plug.

Table 7 shows the plugging efficiency test conducted by incorporating 10 ppb and 30 ppb date seed-based and walnut shell-based LCMs into a divalent salt containing 90 pcf $CaCl_2$ polymer mud. The results demonstrate the effective sealing and blocking capacity of the date seed-based sized particulate LCMs even in the presence of a divalent salt-containing water-based mud.

Field Trial Results and Observation

Two field trials were conducted to evaluate the performance of the newly developed product under downhole conditions. The selection of candidate wells was based on the anticipated severity of the loss of circulation as determined from the offset wells' data. Because the ARC plug was designed to tackle partial loss of circulation events, the two trial tests were carried out in hole sections where mud losses of up to 80 bbl/hr were most likely to be encountered.

For the first field trial, the ARC plug was used as a background additive to the drilling fluid while drilling the anticipated loss zone. The incorporated ARC plug had no detrimental effect on mud properties and was easily pumpable. No mud losses were encountered while drilling. The field trial results confirmed the observations and findings noted during the laboratory evaluation. The particulate nature of the LCM, along with the adequate mechanical properties of the date seeds, allow it to be used as both sealing and bridging materials. It can also be used as a formation strengthening material like commercial bridging-type LCM products.

For the second field trial, the ARC plug was used in the form of a LCM pill after partial losses were encountered while drilling with water-based drilling fluid. Losses started with 160 bph dynamic losses. After pumping two LCM pills with concentrations of 120 ppb and 170 ppb — of which the ARC plug concentrations were 25 ppb and 30 ppb, respectively — losses were partially cured, and ultimately 90% circulation was achieved. The ARC plug showed trouble-free mixing and pumping, and no settlement was observed in the mixing tank. The results from the ARC plug trial tests indicated that the date seed-based sized particulate LCM is a viable local alternative to imported particulate LCMs.

SOCIAL AND ECONOMIC SIGNIFICANCE

The use of waste date seeds to produce sized particulate LCMs will act as a catalyst in encouraging the growth of local industries and enterprises while also creating new job opportunities for the public. It will provide an economic route for recycling palm tree wastes to the benefit of the farming communities. Due to a sustainable source of supply of these raw materials in the Kingdom, it ensures an uninterrupted supply of sized particulate LCMs in the Kingdom no matter the geopolitical situation. The local product development will save foreign currency by reducing the import cost and will also contribute to the growth of the regional as well as the national economy.

CONCLUSIONS

1. The newly developed, date seed-based sized particulate LCM, the ARC plug, has similar or better physical and mechanical properties compared to those of the conventional walnut shell-based sized particulate LCMs provided by service companies.
2. A huge and sustainable supply of waste date seeds accumulates in the Kingdom each year for use in local production of sized particulate LCMs and bridging material.
3. Date seeds are a locally available, eco-friendly, nontoxic and

biodegradable agro-based waste material that can be used to produce green mud additives and ensure a greener environment for future generations.

4. Experimental results indicate that the ARC plug's mechanical properties are similar to or better than those of the conventional sized particulate LCMs, and it is expected to tolerate similar overburden pressure and downhole attrition.
5. Water absorption tests indicate a higher volumetric swelling potential for the ARC plug compared to that of widely used commercially available sized particulate LCMs. Therefore, the ARC plug can create a stronger bridge in the gap due to tighter particle-particle and particle-gap wall contacts.
6. Use of a locally available, agri-based waste material in the production of sized particulate LCMs will accelerate the growth and development of local industries and enterprises along with the improvement of the social and economic condition of the date farming communities.
7. Local product development using available local resources will create new job opportunities for the public and therefore contribute to the growth of the local and national economy.
8. Field trial results and observations confirmed the performance and behavior observed in the laboratory. Therefore, the ARC plug is a viable alternative to equivalent commercial products.
9. The waste date seeds generated yearly in the Middle East region can provide a sustainable supply for production of the sized particulate LCMs, not only for the Middle East region, but also for the global market.
10. The oil and gas industry application of the date seed-based additives and products will act as a catalyst for the growth of local industries and enterprises.

ACKNOWLEDGMENTS

The authors would like to thank the management of Saudi Aramco and the EXPEC Advanced Research Center for their support and permission to publish this article. Our sincere thanks to Eric Mollendick, Chief Technologist, DTT, for his encouragement and support for this innovative research. Special thanks to Turkie Alsubaie and Ali Radwan for their testing and evaluation of the product, and Raed Alouhali for reviewing this article.

This article was presented at the SPE Kingdom of Saudi Arabia Annual Technical Symposium and Exhibition, Dammam, Saudi Arabia, April 24-27, 2017.

REFERENCES

1. Amanullah, M.: "Characteristics, Behavior and Performance of ARC Plug — A Date Seed-based Sized Particulate LCM," SPE paper 182840, presented at the SPE Kingdom of Saudi Arabia Annual Technical Symposium and Exhibition, Dammam, Saudi Arabia, April 25-28, 2016.
2. Kumar, A. and Savari, S.: "Loss Circulation Control and Wellbore Strengthening: Looking beyond Particle Size Distribution," paper AADE-11-NTCE-21, presented at the AADE National Technical Conference Exhibition, Houston, Texas, April 12-14, 2011.
3. Salehi, S. and Nygaad, R.: "Numerical Modeling of Induced Fracture Propagation: A Novel Approach for Lost Circulation Materials (LCM) Design in Borehole Strengthening Applications of Deep Offshore Drilling," SPE paper 135155, presented at the SPE Annual Technical Conference and Exhibition, San Antonio, Texas, October 8-10, 2012.
4. Alberty, M.W. and McLean, M.R.: "A Physical Model for Stress Cages," SPE paper 90493, presented at the SPE Annual Technical Conference and Exhibibition, Houston, Texas, September 26-29, 2004.
5. Dupriest, F.E.: "Fracture Closure Stress (FCS) and Loss Return Practices," SPE paper 92192, presented at the SPE/IADC Drilling Conference, Amsterdam, the Netherlands, February 23-25, 2005.
6. Aadnoy, B.S. and Belayneh, M.: "Elasto-plastic Fracturing Model for Wellbore Stability Using Nonpenetrating Fluids," *Journal of Petroleum Science and Engineering*, Vol. 45, Issues 3-4, December 2004, pp. 179-192.
7. Wang, H., Sweatman, R.E., Engelman, R.E., Deeg, W.F.J., et al.: "The Key to Successfully Applying Today's Lost Circulation Solutions," SPE paper 95895, presented at the SPE Annual Technical Conference and Exhibition, Dallas, Texas, October 9-12, 2005.
8. White, R.J.: "Lost Circulation Materials and Their Evaluations," API paper 56-352, presented at the Drilling and Production Practice Conference, New York, New York, January 1, 1956.
9. Whitfill, D.L.: "Lost Circulation Materials Selection, Particle Size Distribution, and Fracture Modeling with Fracture Simulation Software," SPE paper 115039, presented at the IADC/SPE Asia Pacific Drilling Technical Conference and Exhibition, Jakarta, Indonesia, August 25-27, 2008.
10. Nayberg, T.M.: "Laboratory Study of Lost Circulation Materials for Use in Both Oil-based and Water-based Drilling Muds," *SPE Drilling Engineering*, Vol. 2, Issue 3, September 1987, pp. 229-236.
11. Howard, G.C. and Scott Jr., P.P.: "An Analysis and the Control of Lost Circulation," *Journal of Petroleum Technology*, Vol. 3, Issue 6, June 1951, pp. 171-182.
12. Amanullah, M., Bubshait, A., Allen, T.J. and Foreman, D.: "The Aramco Method — Its Drilling and Production

Engineering Significance," SPE paper 149103, presented at the SPE/DGS Saudi Arabian Section Technical Symposium and Exhibition, al-Khobar, Saudi Arabia, May 15-18, 2011.

13. Tehrani, A., Young, S., Gerrard, D. and Fernandez, J.: "Environmentally Friendly Water-based Fluid for HPHT Drilling," SPE paper 121783, presented at the SPE International Symposium on Oil Field Chemistry, The Woodlands, Texas, April 20-22, 2009.
14. Rae, P., Di Lullo, G. and Ahmad, A.B.: "Toward Environmentally Friendly Additives for Well Completion and Stimulation Operations," SPE paper 68651, presented at the SPE Asia Pacific Oil and Gas Conference and Exhibition, Jakarta, Indonesia, April 17-19, 2001.
15. FAO (Food and Agriculture Organization of United Nations), 2010: Statistical Databases available at website http://faostat.fao.org.
16. MOA: *Agricultural Statistical Yearbook,* Vol. 21, Department of Studies Planning and Statistics, Agricultural Research and Development Affairs, Ministry of Agriculture, Kingdom of Saudi Arabia, 2008.
17. MOA: *Agricultural Statistical Yearbook,* Vol. 22, Department of Studies Planning and Statistics, Agricultural Research and Development Affairs, Ministry of Agriculture, Kingdom of Saudi Arabia, 2009.
18. Besbes, S., Blecker, C., Deroanne, C., Drira, N-E., et al.: "Date Seeds: Chemical Composition and Characteristic Profiles of the Lipid Fraction," *Food Chemistry*, Vol. 84, 2004, pp. 577-584.
19. Nehdi, I., Omri, S., Khalil, M.I. and Al-Resayes, S.I.: "Characteristics and Chemical Composition of Date Palm (Phoenix canariensis) Seeds and Seed Oil," *Industrial Crops and Products*, Vol. 32, November 2010, pp. 360-365.
20. Rahman, M.S., Kasapis, S., Al-Kharusi, N.S.Z., Al-Marhubi, I.M., et al.: "Composition, Characterization and Thermal Transition of Date Pits Powders," *Journal of Food Engineering*, Vol. 80, 2007, pp. 1-10.

BIOGRAPHIES

Dr. Md. Amanullah is a Senior Petroleum Engineering Consultant working at Saudi Aramco's Exploration and Petroleum Engineering Center – Advanced Research Center (EXPEC ARC). Prior to joining Saudi Aramco, he worked as a Principal Research Scientist at CSIRO in Australia.

Aman is the lead inventor of a vegetable oil-based dielectric fluid (patented) that led to the formation of a spinoff company in Australia for commercialization of the product.

He has published more than 85 technical papers and filed 43 patents, with 10 already granted. Two of Aman's patents were highlighted in scholarly editions of two books published in the U.S.

He is one of the recipients of the 2005 Green Chemistry Challenge Award from the Royal Australian Chemical Institute. Aman also received the CSIRO Performance Cash Reward in 2006, the Saudi Aramco Mentorship Award in 2008 and 2010, the World Oil Certificate Award for nano-based drilling fluid development in 2009, the Intellectual Asset Recognition Award in 2014, and the Award of Recognition for Outstanding Contribution to the success of agricultural waste and environmental protection in 2014. His date tree waste-based product development was highlighted in *The Arabian Sun*, the *Arab News* and also in the Al Riyadh newspaper.

Aman is a member of the Society of Petroleum Engineers (SPE). He received the SPE Regional Service Award in 2014 and also SPE Middle East Drilling Engineering Award in 2016 for his contribution to the industry.

Aman received his M.S. degree (First Class) in Mechanical Engineering from the Moscow Oil and Gas Institute, Moscow, Russia, and his Ph.D. degree in Petroleum Engineering from Imperial College, London, U.K.

Mohammed K. Al-Arfaj joined Saudi Aramco in 2006 as a Petroleum Engineer, working with the Drilling Technology Team in the Exploration and Petroleum Engineering Center – Advanced Research Center (EXPEC ARC). He works in the area of drilling and completion, and has conducted several projects in the areas of shale inhibition, drilling nano-fluids, loss circulation materials, spotting fluids, swellable packers, completion fluids and oil well cementing.

Mohammed received his B.S. degree in Chemical Engineering from King Fahd University of Petroleum and Minerals (KFUPM), Dhahran, Saudi Arabia, in 2006. In 2009, he received his M.S. degree in Petroleum Engineering from Heriot-Watt University, Edinburgh, Scotland. Mohammed is currently pursuing a Ph.D. degree in Petroleum Engineering from KFUPM.

Ahmed E. Gadalla joined Saudi Aramco in September 2014 as a Drilling Engineer working in the Drilling Operations Support Unit of the Drilling Technical Department. He has over 18 years of experience in technical and operational procedures, including coordination and supervision of onshore and offshore operations in several countries. Ahmed was trained as a Drilling and Completion Fluids Engineer and has advanced knowledge in the design and field application of oil-based drilling systems (invert emulsions, 100% oil) and water-based systems (conventional, high performance and drill-in fluids).

He received his B.S. degree in Geology from Menoufia University, Al Minufya, Egypt.

Rami F. Saleh is a Drilling Engineering Division Head in the Exploration and Oil Drilling Engineering Department of Saudi Aramco. He has over 15 years of experience in drilling engineering and operations. This experience ranges from onshore and offshore rigs to deep gas drilling, exploration and shale gas drilling, and oil increment development, including the giant Khurais field, and most recently, the Shaybah field expansion increment.

Rami has published several technical papers related to drilling optimization, and he participated in several international technical panels on the subject of drilling automation. He is an active member of the Society of Petroleum Engineers (SPE) and the Saudi Association of Energy Economics, and he is a certified SPE Petroleum Engineer.

Rami received his B.S. degree in Mechanical Engineering from Tufts University, Medford, MA, and his M.S. degree in Petroleum Engineering from Institut Francais du Petrole (IFP), Rueil-Malmaison, France.

Ihab M. El-Habrouk joined Saudi Aramco in July 2014 as a Drilling Fluid Specialist working in the Drilling Operations Support Unit of the Drilling Technical Department. He has over 24 years of oil field experience in technical and operational procedures, including project engineering management of onshore and offshore operations in different countries. Ihab was trained as a Drilling and Completion Fluids Engineer and has advanced knowledge in the design and field application of different types of oil-based and water-based drilling fluids systems.

He has a filed patent, and is a member of the Society of Petroleum Engineers (SPE).

Ihab received his B.S. degree in Mechanical Engineering from Alexandria University, Alexandria, Egypt.

Bader N. Al-Dhafeeri is a Drilling Engineering Supervisor in the High-Pressure Gas Exploration Division of Saudi Aramco's Exploration and Oil Drilling Engineering Department. He joined Saudi Aramco in 2005 and since then has worked in several field development projects such as South Ghawar, Manifa and the Abu Hadriya, Fadhili and Khursaniyah project.

Bander received his B.S. degree in Petroleum Engineering from the University of Tulsa, Tulsa, OK, and his M.S. degree in Petroleum Engineering from Heriot-Watt University, Edinburgh, U.K.

Abdullah M. Khayat is a Petroleum Engineer with Saudi Aramco's Northern Area Oil Operations Drilling Team of the Drilling and Workover organization. His areas of expertise include reservoir engineering, directional drilling, and extending reach drilling engineering and operations.

Abdullah received his B.S. degree in Petroleum Engineering from the University of Louisiana at Lafayette, Lafayette, LA.

Thermal and Geomechanical Dynamics of High-Power Electromagnetic Heating of Rocks

Dr. Damian P. San-Roman Alerigi, Dr. Yanhui Han and Dr. Sameeh I. Batarseh

ABSTRACT

Perforation is an essential step in the cased completion of oil and gas wells, since it provides channels for hydrocarbon fluids to flow from the reservoir into production wells. Traditional methods for perforation cause plastic compaction, resulting in permeability loss in the rock around the perforation channels and reduction of the hydraulic conductivity in the surrounding rock formation. A feasible alternative is to use high-power electromagnetic (HPEM) sources to induce a localized phase change in the rock via dielectric heating and so create a perforation. This method has several crucial benefits: it is contactless and waterless, it improves conductivity, and it reduces general damage to the rock formation.

The physical dynamics that make this possible have been extensively documented in several experimental studies, and some numerical models have been proposed to simulate the thermal mechanical coupling between the HPEM source and the rock designated for perforation or other stimulation operations. Yet, due to the inherent multiscale complexity of the physics involved, a comprehensive model remains a topic of advanced research. Recently, a numerical scheme has been proposed to predict the perforation geometry and production enhancements as a function of the HPEM source parameters — beam shape and energy distribution — the rock properties and the stress configuration.

This article expands this workflow to investigate the effects of material heterogeneity and stress configuration on the perforation rate and the changes to the rock's morphology resulting from HPEM heating. The numerical model is based on a hybrid COMSOL-FLAC coupling. In a companion article, this model is extended to describe the effect of long-pulsed thermal incidence on rock morphology using the thermal and continuum mechanic modules in FLAC.

INTRODUCTION

Photonic technologies, such as the use of high-power electromagnetic (HPEM) sources, provide a high degree of control and are able to deliver, orient and target electromagnetic (EM) energy with unique precision. These qualities of control have made photonics ubiquitous in modern materials processing and engineering, medicine, defense, aerospace and metallurgy. In the oil and gas industry, the technologies' innate versatility has led to a rich application portfolio, encompassing fracturing, drilling, heat treatment and casing, to name a few.

In the first two cases, HPEM sources notably offer a contactless and waterless alternative to drill through a wide range of rocks, increase the rate of penetration (ROP), improve permeability and reduce damage to the neighboring formation[1]. To assess their efficacy, some of these sources have been tested in the drilling and fracturing of sandstone, limestone and shale in several laboratory experiments. The results show a high ROP compared to conventional methods; this is due to the rapid and localized surge in rock temperature, which leads to a thermo-mechanical response, and consequently, a phase change[2]. This thermo-mechanical dynamic is considerably dependent on the transient and spatial distribution of the HPEM beam and the rock properties[1, 3].

Figure 1 summarizes the thermal, EM and mechanical

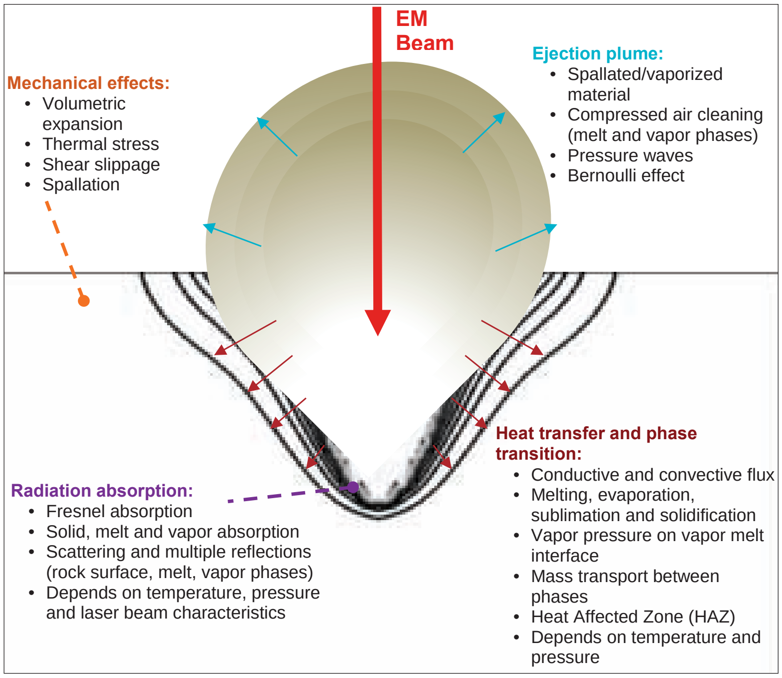

Fig. 1. Schematic representation of the physical dynamics in HPEM field-rock interactions.

physics involved in the EM heating and perforation of rocks. When an HPEM field impinges on a rock, a portion of the incident energy is absorbed and transformed into thermal energy. The stone heats up, which starts a sophisticated thermo-mechanical process that culminates with the rock's vaporization, spallation or melting. What phase change and how the phase change materializes depend on the rock's properties and the structure of the EM heat coupling and flow. For example, if the power is moderate and continuously delivered, the rock will first melt, then dissociate or spall, and finally evaporate. In contrast, if the energy is high enough or switched rapidly, it could sublimate or spall the rock in an instant. These physical dynamics are instantaneous, intricate and extreme, making a careful manipulation of their shape and pace crucial to engineering the next generation of subsurface photonic tools. Therefore, it is essential to understand the underlying physics and build algorithms to predict and optimize their outcome.

To build numerical models, the first step is to quantify and reveal the relations among the vast amount of variables involved. This begins with elucidating a general relation for the specific energy, an analogue of the thermodynamic enthalpy that relates the volume of material (rock) removed to the energy brought to the process[3]. After this step was completed in an earlier study, this relation was applied to explain the effects of both the HPEM irradiation and the rock's porosity, permeability and saturation on the thermodynamic phase change process and perforation geometry. The experimental data collected reveal that the rocks that melted under dielectric heating had larger specific energies than those that dissociated[3-7].

The specific energy can be used to draw a first degree optimization of the HPEM beam parameters for perforation of various rock types under laboratory conditions[1, 3], but it is difficult to predict and optimize the efficiency of the HPEM enabled perforation process under subsurface conditions. Yet, if the process is numerically simulated, then it could be possible to maximize the outcome of the HPEM rock interaction.

A comprehensive numerical model offers a wide prospect: to investigate and improve the process efficiency, to gain greater control and to unlock novel applications. The interaction between the HPEM field and the rocks involves coupled nonlinear processes; consequently, a universal model needs to encompass multiple physics, e.g., EM, thermal, mechanical and fluid dynamics. Over the last three decades, several models have been posited to model these phenomena, with an emphasis on their use in materials processing, yet a comprehensive numerical model remains a work-in-progress. While the fundamental physics are well-known, numerous challenges arise when integrating what is an immanent multiscale problem, given that EM and thermal dynamics occur in temporal and spatial scales several orders of magnitude apart. Furthermore, plenty of technical difficulties complicate the acquisition of the data needed to characterize rocks, minerals and formation fluids over the wide spectrum of temperatures and pressures observed downhole.

The characterization of rock properties in situ can be realized by combining neural networks with experimental methods, in situ measurements and ab-initio simulations[8, 9], and a number of methods have been posited to tackle the former. One possible solution is to separate the dynamics into their constituent physics, evaluate the range of action of each, determine the coupling mechanism and finally integrate a hybrid numerical scheme to calculate the solution[10].

In a recent publication, we used this hybrid numerical method to investigate the effects of continuous HPEM irradiation on idealized sandstone blocks. Our research focused on the thermal mechanical coupling and its effects on the rock structure and geometry. In that context, the HPEM field absorbed by the rock induces a large temperature gradient near the surface of the rock, causes a sudden expansion and triggers a phase change process, all within the heat affected zone.

As the rock transitions through solid, liquid and gaseous phases, the stress condition near the source boundary rapidly transforms from compressive stress to tensile stress. This is due to the elevated heating induced by the HPEM beam on the surface of the rock, which creates an acute temperature gradient near the sample surface and causes a sudden thermal expansion on a time scale of milliseconds. Once the tensile stress becomes larger or equal to the tensile strength, tensile cracking occurs, and fractures are observed near the heat affected zone. If the expansion is unconstrained, then either the temperature induced stress will eventually balance with the boundary loads or the compressive stress will surge. In either case, we showed that locally nonuniform thermal stress could overcome the strength of the rock, resulting in mechanical yielding, such as shearing slip and tensile spallation, which in turn heightens compressive stress[10].

In this article and its companion[11], an expansion on this method is used to characterize the thermal mechanical coupling of HPEM sources and heterogeneous rocks. To this end, the two studies implemented different parametric studies using a hybrid COMSOL-FLAC model and a FLAC3D model, respectively. These articles present an approach to developing a full numerical model that can improve the efficiency of high-power subsurface photonics and predict its effects on the formation rock — i.e., its geometry, morphology and petrology. Ultimately, the intent is to create a numerical assessment tool that guides HPEM assisted or HPEM enabled applications and design operations a priori.

MODELING CONSIDERATIONS

In this section, we briefly review some of the key equations and descriptions that are essential to describing the numerical results. More detailed discussion about the physics and relevant references can be found in San-Roman Alerigi et al. (2016)[10].

Electromagnetic

There are three possible ways to account for the absoprtion of the HPEM field by the rock: a full-wave method that solves Maxwell's equations subject to the rock's EM tensors[12]; a paraxial approximation that solves the ray equation or the radiative transfer method[13-15]; and Beer-Lambert's propagation algorithm. Any of these methods allow us to approximate the dissipated energy, i.e., heat, per unit of volume or area. In the following discussion, it is assumed that the majority of the EM absorption takes place at the boundary of the rock and the air. Consequently, we use Beer-Lambert's approximation and calculate the dissipated power, P_d, as a function of the propagation distance, z:

$$P_d = P_o\left(1 - e^{-\alpha_o k z}\right) \tag{1}$$

where P_o is the transmitted incident power density, α_o is the absorption coefficient, and $k = 2\pi/\lambda$ is the wave number.

Thermal Dynamics

The governing equation of thermodynamics can be written as:

$$\frac{\partial \rho C_p T}{\partial t} = -\vec{v}\cdot\nabla\left(\rho C_p T\right) - \nabla\cdot\vec{Q} + \Theta_v \tag{2}$$

where p is the density of the material, C_p is the specific heat at constant pressure, $\vec{v}$ is the interface velocity between two phases, $\vec{Q}$ is the internal heat flux, and Θ_v is the volumetric heat input. Note that the conserved quantity in a thermal process is the product[16] $b \equiv rhoC_pT, J/m^3$. The continuity condition for Eqn. 2 imposes that:

$$\frac{\partial \rho}{\partial t} + \nabla\cdot(\rho\vec{v}) = 0 \tag{3}$$

where Θ_v is the rate of energy input from the external power sources per unit of volume.

The differential heat flux, $\vec{Q}$, in Eqn. 2 can take different forms depending on the thermal transport phenomena taking place within a given domain and time — including advection, conduction, convection and radiation — and all of them have been observed during HPEM enabled perforation experiments in the past.

Bear in mind that the thermal conductivity, K, emissivity, ε, fluid velocity, $\vec{u}$, and density, p, vary with temperature, pressure, thermodynamic anisotropies and electrical conductivity as well as under the influence of magnetic fields[17-19]; this means the accuracy of any numerical approximation will depend on how these parameters are described.

The interaction encompasses three stages prescribed by the melting temperature, T_m, and evaporation temperature, T_e. Rock heats up if $T < T_m$, melts when $T_m \leq T < T_e$, and evaporates at $T \geq T_e$. Rocks are composite solids made of multiple minerals, each with distinct thermal and EM properties. Therefore, phase change occurs in temperature intervals between $\{T_{m/e} - \Delta T_{pc,m/e}/2, T_{m/e} + \Delta T_{pc,m/e}/2\}$, where ΔT_{pc} is the width of the phase transition zone. Furthermore, experiments have shown that some rocks dissociate prior to melting under HPEM irradiation[6], which adds an additional complication to the thermodynamic properties of rocks.

To characterize these thermodynamic properties and simplify our models, we follow the apparent heat capacity formulation[20, 21] and implement it using COMSOL's module of heat transfer with phase change. This approximation models the material phase using a smooth function, ϑ, such that:

$$\vartheta\left(T_{m/e}\right) = \begin{cases} 1 & T \leq T_{m/e} - \Delta T_{pc,m/e}/2 \\ 0 & T \geq T_{m/e} + \Delta T_{pc,m/e}/2 \\ f(T) & \text{otherwise} \end{cases} \tag{4}$$

where $0 \leq f(T) \leq 1$ is some continuous function, typically the Heaviside function. Equation 4 can then be used to calculate p and K as:

$$\blacksquare = \vartheta\blacksquare_1 + (1-\vartheta)\blacksquare_2 \tag{5}$$

whereas enthalpy, H, mass fraction, Ψ, and equivalent heat capacity, C_{eq}, take the form:

$$\blacksquare = \frac{\vartheta\rho_1\blacksquare_1 + (1-\vartheta)\rho_2\blacksquare_2}{\rho} \tag{6}$$

where ■ is a placeholder for the quantity of interest, and the subscript indicates the material phase.

The latent heat capacity, C_L, is calculated as:

$$C_L = (H_2 - H_1)\frac{d\psi}{dT} \tag{7}$$

The apparent heat capacity is the result of adding this last term to the equivalent heat capacity:

$$C_L = (H_2 - H_1)\frac{d\psi}{dT} \tag{8}$$

Thermal Propagation of the HPEM Beam

The apparent heat capacity method predicts the phase change of the material without the need to implement a moving boundary or Stefan problem. Consequently, it has some drawbacks: it cannot accurately predict problems where the heat source moves with the boundary, and in those cases it may lead to inexact results[22]. This is critical to our application where the HPEM beam impinges on the melt vapor or solid vapor interfaces. A possible workaround is to add a fictitious thermal anisotropy in the vapor phase by assigning a high thermal conductivity ($\kappa_{\parallel} \approx 10^3$ W/(m · K)) along the beam's path[23].

In the numerical simulations, this scheme has accurately resolved the shape of the perforation and temperatures, though it increases the observed perforation time up to a factor of 2[10]. In the companion article[11], an alternative solution is implemeted by adding a thermal heat flow on the moving solid boundary. In this case, the time resolution is reduced by a factor of 2 compared to the experimental results. Nevertheless, these methods allow us to predict the phenomenology of the interaction and the morphology of the perforation.

Thermal Stress

Thermal stress ensues from the balance of thermal and total strains on a material[24, 25]. As the rocks are heated by the HPEM beam, they dilate, creating a thermal strain, which can generate microfractures and macrofractures that affect the morphology of the rock[26]. In downhole conditions, one must also account for the combined effect of thermal and confining stresses, including their effect on the thermodynamic parameters as discussed in the previous section. In the next section, we will present the fundamental relation between temperature and thermal strain, and the use of the FLAC to model the tensile crack regions due to thermal and confining stresses.

The governing relation between thermal strain and the tensile or compressive stress in some particular direction is given by:

$$\sigma_i = E\overline{\alpha}_i \Delta T_i \tag{9}$$

where σ is the thermal induced stress, E is Young's modulus, and $\overline{\alpha}$ is the coefficient of the thermal expansion; the subscript i indicates the direction of measurement.

The heat equation, Eqn. 2, and thermal strain are linked via the thermoelastic damping:

$$\Omega_{te} = -\overline{\alpha} T dS_{pk} \tag{10}$$

where S_{pk} is the second Piola-Kirchoff stress tensor, and dS is the material derivative. Note that Ω_{te} is used explicitly to decribe the thermoelastic damping because, in the heat equation, it can be imagined to act as a heat sink, reducing the material's ability to transfer heat as it expands.

Depending on the temperature level, rocks respond to temperature change differently. Before a rock melts or vaporizes, a temperature increase will cause it to expand. If the expansion is prevented, a compressive stress increment will result; otherwise, it will expand until the temperature induced stress is balanced by the boundary loads. Locally, nonuniform thermal stress can overshoot rock strength, subsequently causing mechanical yielding, such as shearing slip and tensile spallation. When using a HPEM source, the temperature in the surface exposed to the beam could rise up above the melting point in microseconds while the high temperature only penetrates into a very shallow skin. After the melting point is passed, phase change occurs, e.g., rock first transforms into liquid at the melting point and further transforms into vapor/gas at the vaporization point. The temperature increase causes rocks to expand, and as a result, the stress in the region near the surface quickly converts from compressive stress to tensile stress condition. Once the tensile stress reaches the tensile strength, tensile cracking occurs, and fractures are observed near the EM field incidence point.

Modeling Assumptions

This study focuses on the thermal mechanical coupling interaction in the HPEM perforation of rocks. Consequently, some assumptions are made to solve the numerical problem:

1. Rocks are diamagnetic ($\mu = 1$), isotropic and dielectric.
2. The HPEM beam is highly collimated and coherent.
3. The field-rock interaction is circumscribed to the top boundary of the rock-air interface.
4. The phase change of rock materials — solid to liquid and liquid to gas — is approximated by the effective heat capacity.
5. Chemical reactions and nonlinear effects are ignored.
6. Mechanical changes — stress or strain — in the rock do not produce a temperature change.
7. The rock samples are unsaturated, and the thermal advection in the melt is negligible, i.e., melted and vaporized material is removed immediately.

Thermal Boundary. From a thermodynamic perspective, the HPEM energy absorbed by the rock translates into a volumetric heat source that constantly provides thermal energy to the system. This causes a rise in temperature and initiates phase changes. The structure of the thermal source is directly correlated to the spatial and transient distribution of the HPEM beam and the rock properties. In this treatment, we approximate the transversal profile of the field as a Gaussian-like source with a radial intensity distribution:

$$I_r = I_0 e^{-\frac{2r^2}{R^2}}, \tag{11}$$

where r is the radial distance measured from the beam center point, R is the beam radius, and I_o is the on-axis intensity derived from the irradiance power relation as:

$$I_0 = \frac{2P_t}{\pi R^2} \tag{12}$$

with P_t describing the net power of the beam.

Material Properties. The rock sample is approximated by a cube of 12 cm in every direction. The rock samples are subjected to confining stress in two lateral directions (S_X and S_Y), but have no mechanical load at the top surface. The HPEM source, i.e., heat source, is applied and centered on the top surface; the lateral and bottom surfaces are assumed to be adiabatic. Table 1 lists the physical, mechanical and thermal properties of the rock samples in the base case.

Property	Value
Density	2,250 kg/m^3
Young's modulus	100 × 10^9 Pa
Poisson's ratio	0.26
Cohesive strength	26 × 10^6 Pa
Friction angle	26.4°
Dilation angle	6.6°
Tensile strength	2.1 × 10^6 Pa
Thermal conductivity	2.5 W/(m · K)
Specific heat	920 J/(kg · K)
Thermal expansion coefficient	1.16 × 10^{-5} K^{-1}
Melting point	1,813 K
Vaporization point	2,470 K
Latent heat of fusion	2 × 10^6 J/kg
Latent heat of vaporization	1.33 × 10^7 J/kg

Table 1. Rock properties of the base case

Rocks are heterogeneous materials in nature, e.g., the contents and distributions of minerals can vary from location to location even in the same block of rock. Heterogeneity introduces spatial variations in the physical and mechanical properties of rock. In numerical models, the material heterogeneity can be represented through variations of physical and mechanical properties. In this article, heterogeneity is introduced by varying the density, thermal conductivity and specific heat values along the radial and axial direction using a sinusoidal function. The degree of heterogeneity can be controlled by setting the number of periods along the *r* and *z* direction for each property along a chosen axis, independently or simultaneously. Accordingly, the direction and number of periods are identified as: *n.r*, *n.z* and *n.rz*. The range for each is set to be 2, 8, 16, …, 256. Finally, the sinusoidal function is set so that the average value corresponds to the constants previously listed in Table 1.

Mesh Resolution and Geometry. Considering the symmetry of the sample geometry and loading condition, the numerical model is built in 2D axisymmetric mode to maximize the computational efficiency. The simulation model represents a cylinder with a radius of 6 cm and a height of 12 cm. For a millimeter sized element, a uniform mesh is used, i.e., there are 120 elements in the radial direction and 240 elements in the axial direction.

The Numerical Scheme

The HPEM field incident on the rock induces a high thermal gradient in the surface of the rock and in the volume beneath it. In this process, the region near the perforation channel expands in an explosive manner due to the sudden increase in temperature. To capture this effect in numerical modeling, the geomechanical model needs to have a constitutive description that can appropriately account for the critical mechanical behavior of the rock, and it should run in dynamic mode so that the kinetic energy and inertial effects are correctly considered.

This thermal expansion, stress change and mechanical damage process can be modeled by coupling the mesh geometry and the temperature distribution from a thermal solver with the continuum mechanic mesh module of FLAC. In this article, COMSOL is used to approximate the thermal evolution of the rock; however, the algorithm could be implemented with a different thermal solver. In the companion article, a similar scheme is implemented — using, for example, the thermal solvers in FLAC. In the latter, appropriate boundary conditions are applied. In this set of simulations, the roller condition is applied at the bottom, and the right and top boundaries are free.

Ideally, these two steps should be run interactively; i.e., the output at every time step from the COMSOL solver should be passed to the FLAC solver and so resolve the thermo-mechanical evolution of the system. Due to technical limitations, however, for this article we implemented a suboptimal scheme where the thermal steps are calculated first and then fed into the thermo-mechanical model. Yet, the results closely follow the experimental observations, up to the first order. In this suboptimal process, the file saved from the corresponding COMSOL model at the time of zero is loaded and the stored data are mapped into the FLAC model. Next, the geomechanical model is run into equilibrium. After this initiation stage, the following simulation procedure is performed:

1. The data stored in the file saved from the corresponding COMSOL model at the time of 1 second are loaded into FLAC to update the element status — solid, air or mixed — temperature distribution and phase fractions for each element in the model.
2. The mechanical calculation mode is turned off, and the model is run in thermal calculation mode to compute the thermal expansion and thermally induced stress.
3. The thermal calculation mode is turned off, the dynamic calculation mode is turned on, and the model is solved for 20,000 steps — note that the mechanically damaged zones are stabilized under the current thermal load. The stress distribution and mechanical damage in the rock sample are evaluated and can be viewed at this point.

The above procedure is repeated for each file saved from the COMSOL model, and in each repetition the heating time is incremented by 1 second.

NUMERICAL RESULTS

A variable sweep in COMSOL was used to study numerous combinations for the radial and axial variations *n.r*, *n.z* and

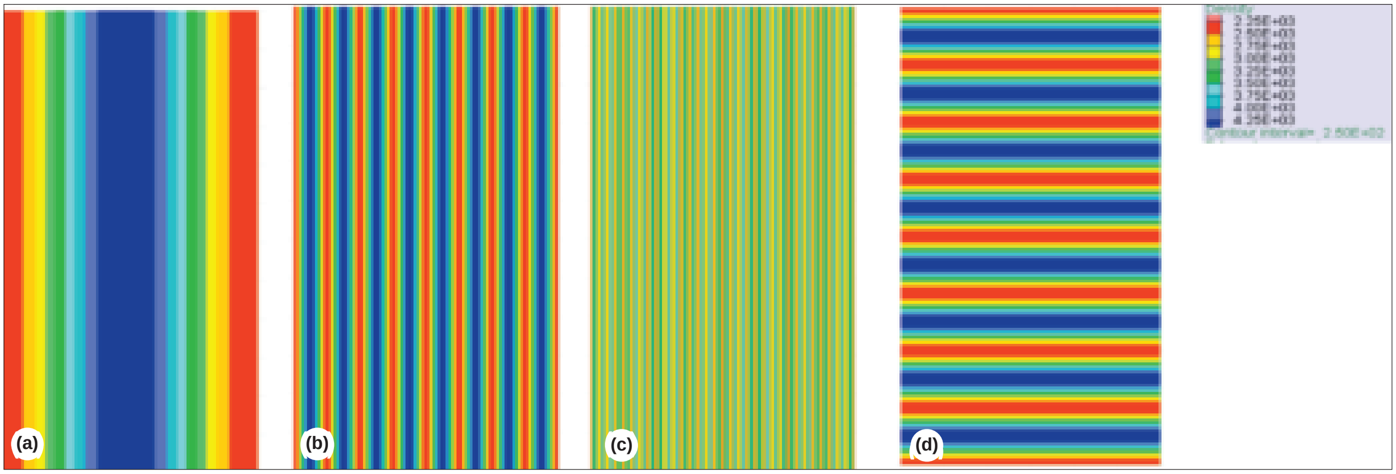

Fig. 2. Visualization of the periodic material property distributions: (a) NSR 001, (b) NSR 008, (c) NSR 032 and (d) NST 008.

n.rz. Figure 2 illustrates a few heterogeneous rocks with their heterogeneity reflected by the periodic distribution of mass density in an axisymmetric configuration. In Figs. 2a to 2c, the density varies periodically in a radial direction, and in Fig. 2d, the density varies periodically along the axial direction.

Figure 3 shows the shape of the perforation channel and the temperature distribution induced by the HPEM beam at different time intervals — 1 second, 10 seconds, 20 seconds and 30 seconds — for *n.r* = 1. The numerical results show that the overall morphology of the perforation follows a similar indistinctive pattern based on the sweeping values; however, the depth and ROP vary with the direction of the heterogeneity and the number of periods.

Figures 4 and 5 summarize the time evaluation of the temperature in regard to position and ROP, respectively, of the highest point of the rock along the axis of symmetry (z-axis). When the heterogeneity is set along the radial direction, *n.r*, it produces a measurable change in the penetration depth (up to 1 cm), and rapid oscillations in the ROP are evident as the rock is removed, particularly as the period of the heterogeneity increases. These changes occur due to the changes in thermal conductivity and heat capacity with the material density; as the number of periods increases, the pace of thermal propagation between neighboring cells becomes irregular, leading to uneven heating. With time, the material evaporates, and the system evolves to a homogeneous temperature due to the regular thermal conduction between the cells. Conversely, when the heterogeneity runs along the axial direction, *n.z,* it shows a narrow variation in the evolution of perforation depth (< 1 mm).

Similarly, the ROP shows a regular stepwise performance that, on average, is smaller than in the previous scenario (< 50%). This is explained by the spatial periodicity of the distribution of thermal parameters, which in this setting ensure that, on average, the ROP is similar between cases regardless of the number of periods. Certainly, the time distribution of the ROP will oscillate and slowly decrease over time; yet, on average, it will follow closely the evolution of the homogeneous system. Finally, the combined case, *n.rz*, results in a significant decrement in the perforation depth — up to 2 cm higher or a factor of 2 — although with a limited variation in depth among the simulated cases (< 5 mm). The ROP, albeit slower, shows wide leaps and seemingly follows a combination of the previous cases.

In the radial direction, however, the results are similar

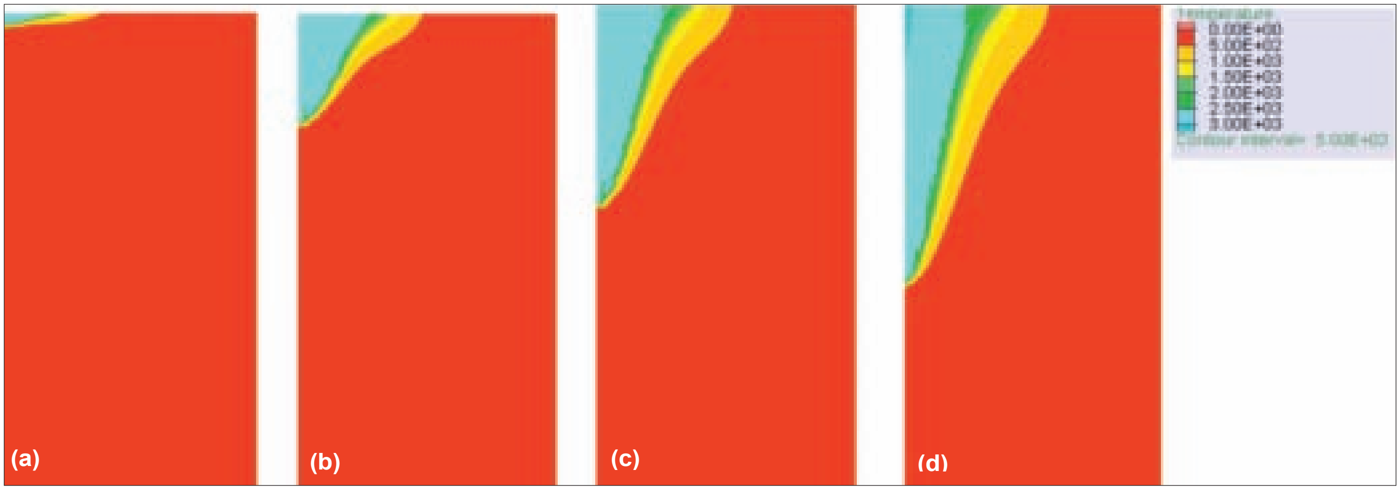

Fig. 3. Contours of temperature distribution over time for n.r = 1 as calculated by the thermal module of COMSOL multiphysics: (a) t = 1 s, (b) t = 10s, (c) t = 20 s, and (d) t = 30 s.

regardless of the case. Figures 6 and 7 plot the radius position and the radial ROP, respectively, along the top boundary for the three simulated scenarios. In all cases, the perforation radius converges to the same maximum value, a constant percentage of the beam's radius (~0.8 R). This is because the beam propagates in the axial direction; therefore, there is no net transfer of energy from the EM field to the material in the radial direction. Due to the material's thermal properties, minor differences exist in the radial ROP. If the heterogeneity is present along the radial direction, the system will swiftly converge (~17 s). If the heterogeneity is set along the axial direction, it will converge at an even faster pace (~14 s). And for the combined case, the ROP is the slowest (~20 s).

Figure 8 shows the mechanical damage introduced by dielectric heating at a time of 5, 10, 15 and 20 seconds in the

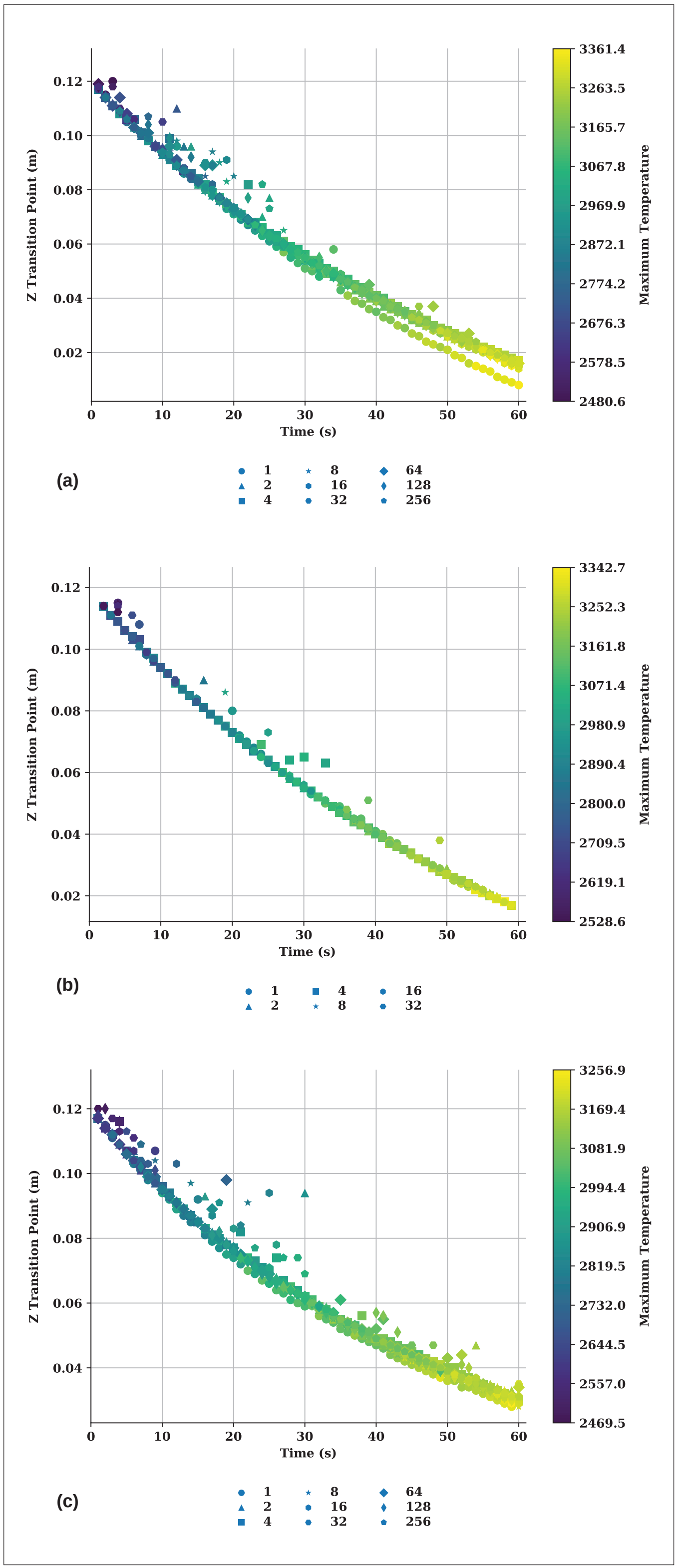

Fig. 4. Time and temperature evolution of the irradiated rock profile along the symmetry (z) axis for the three computed cases: (a) n.r, (b) n.z and (c) n.rz.

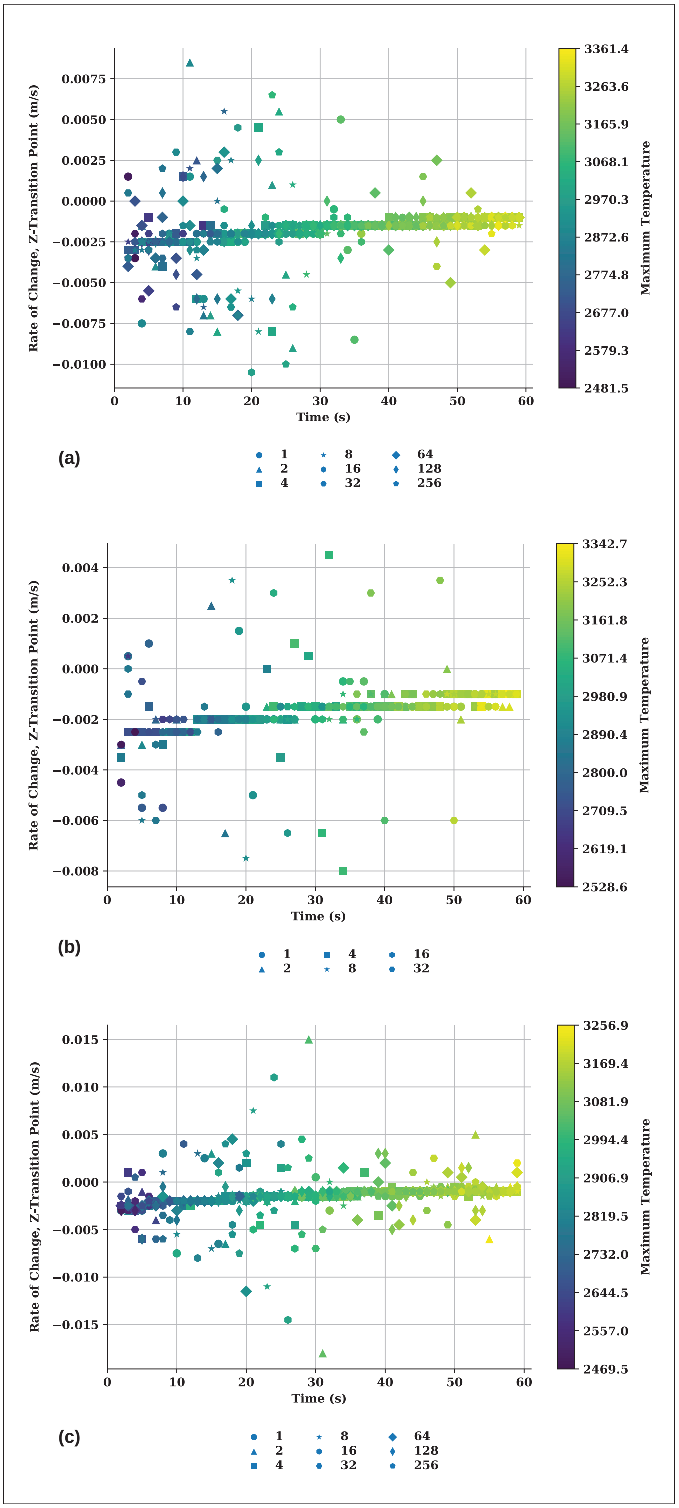

Fig. 5. ROP and temperature evolution of the irradiated rock as measured along the symmetry (z) axis for the three computed cases: (a) n.r, (b) n.z and (c) n.rz.

case of NSR-001. It can be seen that the severe mechanical damage develops and is concentrated at the bottom of the perforation tunnel at an “early” time, e.g., at 5 seconds, when the thickness of the mechanical damage zone near the channel bottom reaches 1.5 cm. As time goes on, the mechanical damage zone is reduced at the bottom region, but increases in the region near the channel entrance and somewhat develops in the middle regions.

It was noticed that the mean stress near the perforation tunnel is around 1 MPa, while the stress in the melted and vaporized region — the perforation channel — is about 50 KPa. Because the melting and vaporization take place at a time scale of microseconds to milliseconds, the gas pressure inside the perforation channel could be comparable to the stress level in the solid sample surrounding the perforation channel.

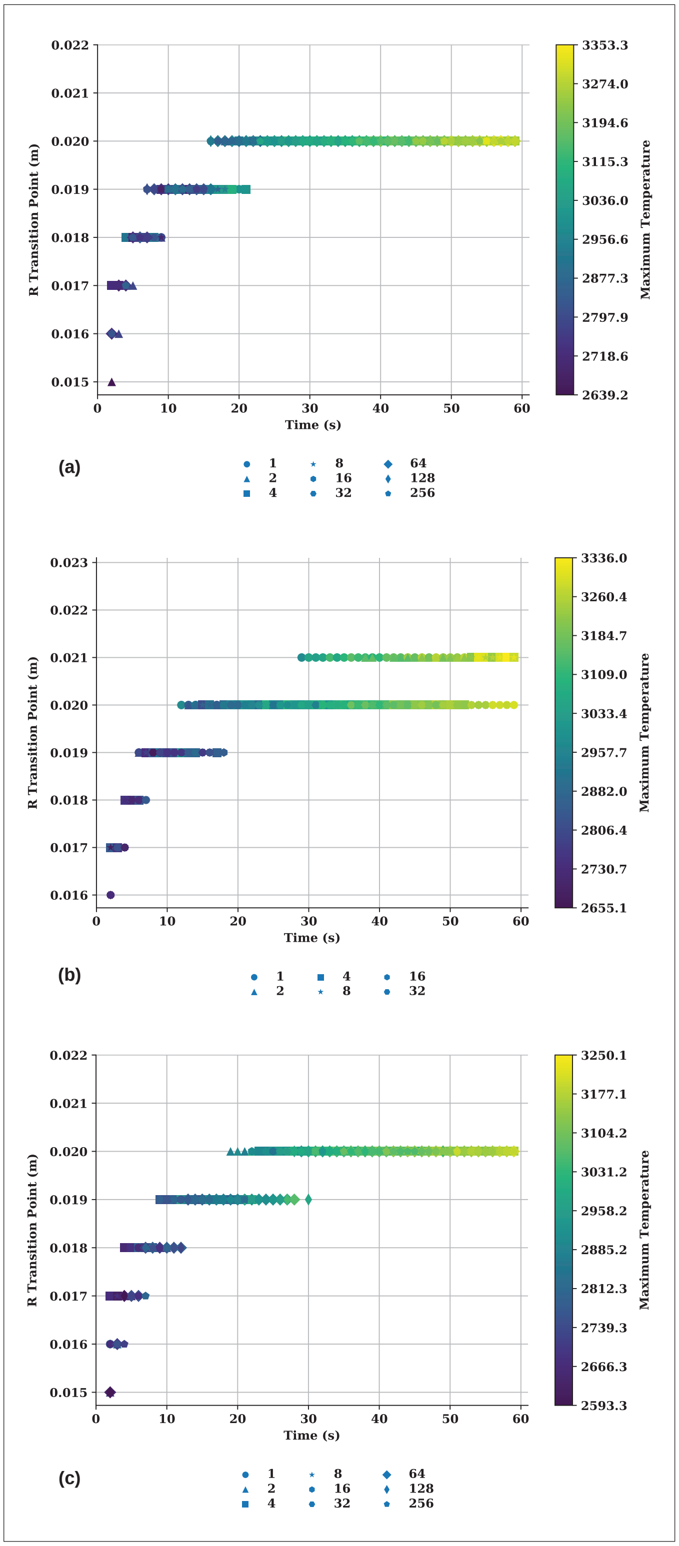

Fig. 6. Time and temperature evolution of the irradiated rock profile along the top boundary, radial (r) axis, for the three computed cases: (a) n.r, (b) n.z and (c) n.rz.

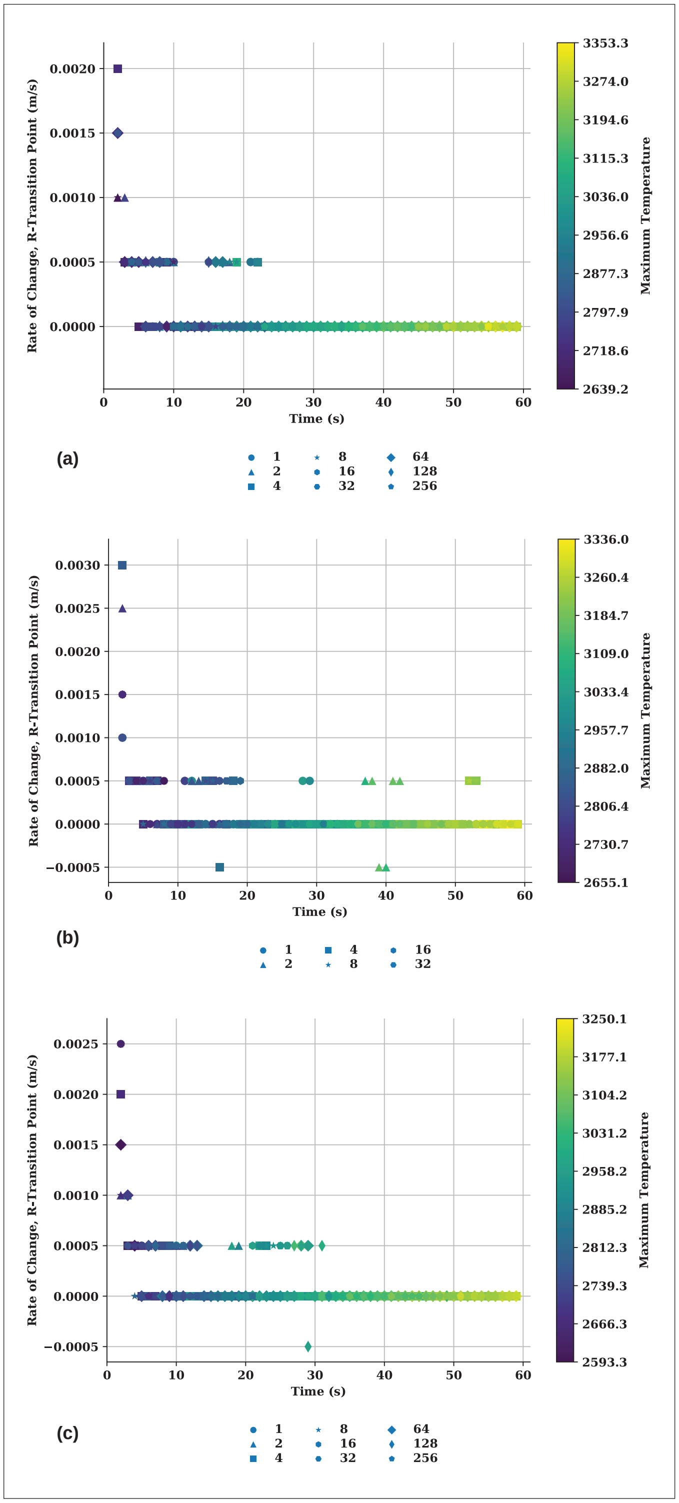

Fig. 7. ROP and temperature evolution of the irradiated rock as measured along the top boundary, radial (r) axis, for the three computed cases: (a) n.r, (b) n.z and (c) n.rz.

To investigate the influence of the pressure in the perforation channel on the mechanical damage in the surrounding region, the simulations are rerun with a pressure boundary condition applied at the grid points along the channel entrance at the top surface. The magnitude of the applied pressure is set to the averaged mean stress of all the elements that have run into plastic yielding. This is arbitrary and should be refined once more accurate data measuring the pressure inside the perforation channel in the dielectric heating process are available. Figure 9 shows the mechanically damaged region around the perforation channel. The damage below the channel bottom does not change significantly. On the one hand, the damage near the channel entrance at 10, 15 and 20 seconds is completely suppressed. On the other hand, the damage in the region surrounding the bottom half of the channel is enhanced, and damage thickness looks uniform.

With a free boundary at the perforation on the top surface, FLAC models are built to couple with the thermal simulation results of COMSOL for all four cases shown in Fig. 2. The mechanically damaged zones at 30 seconds predicted by the FLAC models are provided in Fig. 10. In Figs. 10a to 10c, the mechanical damage near the entrance and bottom of the channel is more severe than in the region around the middle of the perforation channel. The dominant mechanical damage is shear yielding at the bottom, but tensile yielding is shown near the entrance of the perforation channel. The thickness of the broken region near the perforation entrance is more than 1.5 cm.

In Fig. 10d, the mechanical damage is well developed around the whole perforation channel, and the damage distribution is uniform with a thickness of around 1 cm. The difference in the damaged regions between Figs. 10a to 10c and Fig. 10d may be attributed to the different layer distributions in these cases; i.e., the density of the samples varies horizontally in Figs. 10a to 10c, but vertically in Fig. 10d. Therefore, the material property — density — changes quickly on the perforation face in Fig. 10d, which may promote the development of mechanical damage.

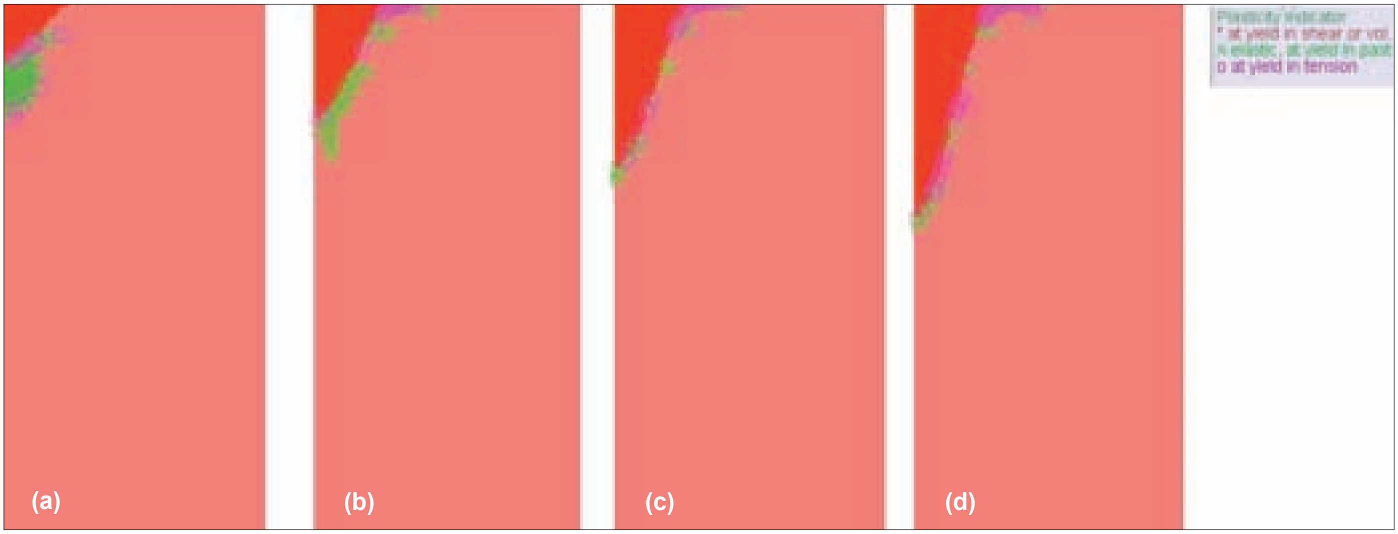

Fig. 8. The mechanical damage zones after being heated for 20 seconds, with a free boundary above the air region, in dynamic simulation mode and in the case of NSR-001: (a) t = 5 s, (b) t = 10 s, (c) t = 15 s and (d) t = 20 s.

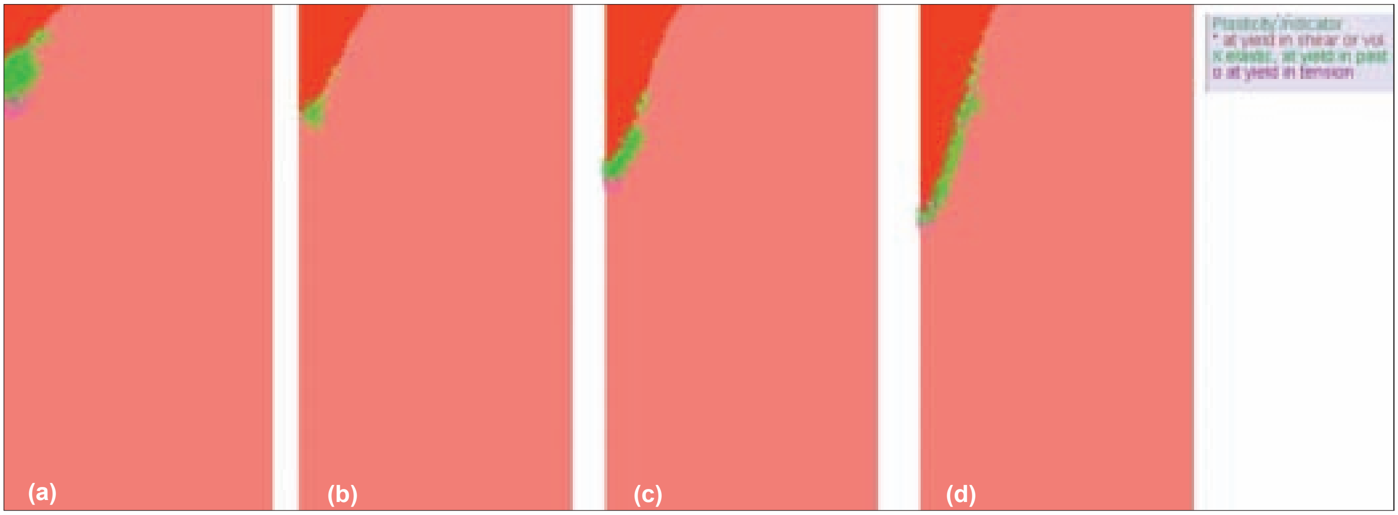

Fig. 9. The mechanical damage zones after being heated for 20 seconds, with a pressure boundary above the air region, in dynamic simulation mode and in the case of NSR-001: (a) t = 5 s, (b) t = 10 s, (c) t = 15 s and (d) t = 20 s.

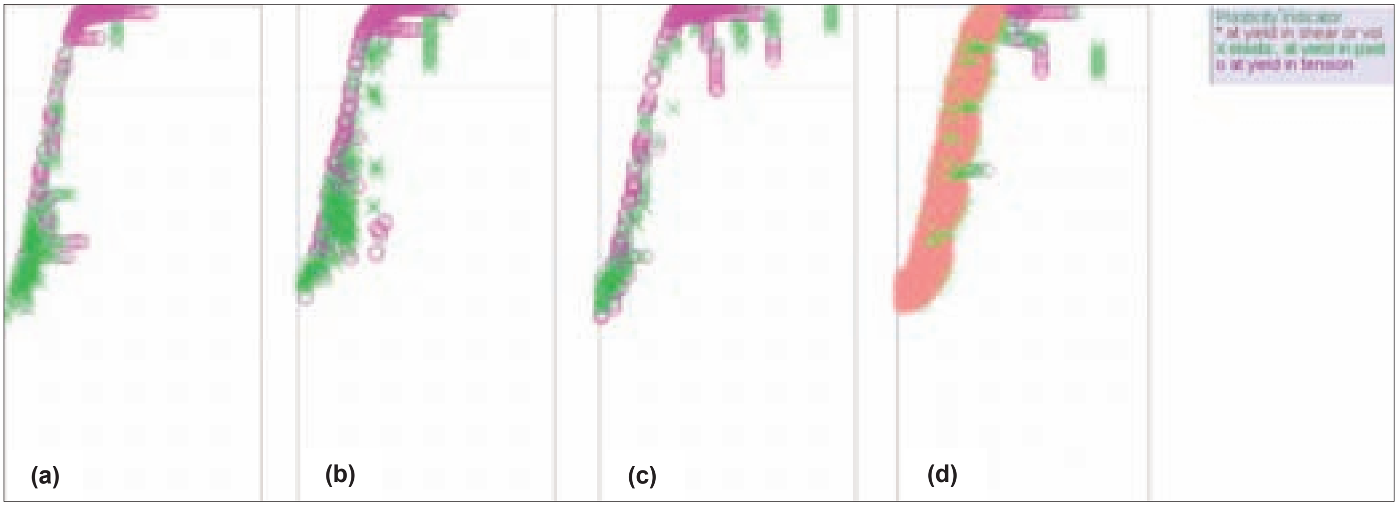

Fig. 10. The mechanical damage zones after being heated for 30 seconds, with a free boundary above the air region, in dynamic simulation mode and in the case of: (a) NSR-001, (b) NSR-008, (c) NSR-032 and (d) NST-008.

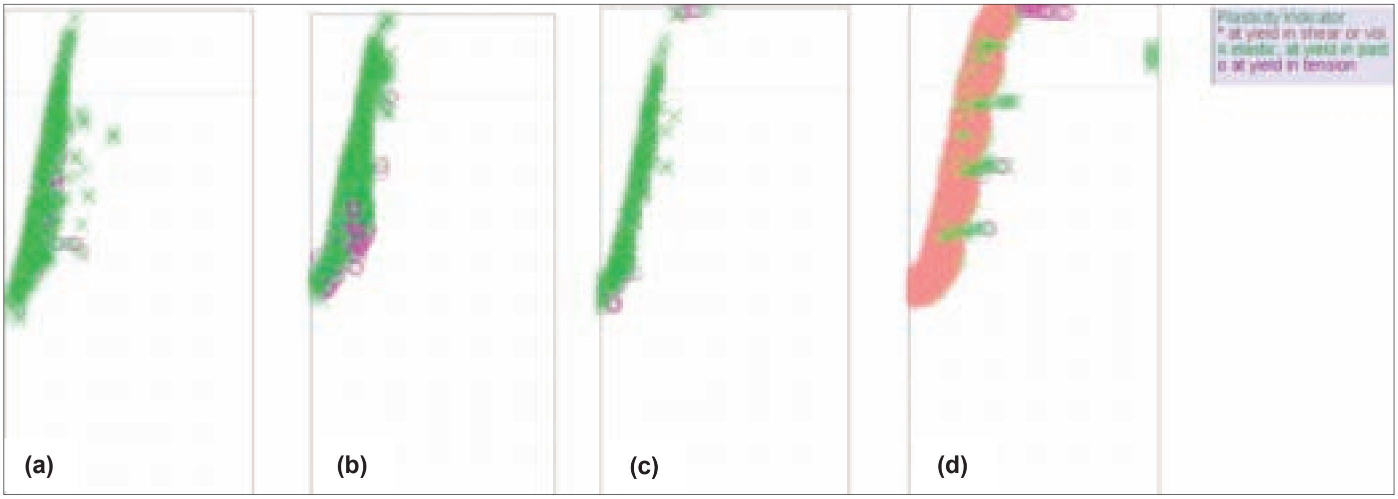

Fig. 11. The mechanical damage zones after being heated for 30 seconds, with a pressure boundary above the air region, in dynamic simulation mode and in the case of: (a) NSR-001, (b) NSR-008, (c) NSR-032 and (d) NST-008.

Figure 11 presents the mechanically damaged zones around the perforation channel at 30 seconds for these four cases with the pressure boundary condition on the top surface of the perforation channel. As can be seen, a higher pressure inside the perforation channel helps suppress the tensile yielding in the region near the perforation entrance in all these cases. In Figs. 11a to 11c, it also helps to enhance the damaged region around the middle section of the perforation channel. In Fig. 11d, it only has negligible effects on the extension of the damaged zone in the near entrance region.

CONCLUSIONS

A set of numerical models were built to simulate the interaction and dynamics between HPEM beams and heterogeneous rock samples. The results characterize the rate of perforation and the thermal induced mechanical damage, as well as their sensitivity to stress configurations. The thermal conduction and thermo-mechanical interaction in the heating process are captured in the simulations by coupling thermal modules and elastoplastic models from COMSOL and FLAC.

In general, these simulations indicate that a well-developed mechanically damaged zone with relatively uniform thickness may be expected if the HPEM beam is applied perpendicularly to the layers of rock. The extension of the tensile cracked or broken region near the perforation entrance is significantly affected by the gas pressure inside the perforation channel. Many other factors, such as bedding planes and in situ stress, that will influence the development of mechanical damage in the perforation process are currently under investigation. The results will be updated in a separate document.

ACKNOWLEDGMENTS

The authors would like to thank the management of Saudi Aramco and Aramco Services Company for their support and permission to publish this article.

This article was presented at the SPE Middle East Oil and Gas Show and Conference, Manama, Kingdom of Bahrain, March 6-9, 2017.

REFERENCES

1. Batarseh, S., Gahan, B.C., Graves, R.M. and Parker, R.A.: "Well Perforation Using High-Power Lasers," SPE paper 84418, presented at the SPE Annual Technical Conference and Exhibition, Denver, Colorado, October 5-8, 2003.
2. Xu, Z., Reed, C.B., Konercki, G., Parker, R.A., et al.: "Specific Energy for Pulsed Laser Rock Drilling," *Journal of Laser Applications*, Vol. 15, Issue 1, January 2003, pp. 25-30.
3. Gahan, B.C., Parker, R.A., Batarseh, S.I., Figueroa, H., et al.: "Laser Drilling: Determination of Energy Required to Remove Rock," SPE paper 71466, presented at the SPE Annual Technical Conference and Exhibition, New Orleans, Louisiana, September 30-October 3, 2001.
4. Graves, R.M., Batarseh, S.I., Parker, R.A. and Gahan, B.C.: "Temperatures Induced by High-Power Lasers: Effects on Reservoir Rock Strength and Mechanical Properties," SPE paper 78154, presented at the SPE/ISRM Rock Mechanics Conference, Irving, Texas, October 20-23, 2002.
5. Gahan, B.C., Batarseh, S.I., Sharma, B. and Gowelly, S.: "Analysis of Efficient High-Power Fiber Lasers for Well Perforation," SPE paper 90661, presented at the SPE Annual Technical Conference and Exhibition, Houston, Texas, September 26-29, 2004.
6. Batarseh, S.I., Gahan, B.C., Sharma, B.C. and Gowelly, S.I.: "Deep Hole Penetration of Rock for Oil Production Using Ytterbium Fiber Laser," *Proceedings of the SPIE*, Vol. 5448, *High-Power Laser Ablation V*, September 2004, pp. 818-826.
7. Ahmadi, M., Erfan, M.R., Torkamany, M.J. and Safian, G.A.: "The Effect of Interaction Time and Saturation of Rock on Specific Energy in ND: YAG Laser Perforating," *Optics and Laser Technology*, Vol. 43, Issue 1, February 2011, pp. 226-231.
8. Vaferi, B., Gitifar, V., Darvishi, P. and Mowla, D.: "Modeling and Analysis of Effective Thermal Conductivity of Sandstone at High Pressure and Temperature Using Optimal Artificial Neural Networks," *Journal of Petroleum Science and Engineering*, Vol. 119, July 2014, pp. 69-78.
9. Abdulagatov, I.M., Abdulagatova, Z.Z., Kallaev, S.N., Bakmaev, A.G., et al.: "Thermal Diffusivity and Heat Capacity Measurements of Sandstone at High Temperatures Using Laser Flash and DSC Methods," *International Journal of Thermophysics*, Vol. 36, Issue 4, April 2015, pp. 658-691.
10. San-Roman Alerigi, D.P., Batarseh, S.I. and Han, Y.: "Numerical Modeling of Thermal and Mechanical Effects in Laser-Rock Interaction — An Overview," ARMA paper 2016-142, presented at the 50th U.S. Rock Mechanics/Geomechanics Symposium, Houston, Texas, June 26-29, 2016.
11. Han, Y., Fang, Y., San-Roman Alerigi, D.P. and Batarseh, S.I.: "Numerical Modeling of Thermal Mechanical Interaction Process in High-Power Electromagnetic Heating of Rocks," SPE paper 183836, presented at the SPE Middle East Oil and Gas Show and Conference, Manama, Bahrain, March 6-9, 2017.
12. Hossan, M.R. and Dutta, P.: "Effects of Temperature Dependent Properties in Electromagnetic Heating," *International Journal of Heat and Mass Transfer*, Vol. 55, Issues 13-14, June 2012, 3412-3422.
13. Chandrasekhar, S.: *Radiative Transfer,* 1st ed., Dover Publications, New York, 1960, 393 p.
14. Cho, J-H. and Na, S-J.: "Implementation of Real-Time Multiple Reflection and Fresnel Absorption of Laser Beam in Keyhole," *Journal of Physics D: Applied Physics,* Vol. 39, Issue 24, December 2006, pp. 5372-5378.
15. San-Roman Alerigi, D.P., Benslimane, A., Ng, T.K., Alsunaidi, M., et al.: "A Possible Approach on Optical Analogues of Gravitational Attractors," *Optics Express*, Vol. 21, Issue 7, 2013, pp. 8298-8310.
16. Deen, W.M.: *Analysis of Transport Phenomena,* 1st ed., Oxford University Press, New York, 1998, 597 p.
17. Atkins, P.: *The Laws of Thermodynamics: A Very Short Introduction*, 1st ed., Dover Publications, New York, 2010, 120 p.
18. Lalena, J.N. and Cleary, D.A.: *Principles of Inorganic Materials Design*, 1st ed., John Wiley & Sons, Hoboken, New Jersey, February 2010, 585 p.
19. Jones, W. and March, N.H.: *Theoretical Solid State Physics,* Vol. 1: *Perfect Lattices in Equilibrium*, 1st ed., Dover Publications, New York, 1985, 704 p.
20. Muhieddine, M., Canot, É. and March, R.: "Various Approaches for Solving Problems in Heat Conduction with Phase Change," *International Journal of Finite Volumes*, Vol. 9, Issue 1, 2009, pp. 1-20.
21. Civan, F. and Sliepcevich, C.M.: "Limitation in the Apparent Heat Capacity Formulation for Heat Transfer with Phase Change," *Proceedings of the Oklahoma Academy of Sciences*, Vol. 67, 1987, pp. 83-88.
22. Bjorndalen, N., Belhaj, H.A., Agha, K.R. and Islam, M.R.: "Numerical Investigation of Laser Drilling," SPE paper 84844, presented at the SPE Eastern Regional Meeting, Pittsburgh, Pennsylvania, September 6-10, 2003.
23. Eppes, T.A., Milanovic, I. and Patlolla, H.: "Early Stage Melt Ejection in Percussion Laser Drilling," *Proceedings of the COMSOL Conference*, Boston, Massachussets, 2012, pp. 2-7.
24. Xu, Z., Yamashita, Y. and Reed, C.: "Modeling of Laser Spallation Drilling of Rocks for Gas and Oil Well Drilling," SPE paper 95746, presented at the SPE Annual Technical Conference and Exhibition, Dallas, Texas, October 9-12, 2005.

25. Sakakura, M., Tochio, T., Eida, M., Shimotsume, Y., et al.: "Observation of Laser-Induced Stress Waves and Mechanism of Structural Changes Inside Rock Salt Crystals," *Optics Express,* Vol. 19, Issue 18, 2011, pp. 17780-17789.
26. Batarseh, S.I., Abass, H.H., Al-Mulhem, A.A. and Habib, N.S.: "High-Power Laser Application in Open Hole Multiple Fracturing with an Overview of Laser Research: Past, Present and Future," SPE paper 160836, presented at the SPE Saudi Arabia Section Technical Symposium and Exhibition, al-Khobar, Saudi Arabia, April 8-11, 2012.

BIOGRAPHIES

Dr. Damian San-Roman Alerigi is a Petroleum Scientist working with the Production Technology Team of Saudi Aramco's Exploration and Petroleum Engineering Center – Advanced Research Center (EXPEC ARC). His focus is on developing the next generation of subsurface photonic and electromagnetic tools.

Damian's previous research focused on the interaction of waves with complex media and its application to subsurface technologies. His work encompasses different areas of science and engineering, from oil and gas to applied mathematics; he has published papers in various international journals and conferences around the world.

Damian received his B.S. degree in Physics from the National Autonomous University of Mexico, Mexico City, Mexico. In 2008, he enrolled in King Abdullah University of Science and Technology (KAUST) as a founding class student where he completed his M.S. degree (2010) and Ph.D. degree (2014), both in Electrical Engineering.

Dr. Yanhui Han is a Petroleum Engineer at the Aramco Research Center – Houston. His research interests are computational geomechanics and petroleum geomechanics-related research, development and applications. Yanhui's previous positions include FLAC Developer and Geomechanics Consultant at Itasca Consulting Group for 10 years, Principal Technical Professional at Halliburton for 1 year and Production Technologist at Shell for 2 years.

He has published around 60 technical papers, served as session chair in various international conferences, e.g., American Rock Mechanics Association (ARMA) symposiums, and served as a technical editor/reviewer for many international journals.

Yanhui is the recipient of the 2013 N.G.W. Cook Award from ARMA. He is also a Registered Professional Engineer in the United States.

Yanhui received his Ph.D. degree in Computational Geomechanics from the University of Minnesota, Minneapolis, MN.

Dr. Sameeh I. Batarseh joined Saudi Aramco in 2011 as a Petroleum Engineering Specialist working with the Production Technology Team in the Exploration and Petroleum Engineering Center – Advanced Research Center (EXPEC ARC). Currently, he is leading the High-Power Laser Program and serving as Focus Area Champion for Unconventional Resources. Sameeh's area of interest is to develop an in situ laser application in drilling, perforation and fracturing, among many other applications with a focus on unconventional reservoirs.

He is an active member of the Society of Petroleum Engineers (SPE), serving the society for several years while holding different positions, including sitting on the SPE Executive Advisory Committee, chairing the Program Committee and serving as session chair. He was also the board and vice chair for the Western Region USA San Joaquin Valley. Sameeh has organized over 52 SPE technical workshops.

He has authored or coauthored more than 48 publications, holds six granted patents and has eight patents in progress.

Sameeh received his Ph.D. degree in Petroleum Engineering from the Colorado School of Mines, Golden, CO.

Shale Gas Reservoir Development Strategies Using Complex Specified Bottom-hole Pressure Well Architectures

Dr. Mari H. Alqahtani and Prof. Turgay Ertekin

ABSTRACT

The principal objective of this article is to develop artificial expert systems capable of instantaneously and accurately predicting the performance of complex wells, proposing complex well designs and predicting average reservoir properties for shale gas wells operating under specified bottom-hole pressure (BHP).

Artificial neural networks (ANNs) provide the backbone of an expert system. Other methods, such as traditional well testing, numerical reservoir simulation and decline curve analysis, have inherent limitations or require significant time and effort to get results. The ANN methodology has the ability to recognize patterns among various parameters in the presence of large databases. It is a powerful tool, especially when the existing relationships between the dependent and independent parameters are vague or are not well understood, as it is capable of instantly solving problems that do not have known analytical or numerical solutions. Complex wells are scarce in shale gas reservoirs, so utilizing real data in ANN training is not possible most of the time. Accordingly, numerical reservoir simulation is used to generate the database necessary for training the expert systems.

The expert systems developed in this research instantly and accurately performs the tasks below for complex wells in shale gas reservoirs operating under constant BHP conditions:

- Predicting production rates for a given complex well design from a given shale gas reservoir.
- Proposing a robust compex well design capable of producing a given production profile from a given set of reservoir properties.
- Predicting unconventional reservoir rock properties corresponding to a given gas production profile from a given complex well design.

Results prove that a well trained ANN is capable of making instantaneous and accurate predictions, which increases confidence in utilizing ANNs to solve complex problems in the oil and gas industry. To increase the accuracy of the expert system and reduce prediction error, data combinations are reintroduced as functional links.

Complex wells consume less water and have a controlled exposure to the reservoir, making them an attractive alternative to the typical horizontal wells with their massive hydraulic fracturing. Field testing of complex wells in shale gas reservoirs allows us to utilize real data in calibrating and testing the expert systems.

INTRODUCTION

Unconventional gas production worldwide has seen an increase in the past years. This increase is dominated by shale gas production. The U.S. Energy Intelligence Agency (EIA)[1] forecasts that shale gas will be the dominant driver in increasing natural gas production for the upcoming 25 years, Fig. 1. The demand for shale gas in particular, and unconventional gas in general, is expected to increase as consumption increases. For example, U.S. gas consumption is forecasted to increase even under conditions of low economic growth and low oil prices, Fig. 2[2].

Although shale gas was discovered a long time ago and has

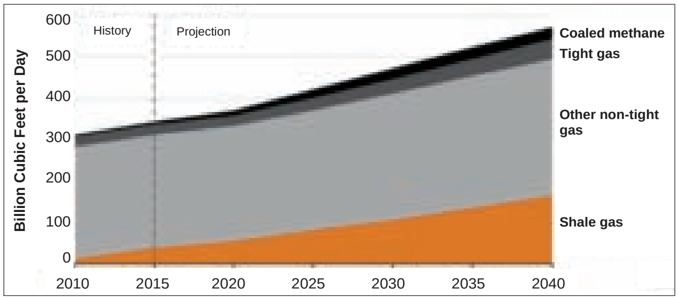

Fig. 1. Projected world natural gas production by type, from 2010 to 2040[1].

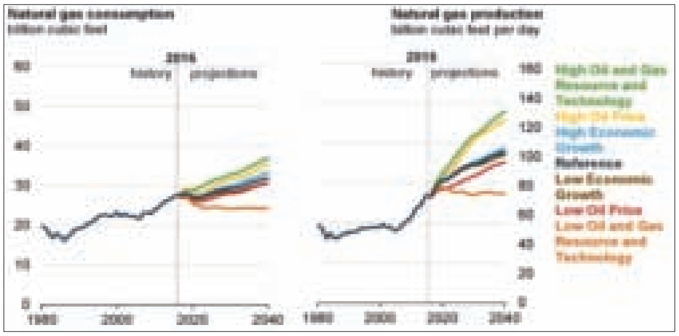

Fig. 2. U.S. historic and forecasted natural gas consumption[2].

been produced for more than a century[3], it wasn't significantly developed and commercially produced until the last decade[4]. This delay in shale gas development wasn't caused solely by supply and demand forces affecting natural gas. Other factors contributed to this delay, such as the high exploitation costs and a lack of sufficient understanding of this unconventional resource. Shale gas is available around the world in large quantities; however, its permeability is lower than 0.001 md, which makes it very difficult to develop[5].

SHALE GAS FORMATIONS AT A GLANCE

Shale is a fine-grained clastic rock that is dark in color. Shale formations are naturally fractured and have an ultra-tight matrix permeability. Shale is organically rich, with total organic carbon (TOC) ranging from 1% to 10%, and its gamma ray signature is usually higher than 140 API[6]. In addition to storing gas in its pore spaces, shale also stores gas by adsorption[7]. The dual porosity model developed by Warren and Root (1963)[8] is widely used to describe shale gas reservoirs, Fig. 3. In their model, gas flows from the ultra-tight matrix to the natural fractures and then to the wellbore. The model assumes no direct flow from the matrix to the wellbore. This model introduces to fracture connectivity terminology a term for dimensionless matrix, lambda (λ), and one for dimensionless fracture storage, omega (ω). As λ gets higher in value, gas flows faster from the matrix to the fractures, and as ω gets higher in value, the gas quantity stored in fractures increases. Equations 1 and 2 define both parameters[8].

$$\lambda = \alpha \frac{k_m}{k} {r_w}^2 \tag{1}$$

where α is the geometric shape factor, which depends on the shape of the matrix block, *k* is permeability, and *rw* is the wellbore radius.

$$\omega = \frac{(\phi\, c_t)_f}{(\phi\, c_t)_f + (\phi\, c_t)_m} \tag{2}$$

where φ is porosity, and *ct* is the total compressibility.

The extremely low permeability of shale gas formations necessitates increasing a well's reservoir exposure to produce economical rates. Accordingly, horizontal wells with massive hydraulic fracturing are widely used to develop shale gas formations. Other alternatives, such as complex wells, are not as widely used as the fractured horizontal wells, yet these alternatives offer more reservoir exposure due to the large number of laterals that drain from existing natural fracture networks.

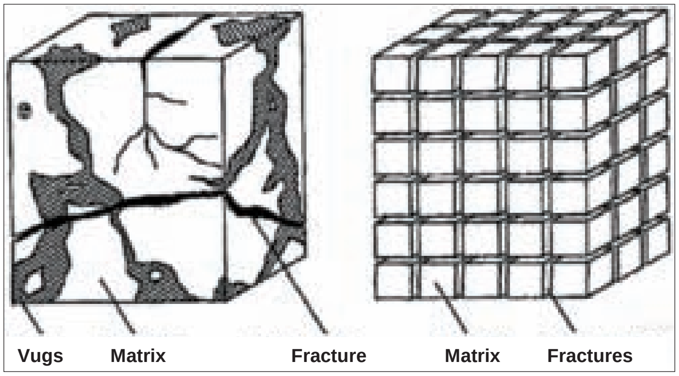

Fig. 3. Modeled idealization of natural fractures in dual porosity reservoirs[8].

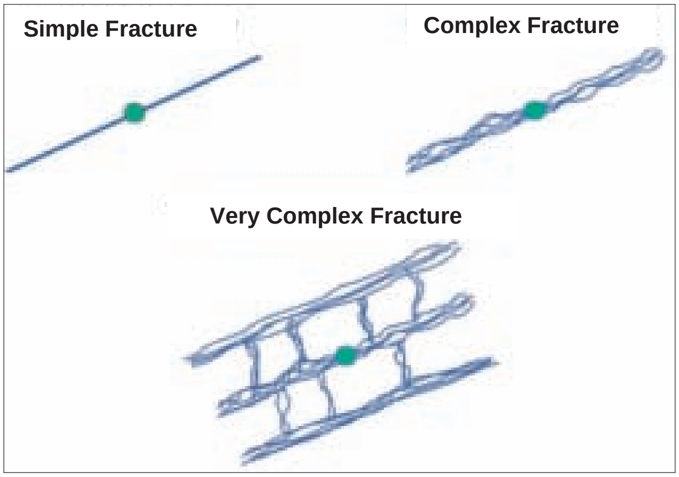

Fig. 4. Hydraulic fracture complexity: simple, complex and very complex fractures[9].

ASSESSING THE LEVEL OF CONFINEMENT IN HYDRAULIC FRACTURES IN SHALE GAS FORMATIONS

In addition to consuming large quantities of water, the hydraulically fracturing of shale formations faces another disadvantage, which is the hydraulic fracture's level of confinement. The longer the half-length of the hydraulic fracture, the lower its level of confinement becomes. Natural fracture networks and their connectivity have an effect on hydraulic fracture propagation. Several studies have indicated that hydraulic fractures in naturally fractured reservoirs, such as shale formations, follow a complex to very complex geometry, Fig. 4[9]. Such a complex hydraulic fracture propagation cannot be captured by existing hydraulic fracture models, and new models are needed to accurately capture their complex geometry[9, 10]. This complex geometry is affected by a number of factors, such as in situ stress, natural fracture connectivity, leakoff, natural fracture orientation and the tip of the fracture effect, all of which have to be modeled.

Not everyone considers all of the aforementioned factors in their studies. For example, some authors consider leakoff in their hydraulic fractures model[11], while others assume zero leakoff[12]. The former considered the shear stress caused by fluid leakoff into the natural fractures and by natural fractures reopening due to the stress caused by the tip effect. Their model assumes that hydraulic fractures will propagate in the direction of intersecting natural fractures[11]. They subsequently modified their model to indicate that when hydraulic fractures intersect a natural fracture, they can either get stopped by it or cut through it, Fig. 5[10]. Most hydraulic fracture analysis and

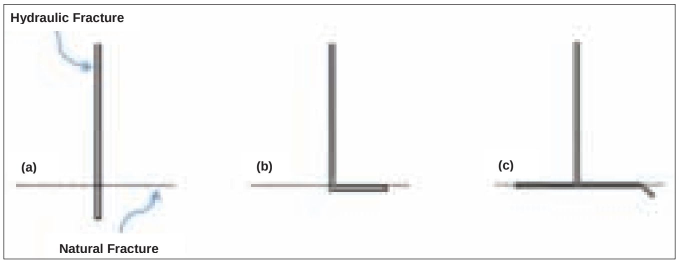

Fig. 5. Possible scenarios at the normal intersection of a hydraulic fracture and a natural fracture: (a) hydraulic fracture crosses natural fracture without incident, (b) hydraulic fracture ends at natural fracture, and (c) hydraulic fracture diverts into natural fracture and propagation continues[10].

models that address conditions in naturally fractured reservoirs highlight the uncertainty associated with the propagation direction and the level of confinement. Low level confinement becomes more pronounced in the massive hydraulic fractures common in shale gas horizontal wells.

Complex Wells

In this research, complex wells are proposed as an attractive alternative to horizontal wells with massive hydraulic fractures. Complex wells have a controlled and increasing reservoir exposure. Complex wells have seen a rise in their field applications since their early beginnings in the 1990s[13, 14]. When compared to single lateral horizontal wells, maximum reservoir contact wells have a lower cost per barrel and higher net present value (NPV)[15]. While both fishbone wells and horizontal wells with massive hydraulic fractures can generate similar NPVs, fishbone wells are preferred since they have a lower uncertainty[16].

The transient behavior of compex well laterals is not fully understood, especially in dual porosity, dual permeability (DPDP) reservoirs. An analytical model that predicts complex well behavior, along with their laterals' interaction, does not exist. Few studies have tried to solve this problem numerically. Segmenting laterals and then superimposing the results to get a final solution has been used in a number of studies[13, 17]. One study represented each lateral as a partial penetration well and then summed their transient and pseudo steady-state solutions[18].

Artificial Intelligence and Its Application to Oil and Gas Reservoirs

Artificial intelligence applications have proven effective in field development and optimization, especially in solving complex well design problems. Fuzzy logic, genetic algorithms and acceleration routines have been used in several studies to select the optimal complex well design, location and trajectory[19-21]. Furthermore, functional transformation, dimension reduction techniques, stochastic modeling, fuzzy logic and parallel predictive models have been used to develop neuro simulators, to forecast natural gas production for 20 years on a national level, and to develop a top-down reservoir model capable of identifying reservoir sweet spots and estimating reserves[22-24].

Artificial neural networks (ANNs) are a powerful tool that can learn the relationships between input parameters and their corresponding outputs. The relationship between a given input and output, or the governing equation, can be linear or nonlinear. The ANN becomes most useful when the relationship between inputs and outputs is not yet known. Although a trained

Name	Input/Output Relation	Icon	MATLAB Function
Hard Limit	$a = 0 \quad n < 0$ $a = 1 \quad n \geq 0$	⎍	Hardlim
Symmetrical Hard Limit	$a = -1 \quad n < 0$ $a = +1 \quad n \geq 0$	⊞	Hardlims
Linear	$a = n$	⧄	Purelin
Saturating Linear	$a = 0 \quad n < 0$ $a = n \quad 0 \leq n \leq 1$ $a = 1 \quad n > 1$	⧄	Satlin
Symmetric Saturating Linear	$a = -1 \quad n < -1$ $a = n \quad -1 \leq n \leq 1$ $a = 1 \quad n > 1$	⧄	Satlins
Log-Sigmoid	$a = \frac{1}{1+e^{-n}}$	∫	Logsig
Hyperbolic Tangent Sigmoid	$a = \frac{e^{n}-e^{-n}}{e^{n}+e^{-n}}$	∫	Tansig
Positive Linear	$a = 0 \quad n < 0$ $a = n \quad 0 \leq n$	⧄	Poslin
Competitive	$a = 1$ neuron with max n $a = 0$ all other neurons	C	Compet

Table 1. Commonly used transfer functions[25]

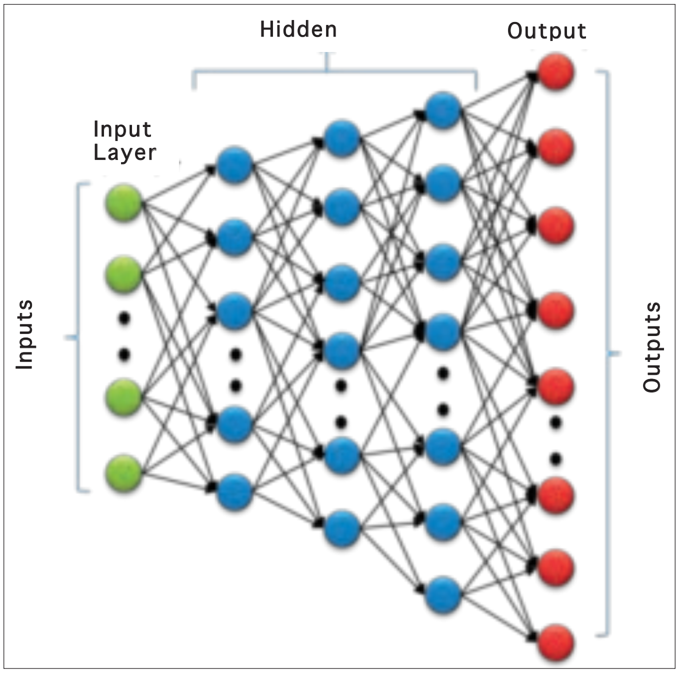

Fig. 6. A schematic showing how the input layer is connected to the output layer through a series of specified layers.

ANN can predict a solution within a specific acceptable error range, it lacks the ability to explicitly state the relationship between input and output parameters.

To predict output parameters, the ANN relies on a number of weights and biases. At the training phase, the ANN develops and calibrates its weights and biases during a trial-and-error process linking the input layer to the output one. To minimize the approximation error, the ANN uses the gradient descent technique in which the input layer is connected to the output layer through a number of user specified hidden layers, Fig. 6. Each layer is connected to the other by neurons and transfer functions. The user choses the transfer functions, which can be linear or nonlinear, that best suit the problem. Table 1 is a list of commonly used transfer functions[25].

METHODOLOGY

The goal of this research is to develop, using ANNs, the following expert systems, which can accurately and instantaneously perform the specified predictions:

1. Forward Production Profile Expert System — Fixed Flowing Bottom-hole Pressure (FEx-FBHP): Reservoir properties and complex well design parameters will be used as an input, and the trained ANN will predict the complex well production profile within an acceptable error range.
2. Inverse Well Architecture Design Expert System — Fixed FBHP (IWEx-FBHP): Reservoir properties and a desired complex well production profile will be used as an input, and the trained ANN will predict a complex well design that can deliver the set production profile from the specified reservoir.
3. Inverse Reservoir Rock Properties Expert System — Fixed FBHP (IREx-FBHP): Complex well design parameters and its production profile will be used as an input, and the trained ANN will predict the corresponding reservoir rock properties.

To achieve the aforementioned goals, the ANN needs to be trained on a database that is large enough to cover all possible ranges.

Data Gathering and Preparation

We cannot rely on available complex well data to train the proposed ANN because an extensive and comprehensive complex well data set does not exist for shale gas formations today. Therefore, a different source of complex well data was used. Currently available commercial numerical reservoir simulation software has the ability to simulate dual porosity, dual permeability reservoirs, so this software was used to generate the needed database to train the ANN.

ANN training requires a database that consists of a large number of data sets. Input parameters in each data set have to capture the maximum and minimum limits set by the user. For example, if the user is interested in complex wells that have between two and six laterals, and lateral lengths between 100 ft and 500 ft, then the database should include complex wells having two, three, four, five and six laterals, which in turn have lengths that vary randomly between 100 ft and 500 ft. In our case, all maximum and minimum limits of reservoir properties and complex well design parameters are shown in Tables 2 and 3, respectively. In addition, Tables 4, 5 and 6 show the input parameters for each expert system developed in this study.

ANN Training and Optimization Workflow

The generated database consists of a large number of data sets. Each data set consists of reservoir properties, complex well design parameters and a corresponding production profile. Data sets are divided into appropriate inputs and outputs based on the prediction mode, with either a forward or an inverse prediction problem. The database is divided into training, validation and testing data sets. In the training phase, the ANN uses trial and error to calibrate its weights and biases until it reaches a desired acceptable error. During the subsequent validation phase, the ANN gets exposed to new data sets, and it further calibrates its weights and biases. If the desired error is not achieved during the validation phase, then the training phase gets repeated again, but the knowledge gained in the validation phase is kept by the ANN to better aid the next training phase. Once an acceptable error is reached, then the testing phase begins. In the testing phase, the trained ANN gets introduced to a testing data set. If the desired error is not

Reservoir Properties			Fluid Composition	
Reservoir Size (acres)	200 – 800		C1	1.00000
Initial Reservoir Pressure P_i (psia)	4,000 – 6,000		C2	0.00000
Reservoir Temperature (°F)	140		C3	0.00000
Matrix Porosity (%)	5 – 10		iC4	0.00000
Fracture Porosity (%)	1% – 10% of Matrix Porosity		nC4	0.00000
Matrix Permeability (i,j) (md)	1.0E-05 – 1.0E-04		iC5	0.00000
Fracture Permeability (i,j) (md)	0.01 – 1.0		nC5	0.00000
Reservoir Thickness (ft)	50 – 300		C6	0.00000
Fracture Spacing (i,j,k) (ft)	1 – 5		C7+	0.00000

Table 2. Shale gas reservoir and fluid properties range

Horizontal Mainbore Length (ft)	864 – 1836
Number of Laterals	1 – 8
Length of Laterals (ft)	382 – 1756
Location of Mainbore (j^{th} row)	(middle row of 55, 77, 95 or 109 cells)
Lateral Spacing (ft)	54 – 1,836
Lateral Phase Angle (degrees)	45
Lateral Placement Pattern	Fishbone Pattern
Wellbore Constant Pressure p_{wf} (psi)	2,000 – 5,500

Table 3. Well design parameters

Category	Parameter	Unit
Well Design Parameters	Mainbore Length	ft
	Well Location with Respect to the Northern Reservoir Boundary	ft
	Well Location with Respect to the Western Reservoir Boundary	ft
	Number of Laterals	
	1st to 8th Lateral Direction	1 - upward 2 - downward
	1st to 8th Lateral Spacing	ft
	1st to 8th Lateral Length	ft
Reservoir Properties	Drainage Area	Acres
	Reservoir Thickness	ft
	Initial Reservoir Pressure (p_i)	psi
Well Operating Condition	Flowing BHP (p_{wf})	psi
Reservoir Properties	Matrix Porosity (ϕm)	fraction
	Natural Fracture Porosity (ϕf)	fraction
	Matrix Permeability (km)	md
	Natural Fracture Permeability (kf)	md
	Natural Fracture Spacing	ft

Table 4. FEx-FBHP input parameters

achieved in the testing phase or the subsequent blind testing phase, then input combinations that are less represented and contribute more to error are identified. More cases representing these input combinations are generated to be introduced to the original database. Figure 7 is a workflow for the training cycle[5].

The very first training of the ANN is always done on the original input and output data, without any modification, data manipulation or functional links. This gives a reference point for the trainer to judge the effect of introducing functional links or using data manipulation techniques. In the optimization process, the trainer strives to reduce the ANN prediction error by testing the ANN response to any modifying of its structure, functions, neurons or data. The user can change the training function, change the learning function, change the transfer function, introduce functional links, use data manipulation techniques, change the number of layers, and/or change the number of neurons in all or some of the layers.

The prediction error is defined differently for forward prediction problems than for inverse prediction problems. An error in the forward prediction problems is defined by a straightforward comparison between simulation outputs and ANN predicted outputs, namely simulation production profiles vs. ANN production profiles. Alternatively, in inverse prediction problems, the error calculation cannot be based on output accuracy due to the principle of the nonuniqueness of the solution. For example, the production profile of a given complex well can be matched by that of a complex well of a total different design in the same reservoir. Figure 8 shows the comparison between the production profiles with an 8.37% error rate. It is clear that the defining error in such an inverse prediction problem, based on the ANN's inability to match the actual complex well design, is misleading since the solution is not unique. Therefore, in this research, inverse prediction problems are judged based on the predicted parameter's ability

Category	Parameter	Unit
Well Design Parameters	Mainbore Length	ft
	Well Location with Respect to the Northern Reservoir Boundary	ft
	Well Location with Respect to the Western Reservoir Boundary	ft
	Number of Laterals	
	1st to 8th Lateral Direction	1 - upward 2 - downward
	1st to 8th Lateral Spacing	ft
	1st to 8th Lateral Length	ft
Reservoir Properties	Reservoir Thickness	ft
	Initial Reservoir Pressure (p_i)	psi
Well Operating Condition	Flowing BHP (p_{wf})	psi
Well Performance	Cumulative Production at Day 1	scf
	Cumulative Production at Day 30	
	Cumulative Production at Day 60	
	… … …	
	… … …	
	Cumulative Production at Day 1,080	

Table 6. IREx-FBHP input parameters

to regenerate production profiles, rather than on an actual comparison between well designs or between rock properties.

RESULTS

The results of this study indicate that a well trained ANN is capable of instantaneously and accurately predicting production profiles, complex well designs and shale gas reservoir properties. The results for the three expert systems are summarized next.

In this research, it has been noted that the ANN prediction ability is improved when production profiles are monotonically increasing; therefore, all production profiles were converted to cumulative production profiles for the ANN training.

FEx-FBHP

For any given complex well design and any given shale gas reservoir with properties within the training range, FEx-FBHP can instantaneously and accurately predict cumulative production profiles. Table 7 shows the ANN design parameters of this expert system.

Category	Parameter	Unit
Reservoir Properties	Drainage Area	Acres
	Reservoir Thickness	ft
	Initial Reservoir Pressure (p_i)	psi
Well Operating Condition	Flowing BHP (p_{wf})	psi
Reservoir Properties	Matrix Porosity (ϕm)	fraction
	Natural Fracture Porosity (ϕf)	fraction
	Matrix Permeability (km)	md
	Natural Fracture Permeability (kf)	md
	Natural Fracture Spacing	ft
Well Performance	Cumulative Production at Day 1	scf
	Cumulative Production at Day 30	
	Cumulative Production at Day 60	
	… … …	
	… … …	
	Cumulative Production at Day 3,600	

Table 5. IWEx-FBHP input parameters

Data manipulation techniques and both simple functional links and complex functional links were introduced to inputs and outputs during the ANN training process to improve its accuracy, shown in Tables 8 and 9, respectively. Simple functional links, e.g., pi – pwf, were added by means of trial and error; however, complex functional links were added after quantifying the major sources of error. For example, the predictions of initial cumulative production values were usually missed, thereby contributing to a large error value. Input parameters were analyzed for initial production patterns. Two input groups were identified and introduced as functional

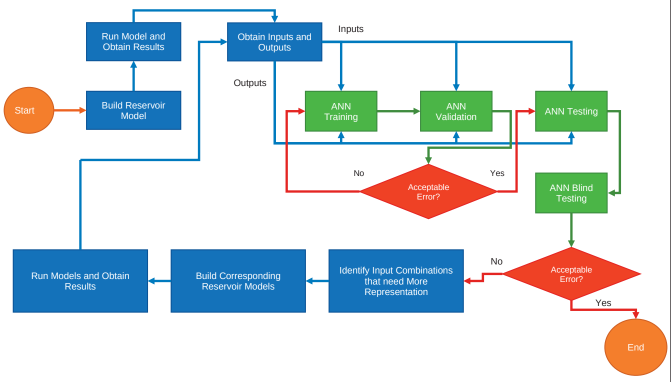

Fig. 7. Workflow for the ANN training process[6].

links (FL #15 and FL #16), Figs. 9 and 10. The introduction of these functional links, and all the other functional links and data manipulation techniques, has contributed to reducing the prediction error of the ANN.

Table 10 lists the minimum, maximum and average prediction errors of FEx-FBHP. The neural network training plot, the training performance plot and the regression plots are shown in Figs. 11, 12, and 13, respectively. The five original test cases are presented in Fig. 14 (3.89% error), Fig. 15 (2.69% error), Fig. 16 (2.62% error), Fig. 17 (3.55% error) and Fig. 18 (7.68% error).

Practicality Test FEx-FBHP

In addition to obtaining error ranges of the FEx-FBHP predictions, a practicality test was performed to test for the ability of the FEx-FBHP to respond accurately to single parameter sensitivities. Two random data sets were selected to perform the practicality test. The first data set had sensitivity on fracture permeability, Table 11, and the second had sensitivity on FBHP, Table 12. The FEx-FBHP showed an accurate signature response to all sensitivities, Figs. 19 and 20.

IWEx-FBHP

The IWEx-FBHP can instantly and accurately propose a complex well design capable of producing the given cumulative production profile from the given reservoir. Table 13 lists the ANN design parameters of this expert system. Data manipulation techniques, simple functional links and complex functional links were introduced to inputs and outputs during the ANN training process to improve its accuracy. Tables 14 and 15 summarize the data manipulation techniques and functional links used in training this ANN.

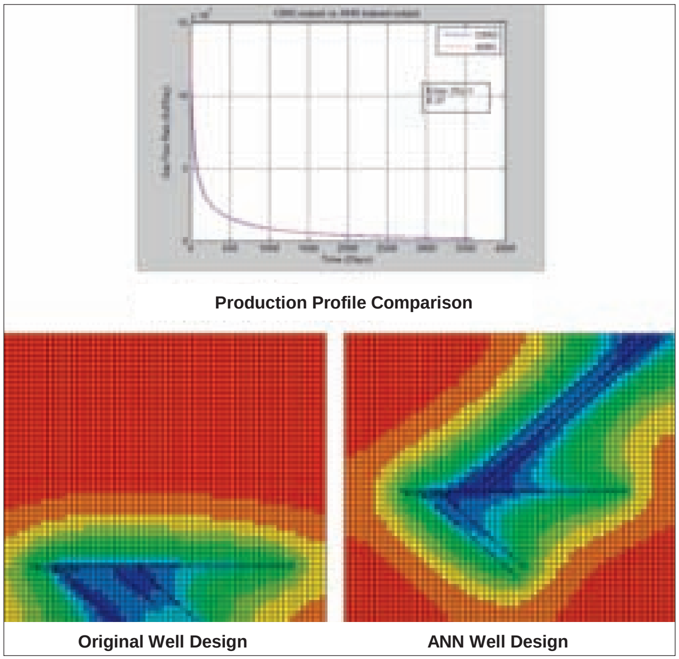

Fig. 8. Comparison of simulation results vs. the ANN results showing different well designs for matching production profiles, with an 8.37% error based on the production profiles.

Network Type	Feed-forward with back Propagation
Number of Hidden Layers	3
Number of Neurons for Hidden Layers	[23, 18, 16]
Number of Case Scenarios	546
Train, Validate, Test Ratio (%)	[75, 24, 1]
Training Function	Trainscg (Scaled Conjugate Gradient)
Transfer Functions	[Tansig, Tansig, Logsig]
Learning Function	Learngdm
Performance Function	Msereg (Mean Square Error with Reg.)
Minimum Performance Goal	5E-05
Maximum Number of Validation Increases	1,000
Maximum Number of Training Iterations	8,000
Minimum Gradient Magnitude	1E-06

Table 7. FEx-FBHP neural network design parameters

Table 16 lists the minimum, maximum and average prediction errors of the IWEx-FBHP. Figures 21, 22 and 23 show the neural network training plot, the training performance plot, and the regression plots, respectively.

A representation of the five original test cases are presented in Fig. 24 (1.89% error), Fig. 25 (3.08% error), Fig. 26 (1.68% error), Fig. 27 (5.43% error) and Fig. 28 (10.26% error). The production profile of the proposed complex well design was generated by commercial numerical reservoir simulation software as well as by the FEx-FBHP.

IREx-FBHP

The IREx-FBHP can instantly and accurately predict a shale gas reservoir property suited for any given three-year

Number	Parameter	Input of Output
DM 1	Ln (Matrix Porosity)	Input
DM 2	Ln (Fracture Porosity)	Input
DM 3	Ln (Matrix Permeability)	Input
DM 4	Ln (Fracture Permeability)	Input
DM 5	1/Ln (Matrix Porosity)	Input
DM 6	1/Ln (Fracture Porosity)	Input
DM 7	1/Ln (Matrix Permeability)	Input
DM 8	1/Ln (Fracture Permeability)	Input

Table 8. FEx-FBHP data manipulation techniques

Number	Functional Link	Input or Output
FL 1	Ln(Matrix Porosity) * Ln (Fracture Porosity)	Input
FL 2	SQRT[Ln (Matrix Permeability)^2 + Ln (Fracture Permeability)^2]	Input
FL 3	Max (Eigen values (Ln (Matrix Porosity), Ln (Fracture Porosity)))	Input
FL 4	Max (Eigen values (Ln (Matrix Permeability), Ln (Fracture Permeability)))	Input
FL 5	Mainbore Length/Reservoir Area	Input
FL 6	Mainbore Length/Reservoir Thickness	Input
FL 7	Pi – pwf	Input
FL 8	Total Wellbore Length (Mainbore + All Laterals)	Input
FL 9	Reservoir Thickness * Reservoir Area * ln (Matrix Porosity)	Input
FL 10	Reservoir Thickness * Reservoir Area * ln (Matrix Porosity) * ln (Matrix Permeability)	Input
FL 11	Reservoir Thickness * Reservoir Area * ln (Matrix Porosity) * ln (Fracture Permeability)	Input
FL 12	Total Wellbore Length/Reservoir Area	Input
FL 13	Total Wellbore Length/Thickness	Input
FL 14	Total Wellbore Length/(Reservoir Thickness * Reservoir Area * ln (Matrix Porosity))	Input
FL 15	(Pi-pwf) * Thickness * Total Wellbore Length	Input
FL 16	Log[(Pi-pwf) * Thickness * Total Wellbore Length * Fracture Permeability * Fracture Porosity/Natural Fracture Spacing]	Input
FL 17	Log[Reservoir Area * Matrix Porosity]	Input
FL 18	-Log[Reservoir Area * Matrix Porosity * Matrix Permeability]	Input

Table 9. FEx-FBHP functional links

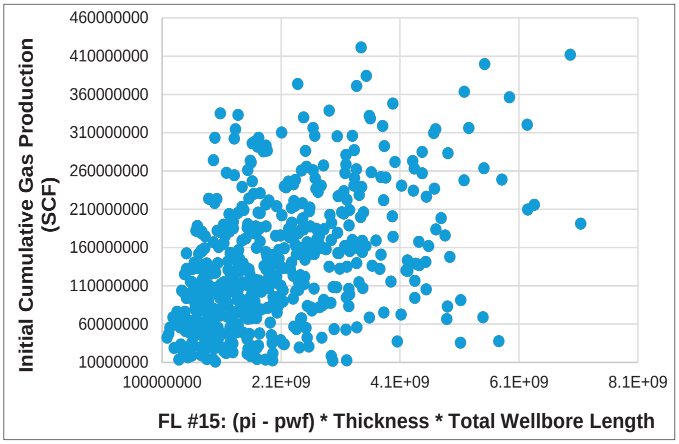

Fig. 9. Initial cumulative production functional link #15.

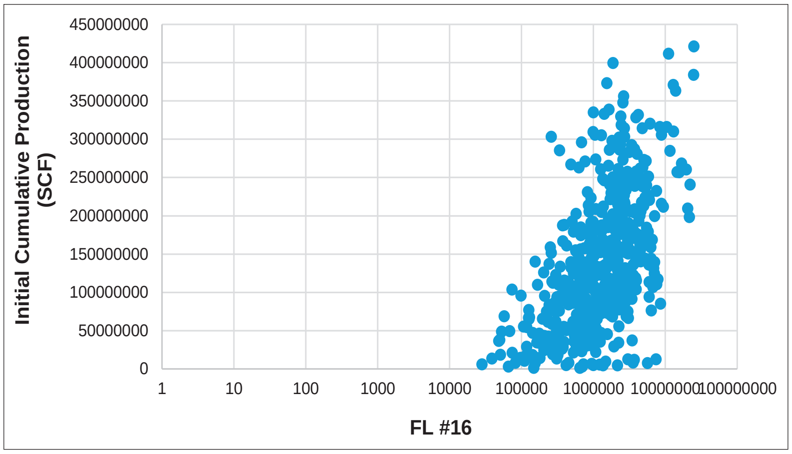

Fig. 10. Initial cumulative production functional link #16. Semi-logarithmic scale.

cumulative gas production profile from any given complex design design. A number of ANNs were trained to achieve the set goals of the IREx-FBHP, but they were not successful in reaching the desired accuracy. Further analysis indicated that the prediction error in natural fracture permeability, drainage area and matrix porosity resulted in the highest production profile error.

To solve this problem, three different ANNs were trained to predict these parameters. The first ANN predicts natural fracture permeability. The second ANN predicts the drainage area, and using the same input parameters used in training the first ANN, adds to it the predicted natural fracture permeability as an additional input. The third ANN predicts matrix porosity, and similar to the second ANN in its use of predicted natural fracture permeability, adds to it the predicted drainage area to predict matrix porosity. After obtaining these critical parameters, they are all used as an additional input in training the final ANN used to generate the IRex-FBHP.

Table 17 lists the minimum, maximum and average prediction errors of the IREx-FBHP. Alqahtani (2015)[5] shows the neural network training plot, the training performance plot, and the regression plots for all four ANNs used in training the IREx-FBHP. Please note that these plots are not presented in this article. The six original test cases are presented in Fig. 29 (0.23% error), Fig. 30 (1.27% error), Fig. 31 (0.95% error), Fig. 32 (6.97% error), Fig. 33 (3.96% error), and Fig. 34 (2.37% error).

	Original Test Cases	Blind Cases
Average Error (%)	4.09	7.61
Maximum Error (%)	7.68	69.47
Minimum Error (%)	2.62	0.45

Table 10. FEx-FBHP original test cases and blind cases errors

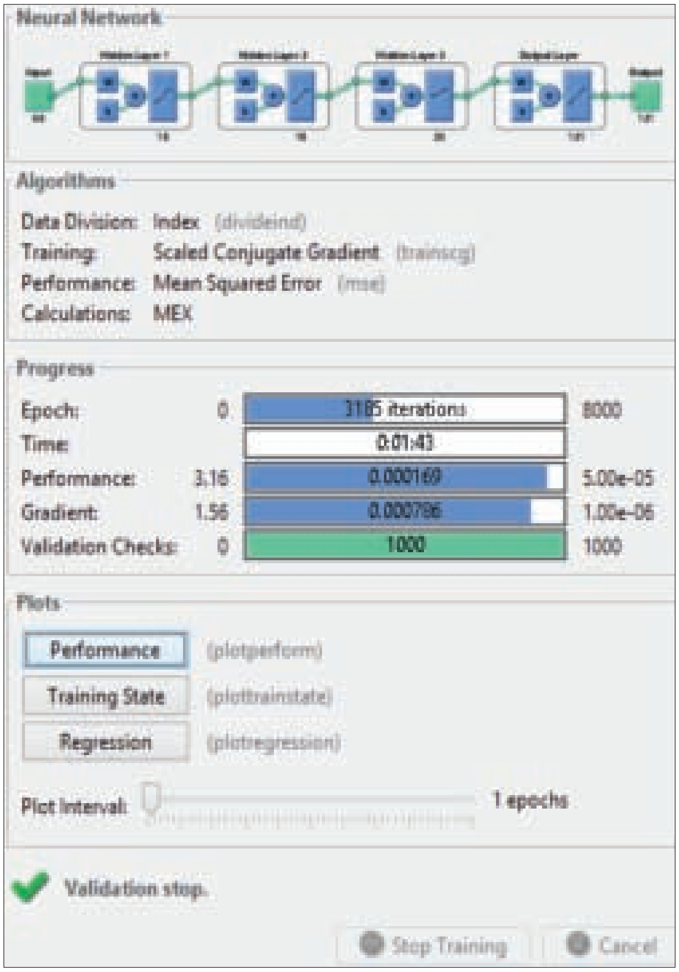

Neural Network

Algorithms

Data Division: Index (divideind)
Training: Scaled Conjugate Gradient (trainscg)
Performance: Mean Squared Error (mse)
Calculations: MEX

Progress

Epoch:	0	3185 iterations	8000
Time:		0:01:43	
Performance:	3.16	0.000169	5.00e-05
Gradient:	1.56	0.000786	1.00e-06
Validation Checks:	0	1000	1000

Plots

Plot Interval: 1 epochs

Validation stop.

Fig. 11. Neural network training pilot for FEx-FBHP.

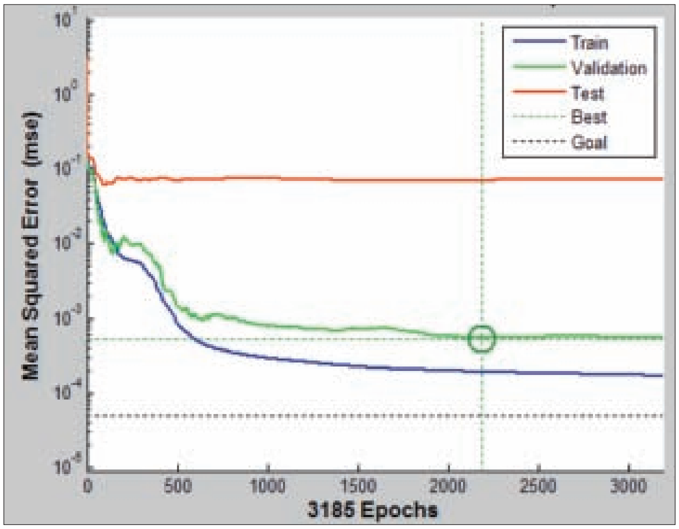

Fig. 12. Training performance pilot for FEx-FBHP.

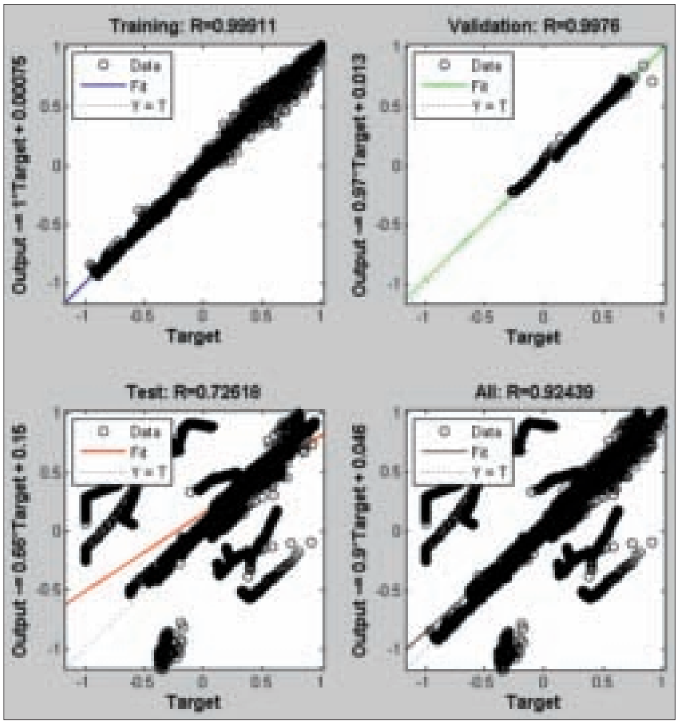

Fig. 13. Regression plots for FEx-FBHP.

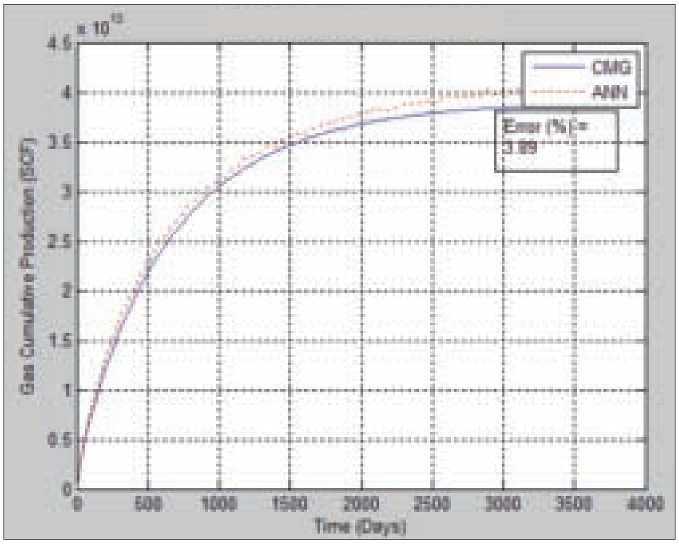

Fig. 14. Comparison of simulation results vs. the ANN results of an original test case, with a 3.89% error.

CONCLUSIONS

The results of the presented expert systems, in forward and inverse prediction modes, prove that a well trained ANN is capable of making fast and accurate predictions. These results increase the confidence in utilizing ANNs to solve petroleum engineering problems. It also opens the door for future work to be done. In addition, these results increase the level of confidence in using complex wells as an alternative to horizontal wells with massive hydraulic fracturing.

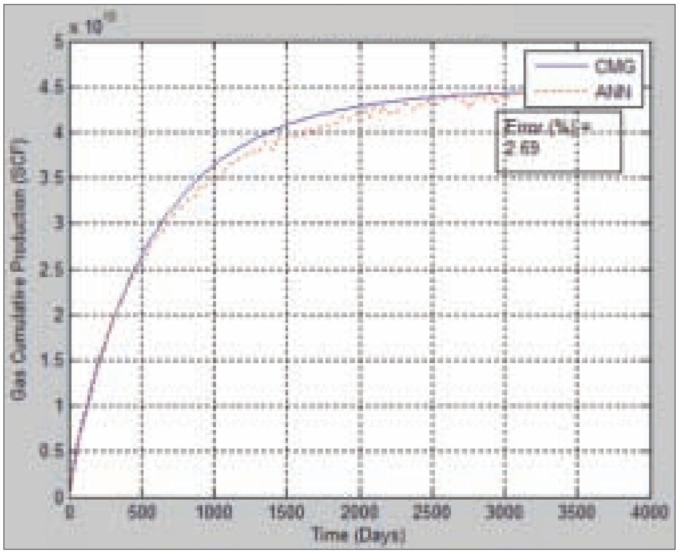

Fig. 15. Comparison of simulation results vs. the ANN results of an original test case, with a 2.69% error.

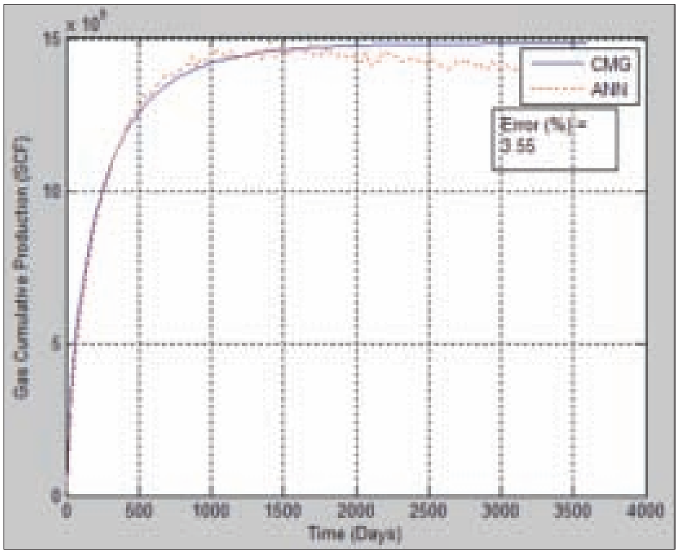

Fig. 17. Comparison of simulation results vs. the ANN results of an original test case, with a 3.55% error.

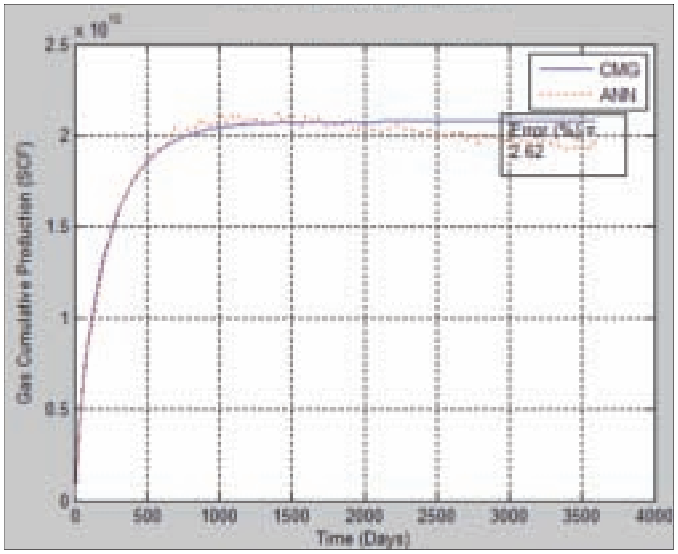

Fig. 16. Comparison of simulation results vs. the ANN results of an original test case, with a 2.62% error.

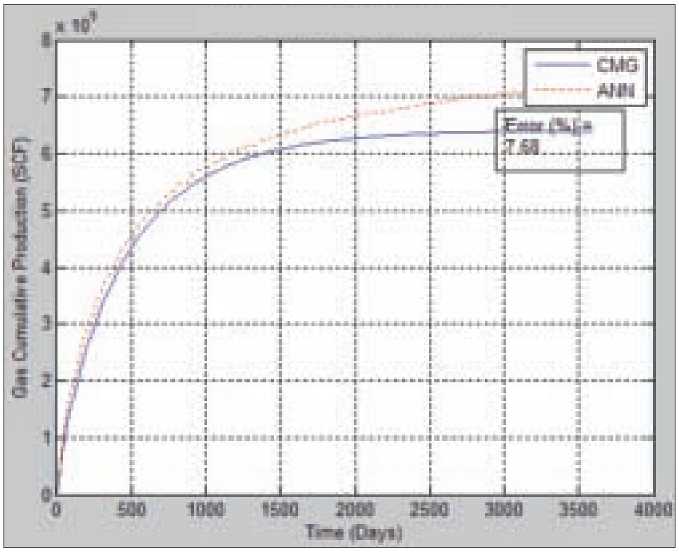

Fig. 18. Comparison of simulation results vs. the ANN results of an original test case, with a 7.68% error.

	Base Case 1	kf - -	kf -	kf +	kf + +
Drainage Area	800	800	800	800	800
Thickness	105	105	105	105	105
pi	5,200	5,200	5,200	5,200	5,200
pwf	1,700	1,700	1,700	1,700	1,700
Matrix Porosity	0.074	0.074	0.074	0.074	0.074
Fracture Porosity	0.0052	0.0052	0.0052	0.0052	0.0052
Matrix Permeability	0.00005	0.00005	0.00005	0.00005	0.00005
Fracture Permeability	0.58	0.1	0.25	0.75	0.9
Natural Fracture Spacing	2	2	2	2	2

Table 11. FEx-FBHP fracture permeability practicality test cases

ACKNOWLEDGMENTS

The authors would like to thank the management of Saudi Aramco for their support and permission to publish this article. The authors would also like to thank The John and Willie Leone Family Department of Energy and Mineral Engineering

	Base Case 2	pwf - -	pwf -	pwf +	pwf + +
Drainage Area	600	600	600	600	600
Thickness	195	195	195	195	195
pi	5,250	5,250	5,250	5,250	5,250
pwf	3,250	3,000	3,150	3,400	3,550
Matrix Porosity	0.089	0.089	0.089	0.089	0.089
Fracture Porosity	0.0013	0.0013	0.0013	0.0013	0.0013
Matrix Permeability	0.00006	0.00006	0.00006	0.00006	0.00006
Fracture Permeability	0.592	0.592	0.592	0.592	0.592
Natural Fracture Spacing	2	2	2	2	2

Table 12. FEx-FBHP practicality test cases

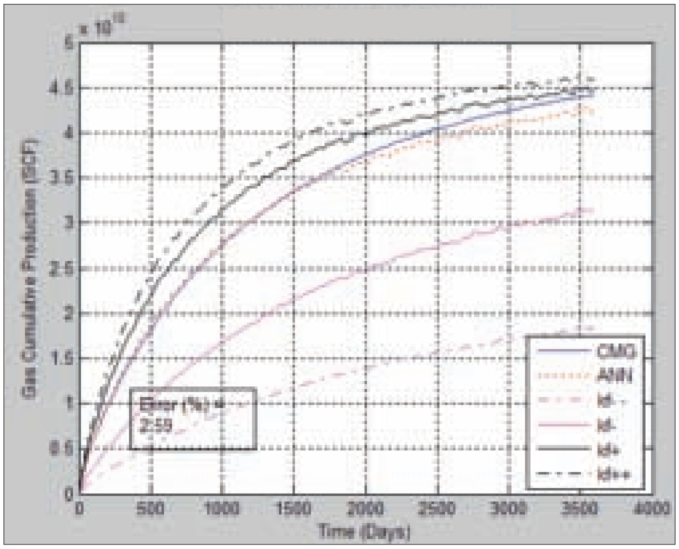

Fig. 19. FEx-FBHP response to natural fracture permeability changes.

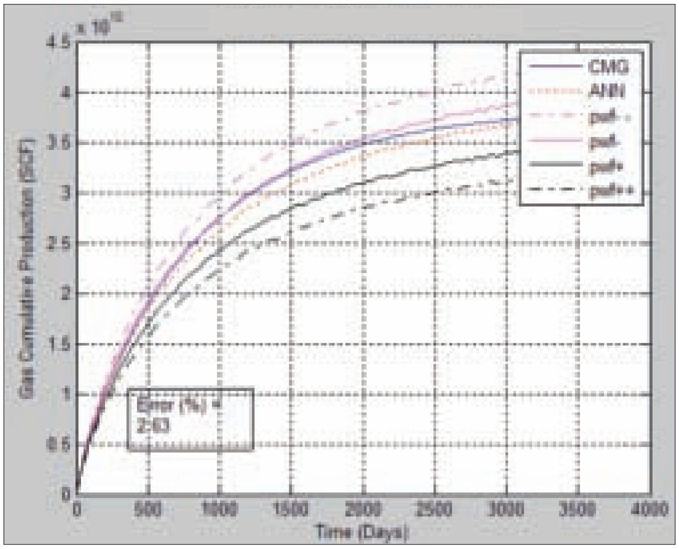

Fig. 20. FEx-FBHP response to FBHP changes.

Network Type	Feed-forward with back propagation
Number of Hidden Layers	3
Number of Neurons for Hidden Layers	[16, 18, 23]
Number of Case Scenarios	1,274
Train, Validate, Test Ratio (%)	[75, 24, 1]
Training Function	Trainscg (Scaled Conjugate Gradient)
Transfer Functions	[Tansig, Tansig, Logsig]
Learning Function	Learngdm
Performance Function	Msereg (Mean Square Error with Reg.)
Minimum Performance Goal	5E-05
Maximum Number of Validation Increases	1,000
Maximum Number of Training Iterations	8,000
Minimum Gradient Magnitude	1E-06

Table 13. IWEx-FBHP neural design parameters

at Pennsylvania State University for their permission to present this article.

This article was presented at the SPE Kingdom of Saudi Arabia Annual Technical Symposium and Exhibition, Dammam, Saudi Arabia, April 24-27, 2017.

REFERENCES

1. EIA: *Annual Energy Outlook 2017 with Projections to 2050*, U.S. Energy Information Administration Report,

Number	Parameter	Input or Output
DM 1	Mainbore Length/54	Input
DM 2	Well distance from the j boundary/54	Input
DM 3	Well distance from the j boundary/54	Input

Table 14. IWEx-FBHP data manipulation techniques

Number	Functional Link	Input or Output
FL 1	$p_i - p_{wf}$	Input
FL 2	Initial cumulative production/($p_i - p_{wf}$)	Input

Table 15. IWEx-FBHP functional links

	Original Test Cases	Blind Cases
Average Error (%)	4.62	13.85
Maximum Error (%)	10.26	32.64
Minimum Error (%)	1.68	4.90

Table 16. IWEx-FBHP original test cases and blink case errors

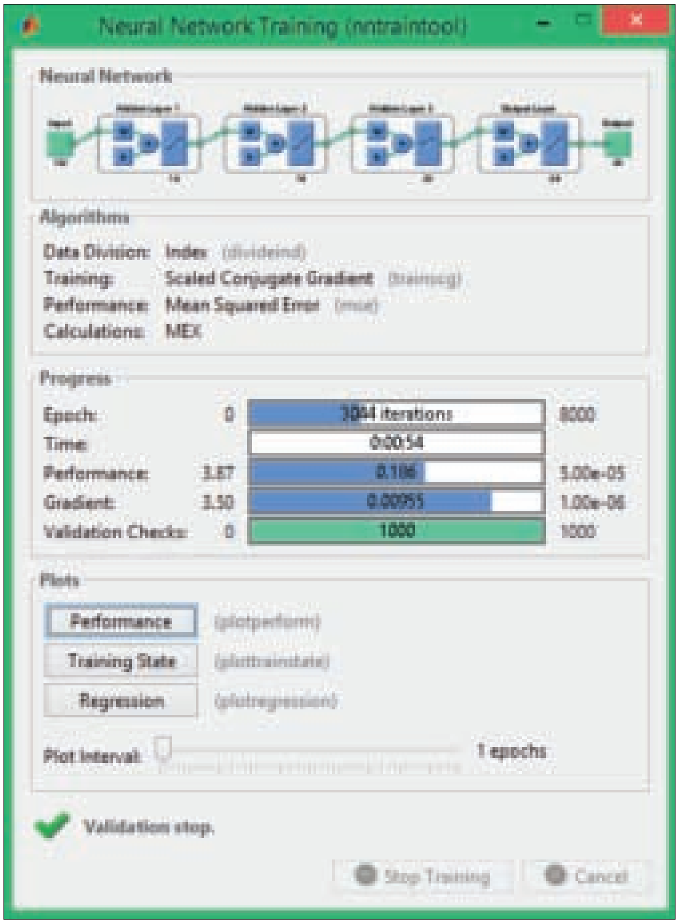

Algorithms

Data Division: Index (divideind)
Training: Scaled Conjugate Gradient (trainscg)
Performance: Mean Squared Error (mse)
Calculations: MEX

Progress

Epoch: 0 3044 iterations 8000
Time: 0:00:54
Performance: 3.87 0.186 5.00e-05
Gradient: 3.50 0.00955 1.00e-06
Validation Checks: 0 1000 1000

Plot Interval: 1 epochs

Validation stop.

Fig. 21. Neural network training plot for the IWEx-FBHP.

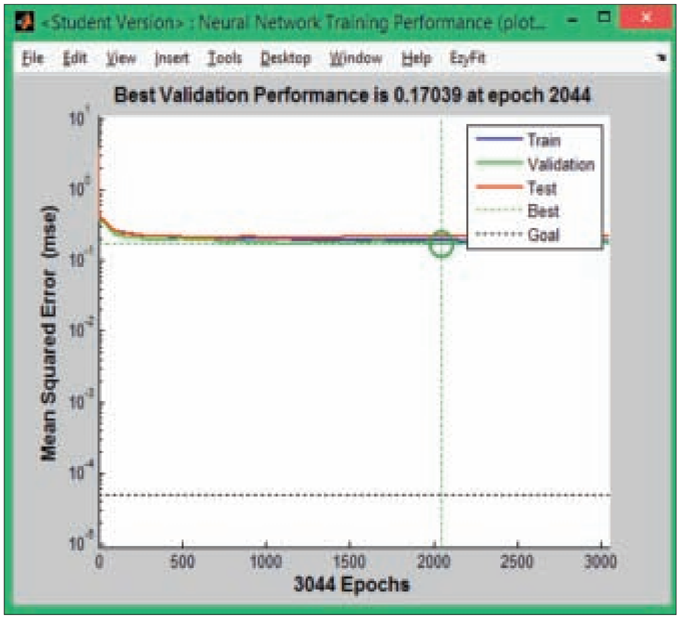

Fig. 22. Training performance plot for IWEx-FBHP.

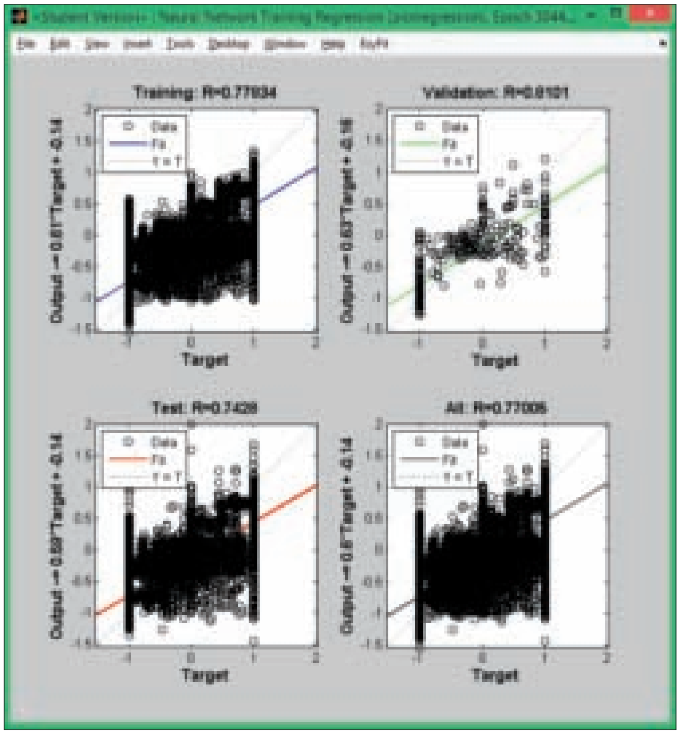

Fig. 23. Regression plots for the IWEx-FBHP.

AEO2017, Washington, D.C., January 2017

2. EIA: *Shale Gas Production Drives World Natural Gas Production Growth*, U.S. Energy Information Administration Report, AEO2016, Washington, D.C., August 2016.

3. U.S. Department of Energy: *Natural Gas from Shale: Questions and Answers*, https://energy.gov/sites/prod/files/2013/04/f0/complete_brochure.pdf, 2013.

4. EIA: *U.S. Natural Gas Gross Withdrawals from Shale Gas*, U.S. Energy Information Administration Report, Washington, D.C., May 2017.

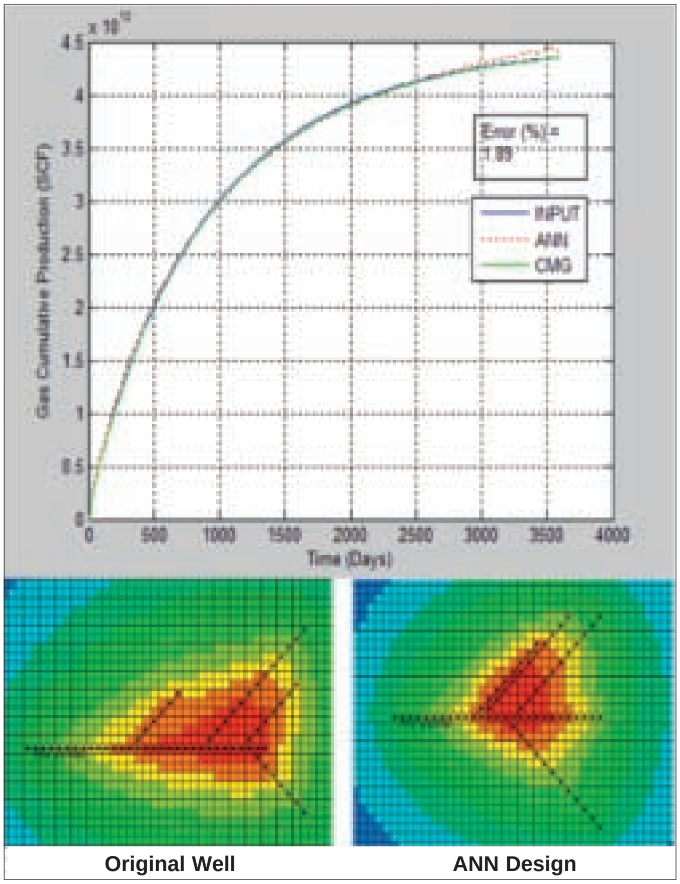

Fig. 24. Comparison of simulation results vs. the ANN results showing well designs and production profiles, with a 1.89% error. An original test case.

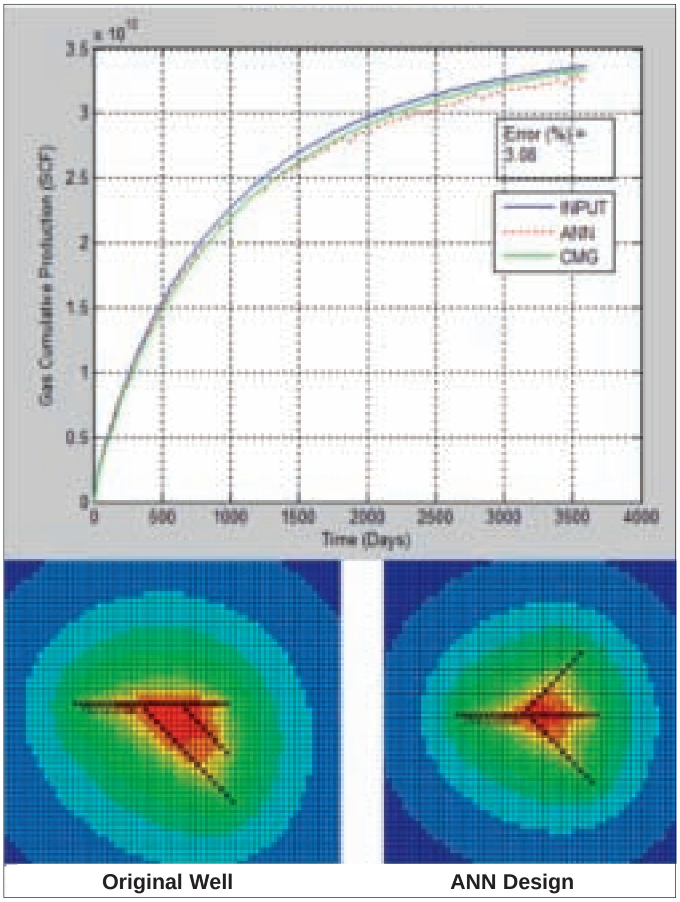

Fig. 25. Comparison of simulation results vs. the ANN results showing well designs and production profiles, with a 3.08% error. An original test case.

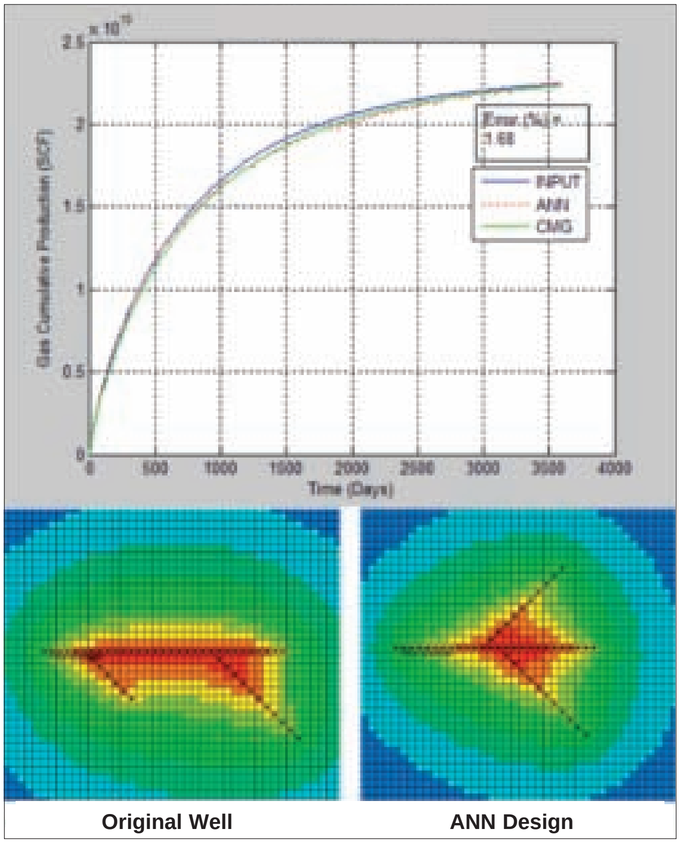

Fig. 26. Comparison of simulation results vs. the ANN results showing well designs and production profiles, with a 1.68% error. An original test case.

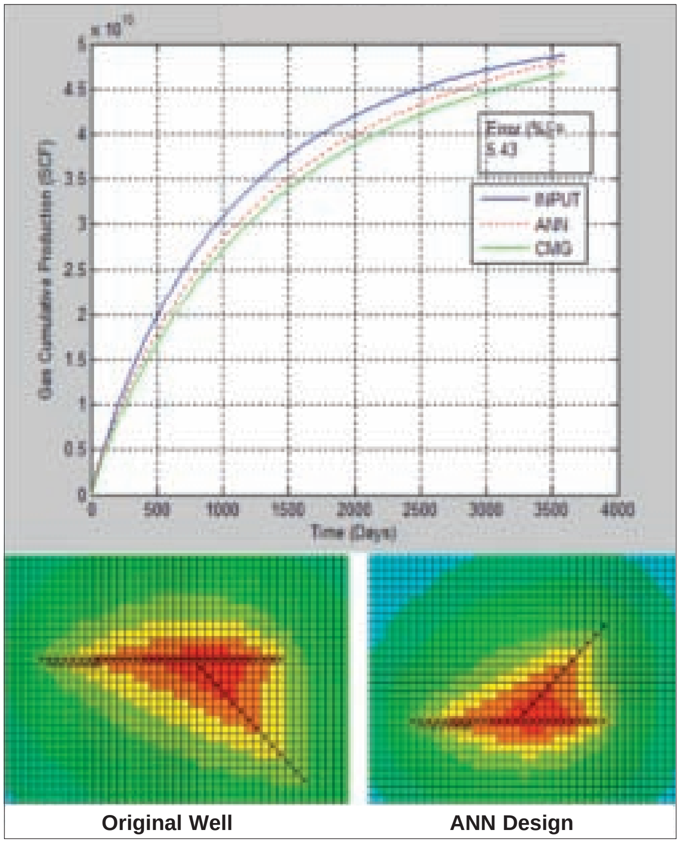

Fig. 27. Comparison of simulation results vs. the ANN results showing well designs and production profiles, with a 5.43% error. An original test case.

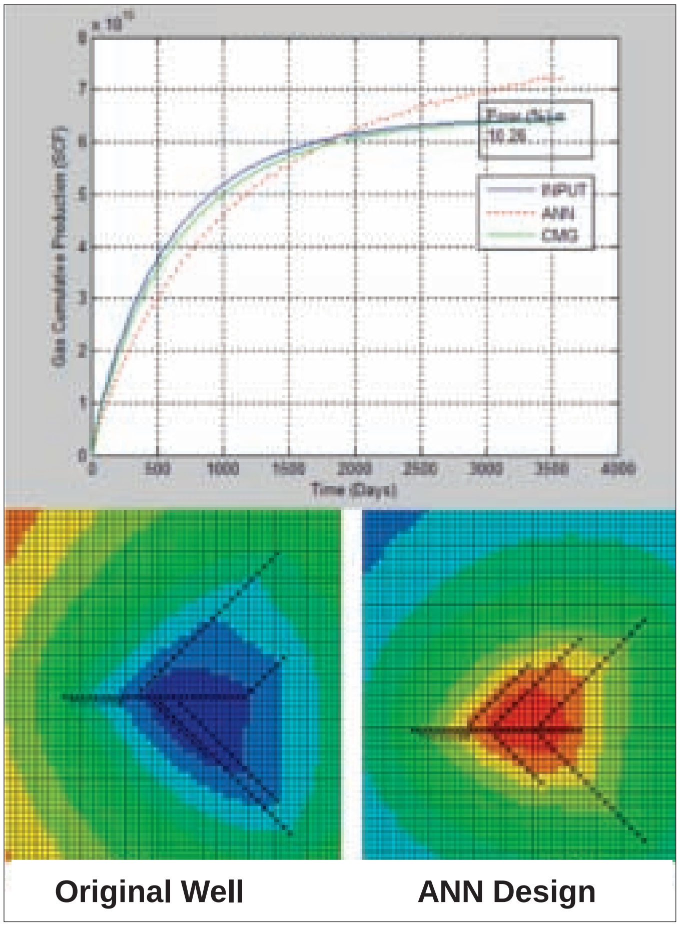

Fig. 28. Comparison of simulation results vs. the ANN results showing well designs and production profiles, with a 10.26% error. An original test case.

	Original Test Cases
Average Error (%)	2.63
Maximum Error (%)	6.97
Minimum Error (%)	0.23

Table 17. IRFx-FBHP original test case errors

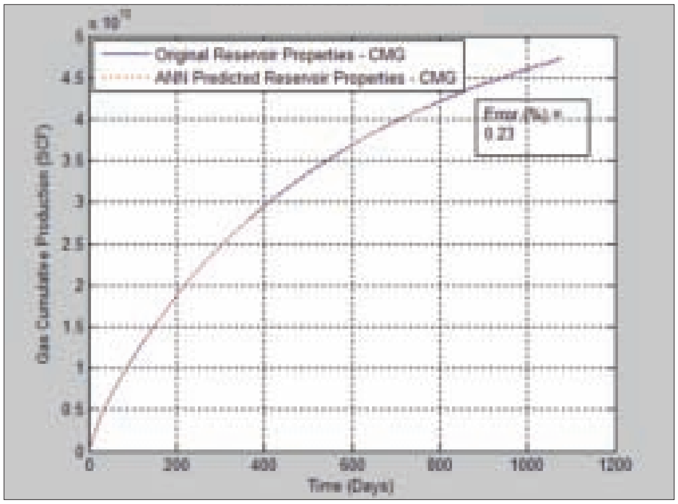

Fig. 29. Comparison of simulation results vs. production of ANN reservoir property prediction, with a 0.23% error. An original test case.

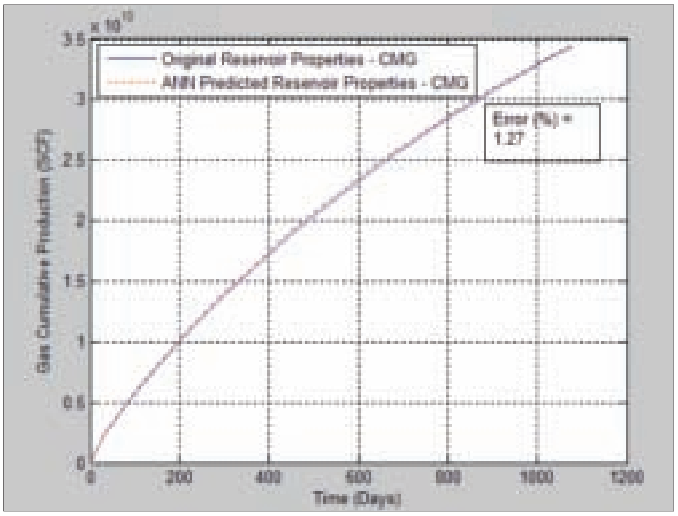

Fig. 30. Comparison of simulation results vs. production of ANN reservoir property prediction, with a 1.27% error. An original test case.

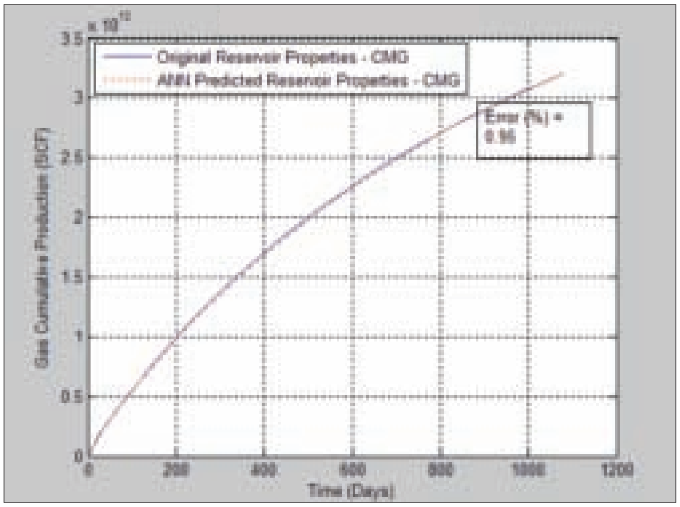

Fig. 31. Comparison of simulation results vs. production of ANN reservoir property prediction, with a 0.95% error. An original test case.

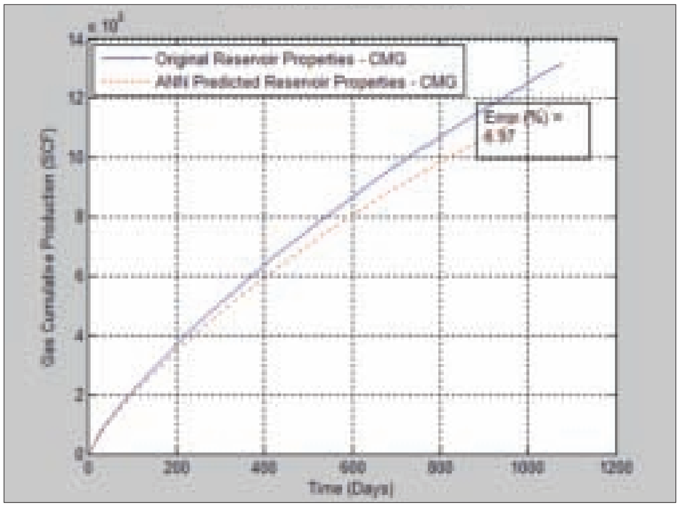

Fig. 32. Comparison of simulation results vs. production of ANN reservoir property prediction, with a 6.97% error. An original test case.

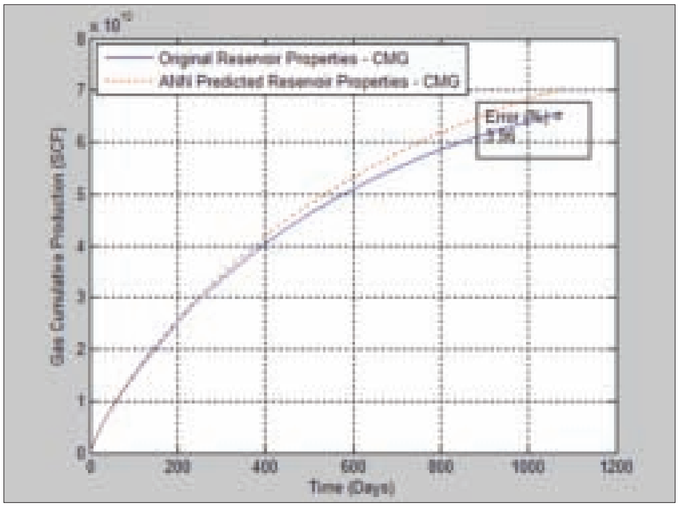

Fig. 33. Comparison of simulation results vs. production of ANN reservoir property prediction, with a 3.96% error. An original test case.

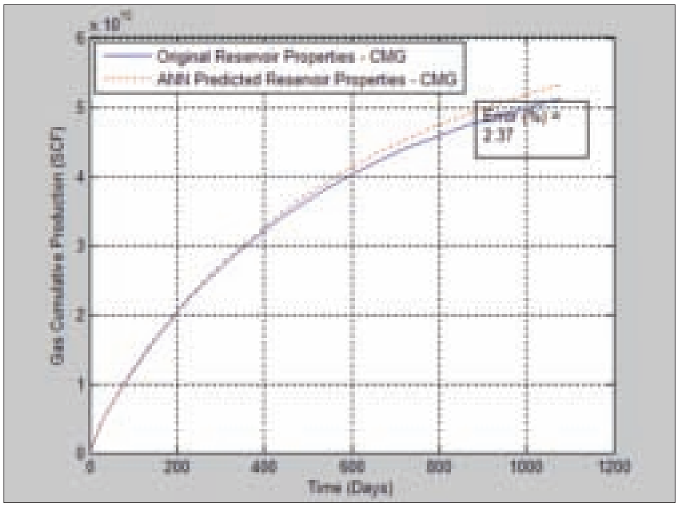

Fig. 34. Comparison of simulation results vs. production of ANN reservoir property prediction, with a 2.37% error. An original test case.

5. Holditch, S.A.: "Tight Gas Sands," *Journal of Petroleum Technology*, Vol. 58, Issue 6, June 2006, pp. 86-93.
6. Alqahtani, M.H.: "Shale Gas Reservoirs Development Strategies via Advanced Well Architectures," Ph.D. Dissertation, Pennsylvania State University, State College, Pennsylvania, June 2015.
7. Mengal, S.A. and Wattenbarger. R.A.: "Accounting for Adsorbed Gas in Shale Gas Reservoirs," SPE paper 141085, presented at the SPE Middle East Oil and Gas Show and Conference, Manama, Bahrain, September 25-28, 2011.
8. Warren, J.E. and Root, P.J.: "The Behavior of Naturally Fractured Reservoirs," *Society of Petroelum Engineers Journal*, Vol. 3, Issue 3, September 1963, pp. 245-255.
9. Fisher, M.K., Wright, C.A., Davidson, B.M., Steinsberger, N.P., et al.: "Integrating Fracture Mapping Technologies to Improve Stimulations in the Barnett Shale," *SPE Production & Facilities*, Vol. 20, Issue 2, May 2005, pp. 85-93.
10. Taleghani, D.A. and Olson, J.E.: "Numerical Modeling of Multistranded Hydraulic Fracture Propagation: Accounting for the Interaction between Induced and Natural Fractures," *SPE Journal*, Vol. 16, Issue 3, September 2011, pp. 575-581.
11. Olson, J.E. and Taleghani, A.D.: "Modeling Simultaneous Growth of Multiple Hydraulic Fractures and Their Interaction with Natural Fractures," SPE paper 119739, presented at the SPE Hydraulic Fracturing Technology Conference, The Woodlands, Texas, January 19-21, 2009.
12. Hossain, M.M., Rahman, M.K. and Rahman, S.S.: "A Shear Dilation Stimulation Model for Production Enhancement from Naturally Fractured Reservoirs," *SPE Journal*, Vol. 7, Issue 2, June 2002, pp. 183-195.
13. Ouyang, L. and Aziz, K.: "A General Single-Phase Wellbore/Reservoir Coupling Model for Multilateral Wells," *SPE Reservoir Evaluation and Engineering*, Vol. 4, Issue 4, August 2001, pp. 327-335.
14. Joshi, S.: "Horizontal and Multilateral Wells: Performance Analysis — An Art or a Science?" *Journal of Canadian Petroleum Technology*, Vol. 39, Issue 10, October 2000, pp. 19-23.
15. Stalder, J.L., York, G.D., Kopper, R.J., Curtis, C.M., et al.: "Multilateral Horizontal Wells Increase Rate and Lower Cost per Barrel in the Zuata Field, Faja, Venezuela," SPE paper 69700, presented at the SPE International Thermal Operations and Heavy Oil Symposium, Portamar, Margarita Island, Venezuela, March 12-14, 2001.
16. Xiance, Y., Guo, B., Ai, C. and Bu, Z.: "A Comparison between Multi-Fractured Horizontal and Fishbone Wells for Development of Low Permeability Fields," SPE paper 120579, presented at the Asia Pacific Oil and Gas Conference and Exhibition, Jakarta, Indonesia, August 4-6, 2009.

17. Iktissanov, V.A.: "Pressure Transient Analysis and Simulation of Nonconventional Wells," SPE paper 133477, presented at the SPE Russian Oil and Gas Technical Conference and Exhibition, Moscow, Russia, October 26-28, 2010.
18. Jordan, C.L., Waeyen, B. and Jackson, R.: "An Alternative Method for Horizontal and Multilateral Pressure Transient Analysis," OMC paper 2009-022, presented at the Offshore Mediterranean Conference and Exhibition, Ravenna, Italy, March 25-27, 2009.
19. Garrouch, A.A., Lababidi, H.M.S. and Ebrahim, A.: "A Novel Expert System for Multilateral Well Completion," SPE paper 83474, presented at the SPE Western Regional/AAPG Pacific Section Joint Meeting, Long Beach, California, May 19-24, 2003.
20. Yeten, B., Durlofsky, L.J. and Aziz, K.: "Optimization of Nonconventional Well Type, Location, and Trajectory," SPE paper 86880, presented at the SPE Annual Technical Conference and Exhibition, San Antonio, Texas, September 29-October 2, 2003.
21. Bukhamsin, A.Y., Farshi, M.M. and Aziz, K.: "Optimization of Multilateral Well Design and Location in a Real Field Using a Continuous Genetic Algorithm," SPE paper 136944, presented at the SPE/DGS Annual Technical Symposium and Exhibition, al-Khobar, Saudi Arabia, April 4-7, 2010.
22. Doraisamy, H., Ertekin, T. and Grader, A.S.: "Methods of Neuro-Simulation for Field Development," SPE paper 39962, presented at the SPE Rocky Mountain Regional/Low Permeability Reservoirs Symposium, Denver, Colorado, April 5-8, 1998.
23. Al-Fattah, S.M. and Startzman, R.A.: "Neural Network Approach Predicts U.S. Natural Gas Production," SPE paper 67260, presented at the SPE Production and Operations Symposium, Oklahoma City, Oklahoma, March 24-27, 2001.
24. Zargari, S. and Mohaghegh, S.D.: "Field Development Strategies for Bakken Shale Formation," SPE Paper 139032, presented at the SPE Eastern Regional Meeting, Morgantown, West Virginia, October 13-15, 2010.
25. Hagan, M.T., Demuth, H.B. and Bearl, M.: *Neural Network Design*, 1st ed., PWS Publishing, Boston, Massachusetts, 1996

BIOGRAPHIES

Dr. Mari H. Algahtani joined Saudi Aramco in 2005 as a Facilities Engineer working in the Production and Facilities Development Department. In 2007, he joined the Upstream Development Strategy and Reserves Division. Mari has held several positions, from a Senior Reservoir Engineer, to a Deputy Team Leader of Integrated Reservoir Studies, to a Unit Supervisor.

He is an active member of the Society of Petroleum Engineers (SPE). In 2014, Mari was elected the SPE Graduate Students' Representative for the SPE Penn State Chapter. He is currently the 2017 ATS&E Pre-Events Courses and Workshops co-chair.

In 2005, Mari received his B.S. degree in Petroleum and Natural Gas Engineering (with honors) from West Virginia University, Morgantown, WV. In 2010, he received his M.S. degree in Petroleum Engineering from Texas A&M University, College Station, TX. Mari's research area was in offshore oil field development.

In 2015, he received his Ph.D. degree in Petroleum Engineering from Pennsylvania State University, State College, PA. Mari's research area was shale gas development. During his tenure at Penn State, he was a Technical Reviewer for the *Journal of Petroleum Exploration and Production Technology*.

Mari holds a U.S. patent in Offshore Recovery Enhancement Mechanism.

Prof. Turgay Ertekin is a Professor of Petroleum and Natural Gas Engineering and Head of the John and Willie Leone Family Department of Energy and Mineral Engineering at Pennsylvania State University. He is also the holder of the George E. Trimble Chair in Earth and Mineral Sciences at the university. Turgay's main research area is mathematical modeling of fluid flow dynamics in porous media and implementation of artificial intelligence technology with respect to various reservoir engineering process analyses.

He is a recipient of several Society of Petroleum Engineers (SPE) international awards, including the 1998 Distinguished Achievement Award for Petroleum Engineering Faculty, the 2001 Lester C. Uren Award for Distinguished Achievement in the Technology of Petroleum Engineering, the 2001 SPE Distinguished Member Award and the 2013 SPE Honorary Membership Award.

At Penn State, Turgay has received the College of Earth and Mineral Sciences' Teaching, Research, Service and Mentorships awards and also the university's Graduate School Teaching Award.

For a two-year period, he served as the Executive Editor of the *SPE Formation Evaluation Journal* and he currently is serving as Editor-in-Chief for the *Journal of Petroleum Exploration and Production Technology*.

Turgay received his B.S. and M.S. degrees in Petroleum Engineering from the Middle East Technical University, Ankara, Turkey, and his Ph.D. degree in Petroleum and Natural Gas Engineering from Pennsylvania State University, State College, PA.

CO_2 Foam Rheology Behavior under Reservoir Conditions

Dr. Abdulaziz S. Al-Qasim, Fawaz M. Al-Otaibi, Dr. Sunil L. Kokal and Xianmin Zhou

ABSTRACT

Supercritical carbon dioxide (sc-CO_2) flooding is one of the most important enhanced oil recovery methods to recover oil from both sandstone and carbonate reservoirs. In many cases, this process is handicapped, especially in thick reservoirs, by sc-CO_2 gravity override. Because sc-CO_2 is lighter than oil and water, there can be extensive gravity override of sc-CO_2, bypassing oil in the lower part of the formation. Different methods have been used to control sc-CO_2 mobility and improve its sweep efficiency by either increasing its density and viscosity or by reducing its relative permeability. Using sc-CO_2 as a foam or as an emulsion is one of these methods and can provide better mobility control of the injected sc-CO_2. This article investigates the impact of various parameters such as a liquid/liquid ratio, different foam qualities and different injection modes on the sc-CO_2 foam quality and its rheological properties.

In this study, various types of surfactants were used to generate sc-CO_2 foam. The sc-CO_2 foam was generated using two different types of injection modes. Experiments were designed and conducted in a high-pressure, high temperature (HPHT) flow loop instrument to identify the optimum surfactant concentration and liquid/liquid ratio to produce high quality foam and increase the sc-CO_2 viscosity. During the experiment, sc-CO_2 foam characteristics were analyzed through a visual cell in terms of bubble size distribution.

The rheological properties of the sc-CO_2 foam were investigated by varying the shear rate, shear stress, foam quality, injection modes and foaming agent concentrations at reservoir conditions. The experimental results show that the foam mobility — total mobility of sc-CO_2 surfactant solution — decreases with increasing foam quality. The results further indicate that the sc-CO_2 foam can make strong and stable foams under certain conditions. Foam quality was correlated to the images of the HPHT foams that were captured through a microscope at different time intervals and analyzed to indicate their stability. Two foaming agents were identified that show excellent foam quality with good foam strength and stability over a period of time at reservoir conditions.

INTRODUCTION

For use as a miscible displacement at the required reservoir conditions, carbon dioxide (CO_2) must exist as a dense or supercritical (sc) CO_2 fluid. The sc-CO_2 presents two distinct disadvantages when it is used to displace crude: (1) an unfavorable viscosity or mobility ratio produces inefficient oil displacement by causing fingering of the CO_2 owing to frontal instability, and (2) gravity override within the reservoir due to the low density of sc-CO_2 reduces sweep efficiency in lower zones. One of the most promising techniques to overcome these challenges is the use of CO_2 foam.

Using CO_2 in the form of foam increases its viscosity, which means CO_2 mobility in porous rock through the reservoir can be decreased if it is contained in a foam-like dispersion[1]. The use of foam for mobility control shows considerable promise in the early work by Bond and Holbrook (1958)[2] and by Fried (1961)[3]. These and later studies suggest that foam injectivity is considerably different from that of either water or gas. Two main types of CO_2 foams can be generated to increase CO_2 viscosity, namely, CO_2 in a water foam and water in a CO_2 foam. These foams are generated using water soluble surfactants, CO_2 soluble surfactants or nanoparticles[4]. Adding surfactant to the injected water during a CO_2 flood improves both the areal and the vertical sweep efficiencies by stabilizing viscous fingering and flow through the more permeable zones.

One of the foam characteristics that needs an assessment is the foam viscosity. Foam viscosity has been defined[5] empirically as:

$$\mu_f = \mu_g * (1 + 3.6\Gamma) \tag{1}$$

where μ_f is the foam viscosity, μ_g is the gas viscosity, and Γ if the foam quality. From this relationship, it is observed that the higher the quality of foam generated, the higher its viscosity. The quality of foam is defined as a ratio of the volume of gas to the volume of gas plus surfactant used. Reducing CO_2 gas mobility decreases the velocity of its flow through the reservoir. From Darcy's equation, and treating the foam — gas and liquid — as a single phase, the foam velocity can be expressed as:

$$v_f = k\ \Delta p/\mu_f.L \tag{2}$$

where v_f is foam velocity, k is permeability, Δp is the pressure difference, μ_f is foam viscosity, and L is the length of the porous medium. Increasing the foam viscosity μ_f in the Eqn. 2 will therefore reduce the foam's velocity while flowing through the reservoir. This reduction of CO_2 flow velocity enables it to contact a larger portion of the reservoir before eventually segregating — due to density differences — or breaking through at the production well.

When used to recover oil, the sc-CO_2 mixes with the oil bank under appropriate miscibility conditions, displacing the remaining oil left behind after waterflooding. The sc-CO_2 is more mobile and less viscous than oil and water, and so tends to create channels or fingers through the oil and water phases. This causes bypassing and results in poor displacement efficiency.

The mobility of the sc-CO_2 foam can be controlled by reducing the sc-CO_2 relative permeability through gas trapping[6, 7] or by increasing the viscosity of the sc-CO_2[8]. Mobility reduction by CO_2 foam has been a topic of considerable research[9-11].

FOAM RHEOLOGY

Gauglitz et al. (2002)[12] defines foam in porous media as "a dispersion of gas in a continuous liquid phase with at least some gas flow paths made discontinuous by thin liquid films called lamellae." Foam quality is defined as the volumetric ratio between the sc-CO_2 phase and the aqueous foaming phase, such as that of surfactants. Aroonsri et al. (2013)[13] suggests that the optimum foam quality can be obtained at around 75% sc-CO_2. The sc-CO_2 density declines as the temperature increases. This effect requires an increased shear rate to generate foam with higher foam quality. Foam texture is a function of the gas bubbles' size distribution. The size of the bubbles may vary from a few microns to a few millimeters.

The rheology of foam has been studied in a capillary viscometer using tubes of different diameters[14]. The apparent viscosity of the foam was determined in this study as a function of the shear stress, in that viscosity decreases with increasing shear stress. Analysis of the data indicates that in a capillary tube the high viscosity foam flows concurrently with a solvent layer around the tube wall. This analysis accounts for why the flow characteristics of the foam vary with tube diameter, and it shows that the foam flows as a viscous fluid. Studies in porous media indicate that foam does not flow as a single fluid even when the liquid and gas are injected as a foam[15]. The liquid phase moves through the porous medium via the film network of bubbles, and the gas phase moves progressively through the system by breaking and reforming bubbles.

In previous studies, CO_2 foams have shown extreme variability in their flow properties. The extrapolation of the results of available tests to a particular reservoir formation therefore is hazardous without more specific insight into foam rheology[16]. Foams are complex mixtures of a gas, a liquid and a surfactant, and its rheological properties are strongly influenced by parameters like temperature, absolute pressure, foam quality, texture, foam channel wall interactions, liquid phase properties, and type and concentration of surfactant[17].

A comparison of the flow properties of foam generated in a shear-type mixer with those of foam formed in situ shows no essential difference. It has been found, however, that the foam from the shear-type mixer is less uniform in bubble size and so was difficult to handle experimentally[16].

CO_2 foams are non-Newtonian in nature, following a power law with or without yield stress. The apparent viscosity of CO_2 foams decreases with increasing pressure or temperature, which decreases its quality. Foam rheology is still a very complex problem and is a matter of debate at the present time[18].

In situ generation of high quality foam depends mainly on the following factors:

- Mixing ratio.
- Temperature resistance.
- Pressure.
- Stability of foam or degree of foam degradation.

The sc-CO_2 foam is used mainly to control sc-CO_2 mobility, improve the conformance control and enhance sweep efficiency in heterogeneous zones with high permeability contrasts. The sc-CO_2 foam also performs other important functions, such as working as a flow barrier or blocking agents for the sealing formation. This is especially true for gelled foams, which act as an aqueous foam — low viscosity — during injection and then form a gel at a later time to enhance the mechanical stability of the sc-CO_2. This minimizes the amount of cycled sc-CO_2 and improves productivity.

Figure 1 shows a conceptual image of the behavior of foam flow in a formation/reservoir. The outcome of this process is highly dependent upon the ease with which each fluid flows through a porous medium.

The quality of a foam can be characterized based on the

Fig. 1. Conceptual image of foam flow within a reservoir.

Foaming Agent	Polymer (gpt)	Surfactant (gpt)	Stabilizer (gpt)
Type I	8.9	10.0	0.0

Table 1. Type I foaming agent

Foaming Agent	Alpha Olefin Sulfonate (wt%)	Isopropyl Alcohol (wt%)	Citrus Terpenes (wt%)
Type II	10-30	1-5	1-5

Table 2. Type II foaming agent

percentage (%), or fraction, of the gas volume, i.e., the sc-CO_2, to the total volume present in the foam, which includes the foaming agent. For example, a foam quality of 70% contains 70% gas by volume. Another way of characterizing the quality is simply by writing the ratio of the gas fraction volume to the liquid volume, i.e., the foaming agent. So, a 70/30 ratio means we have 70% gas and 30% liquid. The ratio format was used to express foam qualities in the experimental work performed and presented in this article.

EXPERIMENTAL SETUP AND PROCEDURES

Foaming Agents

Two commercial foaming agents were used in this study: Type I and Type II. They were obtained from different chemical providers. The Type I foaming agent is used to enhance CO_2 viscosity in well treatments. It consists of a polysaccharide-based gelling agent and a foaming agent, or surfactant, that is added to stabilize the emulsion between the CO_2 and base gel. The Type II foaming agent is designed specifically for use in foam flooding and conformance control in enhanced oil recovery/improved oil recovery applications. It is a mixture of solvent, co-solvent foamer and surfactants. More information about the Type I and Type II foaming agents are shown in Tables 1 and 2, respectively.

The properties of all foaming agents are sensitive to high temperatures and high salinities (especially hardness), which may have a detrimental effect on their performance. Some of the selected foaming agents use temperature stabilizers to stabilize the foams and as a means to delay viscosity degradation at higher temperatures.

Foam Quality

The selected Type I and Type II foaming agents were used to study the apparent viscosity achieved under different foam qualities and to optimize the amount of the foaming agents used. Two injection modes, i.e., injecting larger volumes of the foaming agents or injecting at a faster rate to reduce the exposure time, were tested for high temperature sensitivity.

Injection Schemes

Different injection schemes were used in the experiments to test their ability to optimize the amount of foaming agent and to determine the best foaming conditions. The following injection schemes were tested:

- Injecting the sc-CO_2 first, then the foaming agent.
- Injecting the foaming agent first, followed by a gradual and slow injection of the sc-CO_2.
- Injecting the foaming agent first, then injecting sc-N_2, followed by gradual and slow injection of the sc-CO_2.

Procedure

A new procedure was developed and tested to evaluate the rheology of sc-CO_2 foams at different sc-CO_2/foam ratios and qualities, all at reservoir conditions, i.e., high-pressure, high temperature (HPHT). It utilized a rheometer device especially built to conduct rheology studies for complex non-Newtonian fluids at reservoir conditions. The foam rheometer was calibrated using standard non-Newtonian fluids under different reservoir conditions to test the full extent of its viscosity range. The viscosity results obtained from the device were validated with theoretical calculations. This step is fundamental to the correct estimation of sc-CO_2/foam rheology as a function of foam quality.

The rheology of the foams was determined by measuring their average apparent viscosity and shear rates. From these data, plots of the viscosity shear rate relationship were generated to help understand the rheology of foam, i.e., to indicate whether the foam exhibited a shear thinning or shear thickening behavior. Figure 2 shows a schematic of the experimental setup used here for studying the rheology of sc-CO_2 foams. The experiment included a visual pressure-volume-temperature cell and a flow loop. The flow loop was designed to measure foam rheology under flowing conditions and consists of a circulating loop made of capillary steel tubes. Figure 3 shows a photograph of the foam rheology apparatus.

The test procedure was as follows. First, the foaming agent is introduced into the cell/apparatus that has been equilibrated at the desired temperature in the oven. The amount of the foaming agent injected is based on the foam quality value for that particular experiment. Then, the sc-CO_2 is slowly pumped into the system to bring the pressure up to the desired pressure. The amount of the foaming agent and sc-CO_2 are recorded. From this data, the foam quality is determined using the gas/foaming agent ratio. After building up the apparatus to the desired reservoir conditions (P = 3,250 psi and T = 212 °F), the fluids inside the cell are circulated through the loop. They mix together and generate sc-CO_2 foam. This process is very important to allow foam equilibrium.

The initial shear rate is set around 400 s^{-1} for about 20

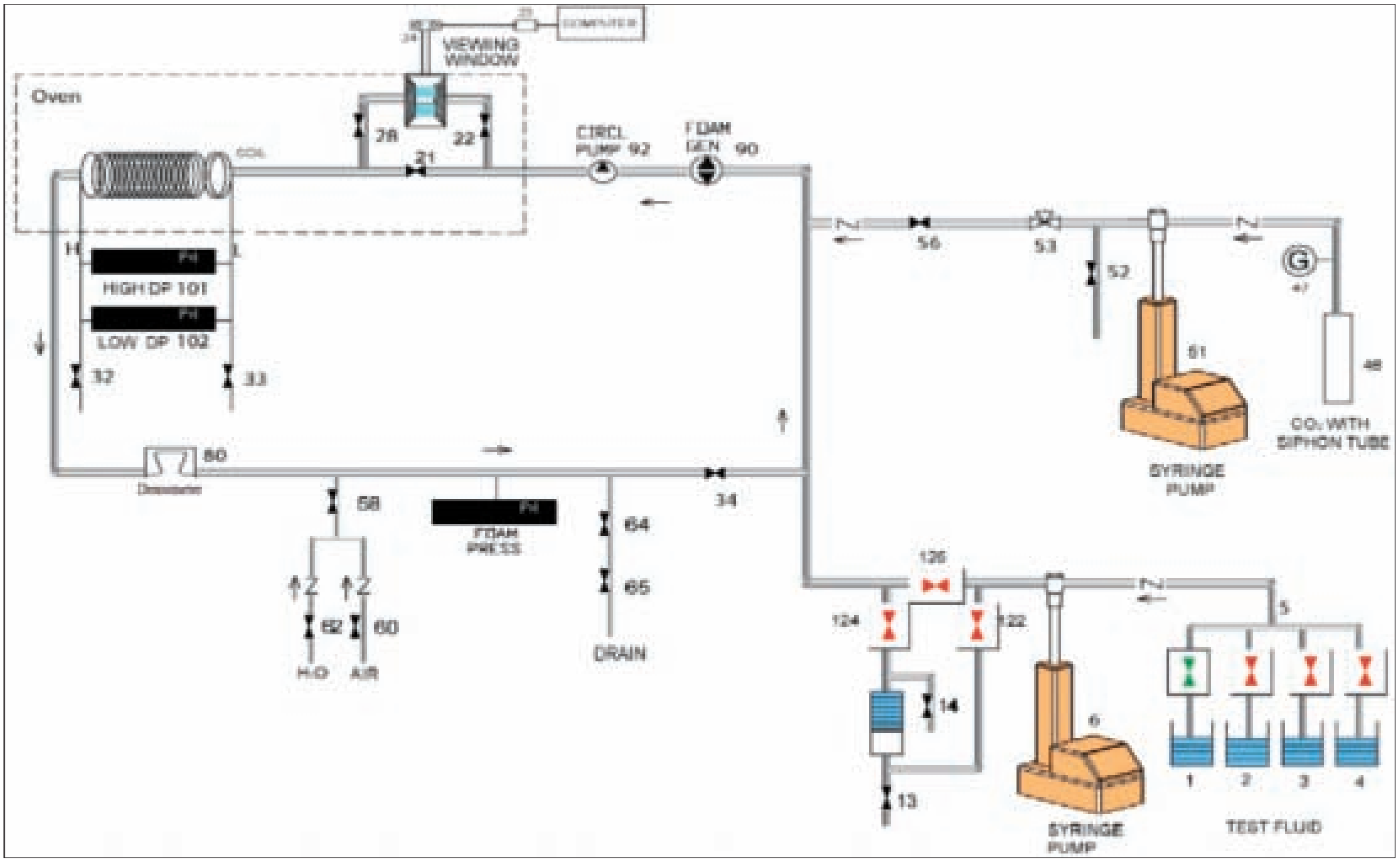

Fig. 2. *Schematic of the foam rheology test apparatus.*

Fig. 3. *Photograph of the foam rheology test apparatus.*

Fig. 4. Collected samples of the foam generated inside the flow loop.

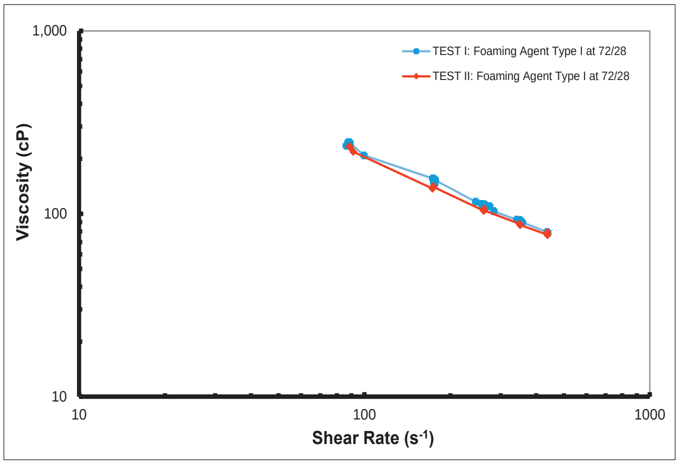

Fig. 5. Shear rate vs. apparent viscosity for the Type 1 repeatability test.

minutes to create the foam in the loop during which the foam generation, bubble size, texture and quality are monitored using the viewing cell. Then, the flow rate is changed, and the shear rate and viscosity are recorded. The apparent viscosity is calculated based on the capillary tube geometry and circulating flow rate data. Other rheological characteristics of the sc-CO_2 foam, such as density, can also be determined as a function of time and shear rate. At the end of the experiment, the foam can be collected, Fig. 4.

RESULTS AND DISCUSSION

To first test conducted was to confirm the repeatability of the foam rheology in the apparatus under identical test conditions. The repeatability experiment was conducted with the Type I foaming agent at the same HPHT conditions and the same foam quality of 72/28. Figure 5 shows the results of these two tests. The results are close and indicate that the data generated are repeatable.

Foaming Agents

Figure 6 shows the apparent viscosity vs. the shear rates for the Type I and Type II foaming agents with sc-CO_2 at different foam quality ratios. The results indicate that the CO_2 foams behave as non-Newtonian fluids and exhibit a shear thinning behavior. In most cases, their behavior can be approximated with a power-law fluid. The Type I foaming agent created foams that had significantly high viscosities, both in terms of absolute values and relative to the sc-CO_2 viscosity. The viscosity of foams with the Type I foaming agent increased by three to four orders of magnitude compared to the sc-CO_2.

The viscosity of foams with the Type II foaming agent was lower, increasing by less than two orders of magnitude. When the Type I foaming agents were compared to the Type II agents, each at a given foam quality, the bubble size distribution was larger, and the texture was different, in the case of the Type I agent, Fig. 7. The visual observations from the viewing cell, Fig. 8, are consistent with the trends previously shown in Fig. 6. The results indicate that the foam texture and bubble size distribution for Type I foaming agents are better than those of Type II.

Foam Quality

Different quality ranges of the foaming agents and sc-CO_2 were also investigated. The goal of these experiments was to study the apparent viscosity under different foam qualities so as to optimize the amount of the foaming agents used. An examination of the three curves plotted in Fig. 6 for foams at different foam qualities with the Type I foaming agent indicates that the foam's apparent viscosity exhibits a direct relationship to the volume fraction or quality of the foam. As the volume fraction of the foaming agent increases, the apparent viscosity increases — at a given shear rate. This is attributed to the higher amount of foaming agent in the foam. But this is true up to a point only and varies by foaming agent.

A similar behavior was observed with the Type II foaming

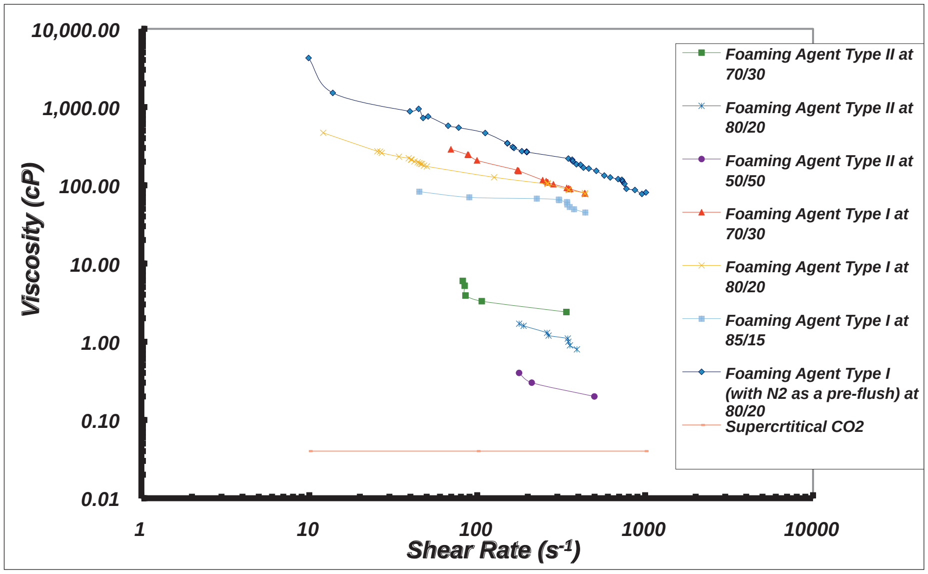

Fig. 6. Shear rate vs. apparent viscosity for Type I and Type II foaming agents.

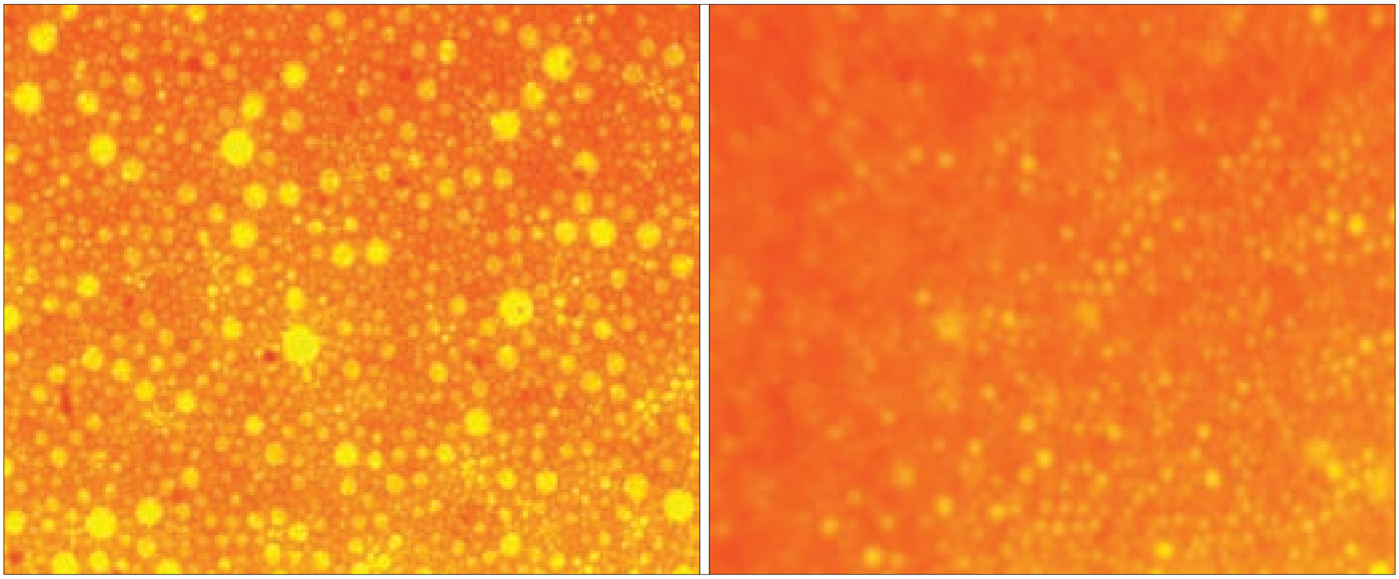

Fig. 7. Bubble size distribution from the viewing cell for the Type I (left) and the Type II (right) foaming agents.

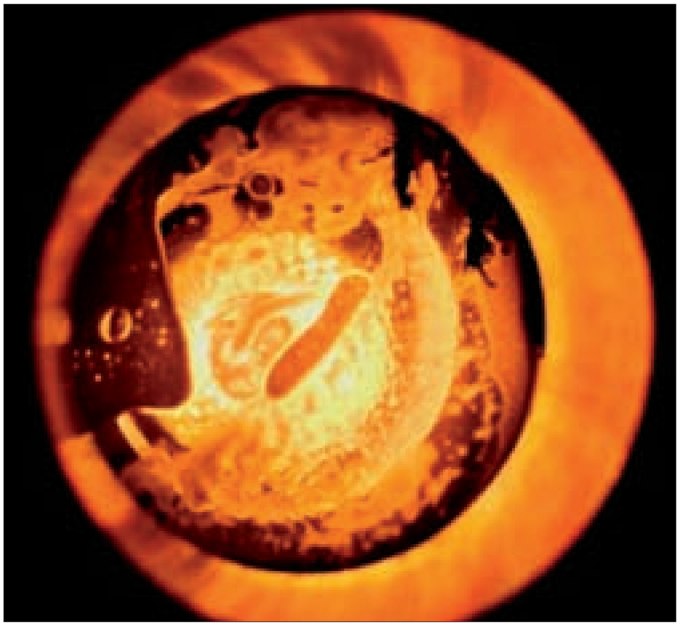

Fig. 8. Viewing cell for Type I at 50/50 ratio.

agent in which the 70/30 foam yielded higher apparent viscosity compared to the 80/20 foam. Going beyond a certain foaming agent volume fraction, however, actually reduces the foam viscosity, as seen in the 50/50 foam for Type II. This behavior was also seen in the Type I foaming agent (but not shown in Fig. 6).

The results indicate that a certain volume of foaming agent is necessary to form a stable foam. Increasing the amount of foaming agent beyond some value results in poor viscosity behavior. This is attributable to the fact that a stable foam requires a minimum amount of sc-CO_2. The Type I and Type II foaming agents could not form a stable foam with less than 50% sc-CO_2.

The same applies for creating a foam at very high sc-CO_2 volume fractions. Using less than 10% of the foaming agent results in a collapse of the foam and difficulty in sustaining a stable foam. One explanation is that the foam may be unable to form at a very high quality, due to the lack of a sufficient amount of the foaming agent to support foam generation, and the gas mobility may then become unfavorable resulting in stability issues. The quality of foam therefore plays an important role in the creation and the subsequent sustainability and stability of foams. Too much, or not enough, of the foaming agent causes segregation between the sc-CO_2 and the foaming agent, resulting in poor foam stability. The results from our study indicate that the best quality for a stable and high viscosity foam is between 15% to 25% of foaming agent volumes.

Injection Schemes

Different injection schemes were experimented with to test and evaluate the optimum foaming conditions. Injecting the sc-CO_2 first, followed by the foaming agent, did not result in the formation of stable foams. This could be an apparatus effect or a procedural effect. The second scheme in which the foaming agent is injected first and followed by gradual injection of the sc-CO_2 provides the optimum foaming conditions. All the data shown in Fig. 6 were generated using this scheme.

The last experiment assessed the benefit of using a small amount of sc-N_2 as a pre-flush agent in the case of an 80/20 quality foam with the Type I foaming agent. The sc-N_2 was injected as a small slug ahead of the sc-CO_2. This particular foam therefore contained about 10% sc-N_2, 70% sc-CO_2 and 20% of the Type I foaming agent. The foaming agent was injected first, then the sc-N_2 was injected, followed by gradual injection of the sc-CO_2. The use of sc-N_2 as a pre-flush of sc-CO_2 improved the foam quality and yielded a higher apparent viscosity. This apparent viscosity was approximately two to three times the value observed in the 80/20 experiment without using sc-N_2 as a pre-flush, as previously shown in Fig. 6. The use of sc-N_2 vs. sc-CO_2 in foams is currently being investigated and will be the topic of a future SPE publication.

The time frame for all the data obtained in this study was about 40 minutes. The results may change as the foam behavior, texture and bubble distribution changes with time. The stability of the foam is an important aspect in foam rheology and will be addressed in a forthcoming publication.

CONCLUSIONS

1. The foam's apparent viscosity can be increased substantially by using good foaming and polymeric agents. This increase can be several orders of magnitude greater compared to the sc-CO_2 alone.
2. There is an optimum range of foam quality in which the foam is relatively stable and provides high apparent viscosities. For each foaming agent, this will be different, but generally the best quality is achieved with between 10% to 25% of the foaming agent.
3. Adding a small amount of sc-N_2 as a pre-flush of the sc-CO_2 improved the results, but this finding needs to be studied further and validated.
4. Further studies need to be performed to determine the optimum foaming conditions for different concentrations using different foaming agents.

ACKNOWLEDGMENTS

The authors would like to thank the management of Saudi Aramco for their support and permission to publish this article. Special thanks are extended to Amin M. Al-Abdulwahab for the preparation of the rheometer experiments.

This article was presented at the SPE Annual Technical Conference and Exhibition, Dhahran, Saudi Arabia, April 24-27, 2017.

REFERENCES

1. Lee, H.O. and Heller, J.P.: "Laboratory Measurements of CO_2 Foam Mobility," *SPE Reservoir Engineering*, Vol. 5, Issue 2, May 1990, pp. 193-197.
2. Bond, D.C. and Holbrook, O.C.: *Gas Drive Oil Recovery Process*, U.S. Patent 2,866,507, 1958.
3. Fried, A.N.: *The Foam-Drive for Increasing the Recovery of Oil*, U.S. Bureau of Mines, Washington, D.C., 1961, 65 p.
4. Al-Otaibi, F.M., Kokal, S.L., Chang, Y., Al-Qahtani, J.F., et al.: "Gelled Emulsion of CO-Water-Nanoparticles," SPE paper 166072, presented at the SPE Annual Technical Conference and Exhibition, New Orleans, Louisiana, September 30-October 2, 2013.
5. Mitchell, B.J.: *Viscosity of Foam*, University of Oklahoma, Norman, Oklahoma, 1969, 292 p.
6. Friedmann, F., Chen, W.H. and Gauglitz, P.A.: "Experimental and Simulation Study of High Temperature Foam Displacement in Porous Media," *SPE Reservoir Engineering*, Vol. 6, Issue 1, February 1991, pp. 37-45.
7. Rossen, W.R. and Renkema, W.J.: "Success of Foam SAG Processes in Heterogeneous Reservoirs," SPE paper 110408, presented at the SPE Annual Technical Conference and Exhibition, Anaheim, California, November 11-14, 2007.
8. Hirasaki, G.J. and Lawson, J.B.: "Mechanisms of Foam Flow in Porous Media: Apparent Viscosity in Smooth Capillaries," *Society of Petroleum Engineers Journal*, Vol. 25, Issue 2, April 1985, pp. 176-190.
9. Yang, S.H. and Reed, R.L.: "Mobility Control Using CO_2 Forms," SPE paper 19689, presented at the SPE Annual Technical Conference and Exhibition, San Antonio, Texas, October 8-11, 1989.
10. Tsau, J-S. and Grigg, R.B.: "Assessment of Foam Properties and Effectiveness in Mobility Reduction for CO_2 Foam Floods," SPE paper 37221, presented at the International Symposium on Oil Field Chemistry, Houston, Texas, February 18-21, 1997.
11. Al-Otaibi, F.M., Zhou, X., Kokal, S.L., Balasubramanian, S., et al.: "A Novel Technique for Enhanced Oil Recovery: In Situ CO_2 Emulsion Generation," SPE paper 174567, presented at the SPE Asia Pacific Enhanced Oil Recovery Conference, Kuala Lumpur, Malaysia, August 11-13, 2015.
12. Gauglitz, P.A., Friedmann, F., Kam, S.I. and Rossen, W.R.: "Foam Generation in Porous Media," SPE paper 75177, presented at the SPE/DOE Improved Oil Recovery Symposium, Tulsa, Oklahoma, April 13-17, 2002.
13. Aroonsri, A., Worthen, A.J., Hariz, T., Johnston, K.P., et al.: "Conditions for Generating Nanoparticle Stabilized CO_2 Foams in Fracture and Matrix Flow," SPE paper 166319, presented at the SPE Annual Technical Conference and Exhibition, New Orleans, Louisiana, September 30-October 2, 2013.
14. David, A. and Marsden Jr., S.S.: "The Rheology of Foam," SPE paper 2544, presented at the Fall Meeting of the Society of Petroleum Engineers of AIME, Denver, Colorado, September 28-October 1, 1969.
15. Holm, L.W.: "The Mechanism of Gas and Liquid Flow Through Porous Media in the Presence of Foam," *Society of Petroleum Engineers Journal*, Vol. 8, Issue 4, December 1968, pp. 359-369.
16. Patton, J.T., Holbrook, S.T. and Hsu, W.: "Rheology of Mobility-Control Foams," *Society of Petroleum Engineers Journal*, Vol. 23, Issue 3, June 1983, pp. 456-460.
17. Bonilla, L.F. and Shah, S.N.: "Experimental Investigation

on the Rheology of Foams," SPE paper 59752, presented at the SPE/CERI Gas Technology Symposium, Calgary, Alberta, Canada, April 3-5, 2000.

18. Herzhaft, B. and Guazzelli, É.: "Experimental Study of the Sedimentation of Dilute and Semi-Dilute Suspensions of Fibers," *Journal of Fluid Mechanics*, Vol. 384, April 1999, pp. 133-158.

BIOGRAPHIES

Dr. Abdulaziz S. Al-Qasim has been working with Saudi Aramco as a Petroleum Engineer since 2007. In that time, he has worked in a variety of departments within Saudi Aramco. The emphasis of Abdulaziz's work has been on enhanced oil recovery projects (EOR). Most recently, he has worked in carbon dioxide (CO_2) EOR pilot management, and he is currently leading the gravity override mitigation research, which focuses mainly on CO_2 foams (water soluble surfactants, CO_2 soluble surfactants and nanoparticle stabilized foams) and direct thickeners for CO_2 (polymers).

Abdulaziz has authored and coauthored more than 10 papers, including several peer reviewed articles. He has also mentored and coached a number of summer students.

Abdulaziz previously served as a Vice Chairman of the Society of Petroleum Engineers-Young Professionals (SPE-YP) regional symposium held in Oman in February 2009. He has served in numerous SPE events at different levels.

Abdulaziz received his B.S. degree in 2007 from King Fahd University of Petroleum and Minerals (KFUPM), Dhahran, Saudi Arabia; his M.S. degree in 2011 from the University of Texas at Austin, Austin, TX; and his Ph.D. degree in 2016 from the University of Tulsa, Tulsa, OK, all in Petroleum Engineering.

Fawaz M. Al-Otaibi is a Petroleum Engineer at Saudi Aramco's Reservoir Characterization Department. Prior to that, he worked as a Supervisor of the Petrophysics Unit in the Exploration and Petroleum Engineering Center – Advanced Research Center (EXPEC ARC). Fawaz has worked in many technical positions and a variety of disciplines, including production engineering and reservoir management, within Saudi Aramco. He has led research projects on both enhanced oil recovery using carbon dioxide (CO_2 EOR) and reservoir fluids. Fawaz has evaluated different CO_2 EOR methods, such as water-alternating gas (WAG) and tapered WAG during CO_2 EOR flooding. He has also taught courses on CO_2 EOR and coreflooding theories and applications. Currently, Fawaz is leading a group of scientists and technicians to conduct studies to investigate several techniques in overcoming the gravity override during CO_2 EOR.

He is an active member of the Society of Petroleum Engineers (SPE) and has published numerous SPE papers and technical journals. Fawaz also has five filed patents. He is a Certified Petroleum Engineer and has received several awards and other recognitions from SPE.

In December 1997, Fawaz received his B.S. degree in Chemical Engineering from King Fahd University of Petroleum and Minerals (KFUPM), Dhahran, Saudi Arabia.

Dr. Sunil L. Kokal is a Principal Professional and a Focus Area Champion of enhanced oil recovery (EOR) on the Reservoir Engineering Technology team of Saudi Aramco's Exploration and Petroleum Engineering Center – Advanced Research Center (EXPEC ARC). Since joining Saudi Aramco in 1993, he has been involved in applied research projects on EOR/improved oil recovery, reservoir fluids, hydrocarbon phase behavior, crude oil emulsions and production-related challenges. Currently Sunil is leading a group of scientists, engineers and technicians in efforts to develop a program for carbon dioxide EOR and to conduct appropriate studies and field demonstration projects. Prior to joining Saudi Aramco, he worked at the Petroleum Recovery Institute, Calgary, Canada.

Sunil is a member of the Society of Petroleum Engineers (SPE), and he is a Registered Professional Engineer and a member of the Association of Professional Engineers, Geologists and Geophysicists of Alberta, Canada.

He has written over 100 technical papers. Sunil has served as an associate editor for the *Journal of Petroleum Science and Engineering* and for SPE's *Reservoir Evaluation and Engineering Journal*, and he earlier served on the Editorial Review Board of the *Journal of Canadian Petroleum Technology*.

He is the recipient of the prestigious 2016 SPE Honorary Member Award, the 2012 SPE DeGolyer Distinguished Service Medal, the 2011 SPE Distinguished Service Award, the 2010 SPE Regional Technical Award for Reservoir Description & Dynamics, and the 2008 SPE Distinguished Member Award for his services to the society. Sunil also served as a SPE Distinguished Lecturer during 2007-2008. Currently he is the Chair of the SPE Distinguished Lecturer Committee.

In 1982, Sunil received his B.S. degree in Chemical Engineering from the Indian Institute of Technology, New Delhi, India, and in 1987, he received his Ph.D. degree in Chemical Engineering from the University of Calgary, Calgary, Alberta, Canada.

Xianmin Zhou is currently a Petroleum Engineer with 41 years of experience working in the Center for Integrative Petroleum Research (CIPR), College of Petroleum Engineering and Geosciences, King Fahd University of Petroleum and Minerals (KFUPM), Saudi Arabia. Prior to joining KFUPM, Xianmin worked as a Petroleum Engineer at Saudi Aramco's Exploration and Petroleum Engineering Center – Advanced Research Center (EXPEC ARC), and as a Senior Petroleum Engineer/Senior Core Analyst for four major oil companies: Daqing Petroleum Research Center, China; Core Lab Inc., Omni Labs Inc. and Intertek Westport Technology Center in the U.S.

His current research interests include supercritical carbon dioxide enhanced oil recovery (EOR), chemical EOR, special core analysis, rock wettability studies and reservoir characterization. Xianmin's specialty is designing and developing lab equipment at reservoir conditions to meet research needs.

He has authored or coauthored 16 journal papers on the above subjects in Chinese and Canadian and SPE journals and presented 18 papers at SPE conferences, and holds five patents.

Xianmin received his B.S. degree in Petroleum Engineering from Daqing Petroleum Institute, Heilongjiang, China, and he received his M.S. degree in Chemical and Petroleum Engineering from the University of Wyoming, Laramie, WY.

Xianmin is member of the Society of Petroleum Engineers (SPE), the Society of Core Analysts (SCA) and the European Association of Geoscientists and Engineers (EAGE).

SUBSCRIPTION ORDER FORM

To begin receiving the *Saudi Aramco Journal of Technology* at no charge, please complete this form.

Please print clearly.

Name ____
Title ____
Organization ____
Address ____
City ____
State/Province ____
Postal code ____
Country ____
E-mail address ____
Number of copies ____

TO ORDER

By phone/email:

Saudi Aramco Public Relations Department
JOT Distribution
+966-013-876-0498
william.bradshaw.1@aramco.com

By mail:

Saudi Aramco Public Relations Department
JOT Distribution
Box 5000
Dhahran 31311
Saudi Arabia

Current issues, select back issues and multiple copies of some issues are available upon request.

The *Saudi Aramco Journal of Technology* is published by the Saudi Aramco Public Relations Department, Saudi Arabian Oil Company, Dhahran, Saudi Arabia.

GUIDELINES FOR SUBMITTING AN ARTICLE TO THE SAUDI ARAMCO JOURNAL OF TECHNOLOGY

These guidelines are designed to simplify and help standardize submissions. They need not be followed rigorously. If you have additional questions, please feel free to contact us at Public Relations. Our address and phone numbers are listed on page 77.

Length

Varies, but an average of 2,500-3,500 words, plus illustrations/photos and captions. Maximum length should be 5,000 words. Articles in excess will be shortened.

What to send

Send text in Microsoft Word format via email or on disc, plus one hard copy. Send illustrations/photos and captions separately but concurrently, both as email or as hard copy (more information follows under file formats).

Procedure

Notification of acceptance is usually within three weeks after the submission deadline. The article will be edited for style and clarity and returned to the author for review. All articles are subject to the company's normal review. No paper can be published without a signature at the manager level or above.

Format

No single article need include all of the following parts. The type of article and subject covered will determine which parts to include.

Working title

Abstract

Usually 100-150 words to summarize the main points.

Introduction

Different from the abstract in that it "sets the stage" for the content of the article, rather than telling the reader what it is about.

Main body

May incorporate subtitles, artwork, photos, etc.

Conclusion/summary

Assessment of results or restatement of points in introduction.

Endnotes/references/bibliography

Use only when essential. Use author/date citation method in the main body. Numbered footnotes or endnotes will be converted. Include complete publication information. Standard is *The Associated Press Stylebook*, 52nd ed. and *Webster's New World College Dictionary*, 5th ed.

Acknowledgments

Use to thank those who helped make the article possible.

Illustrations/tables/photos and explanatory text

Submit these separately. **Do not place in the text.** Positioning in the text may be indicated with placeholders. Initial submission may include copies of originals; however, publication will require the originals. When possible, submit both electronic versions, printouts and/or slides. Color is preferable.

File formats

Illustration files with .EPS extensions work best. Other acceptable extensions are .TIFF, .JPEG and .PICT.

Permission(s) to reprint, if appropriate

Previously published articles are acceptable but can be published only with written permission from the copyright holder.

Author(s)/contributor(s)

Please include a brief biographical statement.

Submission/Acceptance Procedures

Papers are submitted on a competitive basis and are evaluated by an editorial review board comprised of various department managers and subject matter experts. Following initial selection, authors whose papers have been accepted for publication will be notified by email.

Papers submitted for a particular issue but not accepted for that issue will be carried forward as submissions for subsequent issues, unless the author specifically requests in writing that there be no further consideration. Papers previously published or presented may be submitted.

Submit articles to:

Editor
The *Saudi Aramco Journal of Technology*
C-11B, Room AN-1080
North Admin Building #175
Dhahran 31311, Saudi Arabia
Tel: +966-013-876-0498
E-mail: william.bradshaw.1@aramco.com.sa

Submission deadlines

Issue	Paper submission deadline	Release date
Spring 2018	November 26, 2017	March 31, 2018
Summer 2018	February 21, 2018	June 30, 2018
Fall 2018	May 23, 2018	September 30, 2018
Winter 2018	August 16, 2018	December 31, 2018